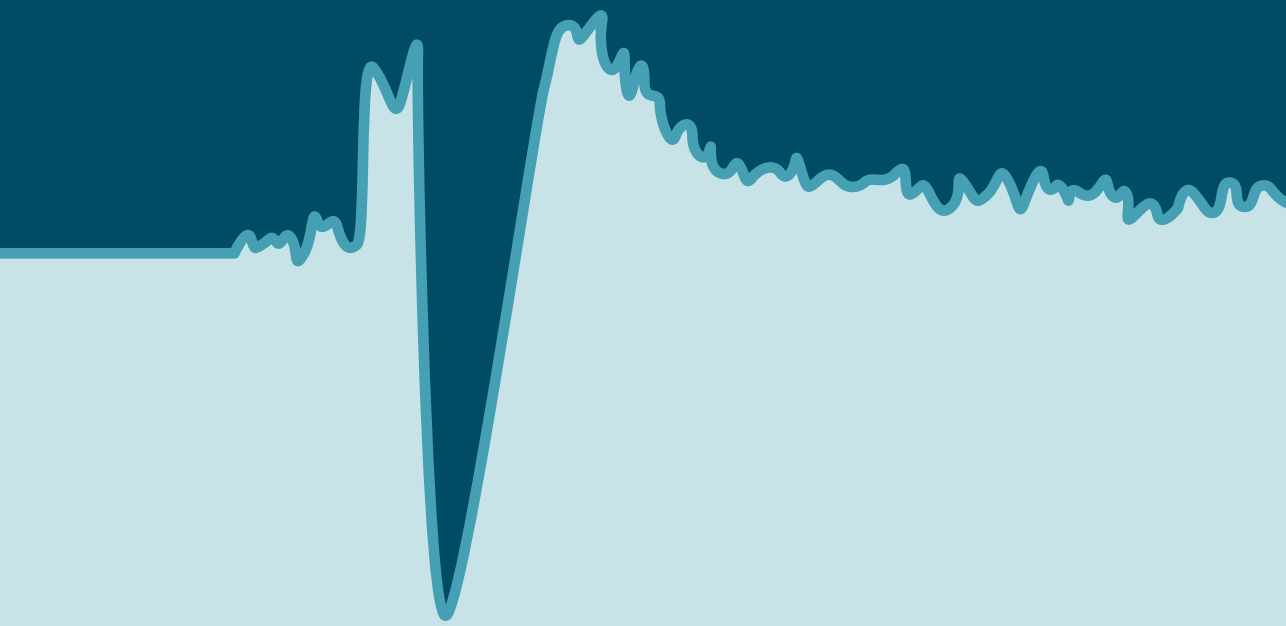

A CLOSER LOOK AT STIMULATION THRESHOLDS AND SPREAD OF EXCITATION IN COCHLEAR IMPLANTS

RECORDING ASPECTS AND CLINICAL IMPLICATIONS

DICK BIESHEUVEL

A CLOSER LOOK AT STIMULATION THRESHOLDS AND SPREAD OF EXCITATION IN COCHLEAR IMPLANTS

RECORDING ASPECTS AND CLINICAL IMPLICATIONS

JAN DIRK BIESHEUVEL

Cover: Bregje Jaspers || www.ProefschriftOntwerp.nl
Layout: Dennis Hendriks || www.ProefschriftMaken.nl
Printing: www.ProefschriftMaken.nl

ISBN: 978-94-6469-153-5

This research was funded by: Dutch Research Council (NWO/STW), project number 11693
The publication of this thesis was financially supported by: Advanced Bionics, Cochlear, Oticon Medical, MED-EL, ChipSoft.

A CLOSER LOOK AT STIMULATION THRESHOLDS AND SPREAD OF EXCITATION IN COCHLEAR IMPLANTS

RECORDING ASPECTS AND CLINICAL IMPLICATIONS

Proefschrift

ter verkrijging van
de graad van doctor aan de Universiteit Leiden,
op gezag van rector magnificus prof. dr. ir. H. Bijl,
volgens besluit van het college voor promoties
te verdedigen op woensdag 1 februari 2023
klokke 13.45 uur

door

Jan Dirk Biesheuvel
geboren te Lienden
in 1990

Promotores:	Prof. dr. ir. J.H.M. Frijns Prof. dr. ir. W.A. Serdijn (TU Delft)
Copromotor:	Dr. ir. J.J. Briaire
Leden promotiecommissie:	Prof. dr. P.P.G. van Benthem Prof. dr. R.P. Carlyon (University of Cambridge) Dr. R. Gransier (KU Leuven) Dr. ir. M.W. Kaandorp (Amsterdam UMC)

Content

CHAPTER

1

General introduction

Hearing is an important element in communication, social interaction, and human wellbeing. It is, therefore, essential to identify hearing loss in an early stage and to rehabilitate hearing loss adequately. Hearing loss can generally be rehabilitated with a hearing aid, except if there is a severe sensorineural hearing loss. Sensorineural hearing loss is often associated with damaged or deficient cochlear hair cells, resulting in an inability to translate sounds into neural signals traveling toward the brain. In that case, just sound amplification by a hearing aid is no longer effective and other means of rehabilitations need to be sought. Some decades ago, the population of deaf and hard of hearing people was dependent on written language, sign language or lip reading. However, with the advent of cochlear implants (CIs) new perspectives arose (Shannon 1983). A CI is a device that delivers sound directly to the auditory nerve by electrical stimulation via an electrode array in the cochlea. Although CIs do not work equally well for everyone, most people with a CI can again communicate via spoken language.

1.1. Cochlear implant

A CI consists of two parts: (1) an external part, which is called the sound processor and is worn on the ear, and (2) an internal part, which is the actual implant located under the skin. Figure 1.1 shows the different components of a CI and their position relative to the human anatomy. The first step in hearing with a CI is the recording of sound signals by the microphones of the sound processor. Next, the sound is pre-processed, e.g., noise is reduced and speech is amplified. The optimized sound signal is then divided over different frequency bands using bandpass filters. The sound energy per frequency band, typically coded by the envelope of the signal, forms the basis for calculating the stimulation pattern across the spectral channels. After calculating the stimulation pattern, the pattern is sent wirelessly to the implant via a coil located in the headpiece. In the implant, the stimulation pattern is transformed into electrical current pulses. These pulses go through multiple wires bundled in the electrode lead to different electrode contacts in the cochlea, where they deliver frequency specific stimulation. Finally, the electrical pulses will stimulate the auditory nerve and the CI-user perceives a sound. The CI uses the tonotopical organization of the cochlea, whereby high-frequency sounds are encoded at the base of the cochlea and low-frequency sounds in the apex of the cochlea.

1.2. Electrically evoked compound action potential

After electrical stimulation, the current spreads through the cochlea and excites multiple nerve fibers. In each excited nerve fiber, an action potential arises, which is a wave of electrical charge traveling over the nerve fiber membrane towards the brain. Due to the short and strong stimulus, all action potentials are generated simultaneously and together they form

an electrically evoked compound action potential (eCAP). The eCAP is a measurable electrical potential that represents the synchronous firing of multiple nerve fibers (Abbas et al. 1999; Hughes 2013). It is important to realize that the eCAP is a complex result of several factors: the number of firing nerve fibers, the position of the measuring electrodes, synchronicity of the excitation and the electrical conduction of the tissue (Mens 2007).

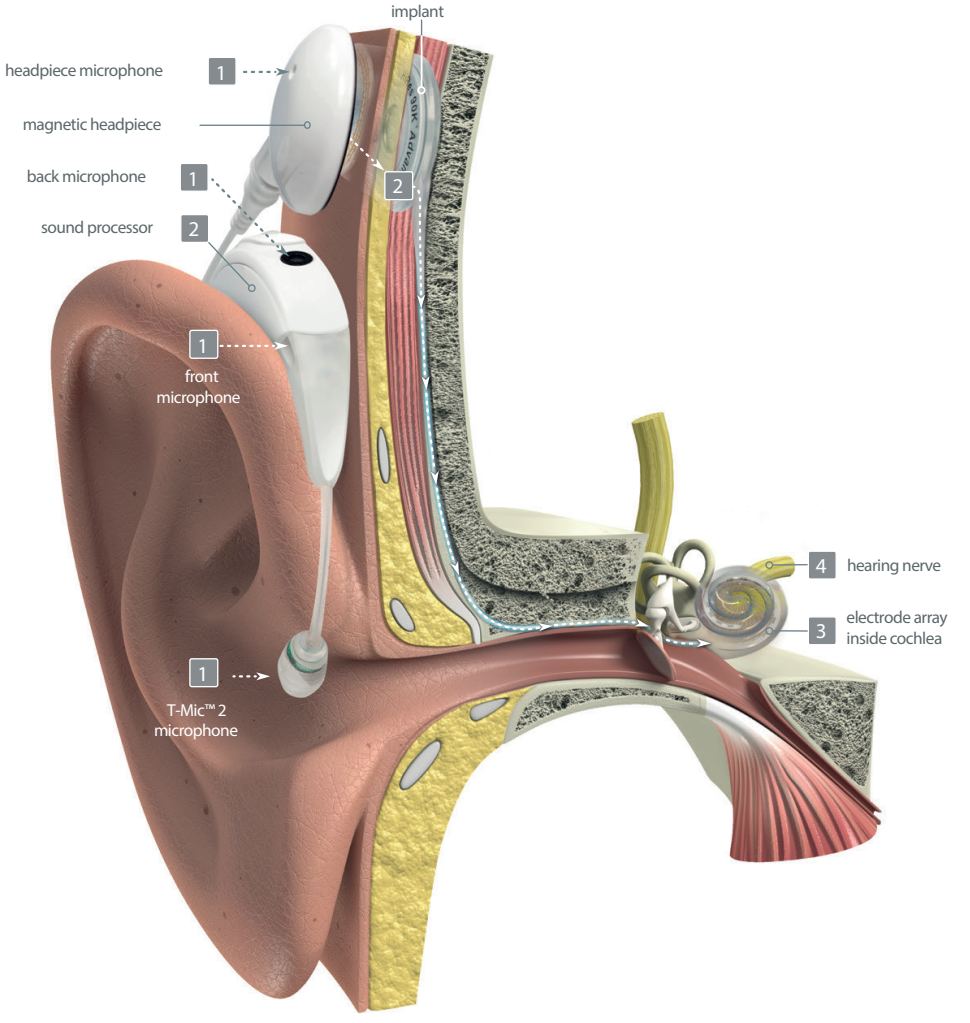

Figure 1.1. A cochlear implant consists of several components: microphones (1), sound processor and implant (2), and the electrode array in the cochlea (3). Via these components acoustic sounds are converted into electrical signals that directly stimulates the auditory nerve (4). Image courtesy of Advanced Bionics.

1.2.1. Recording eCAPs

All modern CIs have a built-in telemetry function for recording eCAP signals (Hughes 2013). Figure 1.2 schematically shows how an eCAP signal can be measured. A CI contains a current source that provides electrical stimulation via one of the electrode contacts located in the cochlea. Subsequently, an eCAP arises, which can be measured via an adjacent electrode contact and a reference contact located outside the cochlea. In general, the eCAP is measured using an intra-cochlear contact close to the source, i.e., the excited neurons. This is favorable for the amplitude of the signal and therefore for the signal-to-noise ratio. The recorded signal can be read-out via the speech processor and a computer. Typically, the eCAP is recorded as a waveform with a negative peak (N1) followed by a positive peak or plateau (P1). The amplitude of the eCAP is measured from N1 to P1 and can reach values up to 1.5 mV.

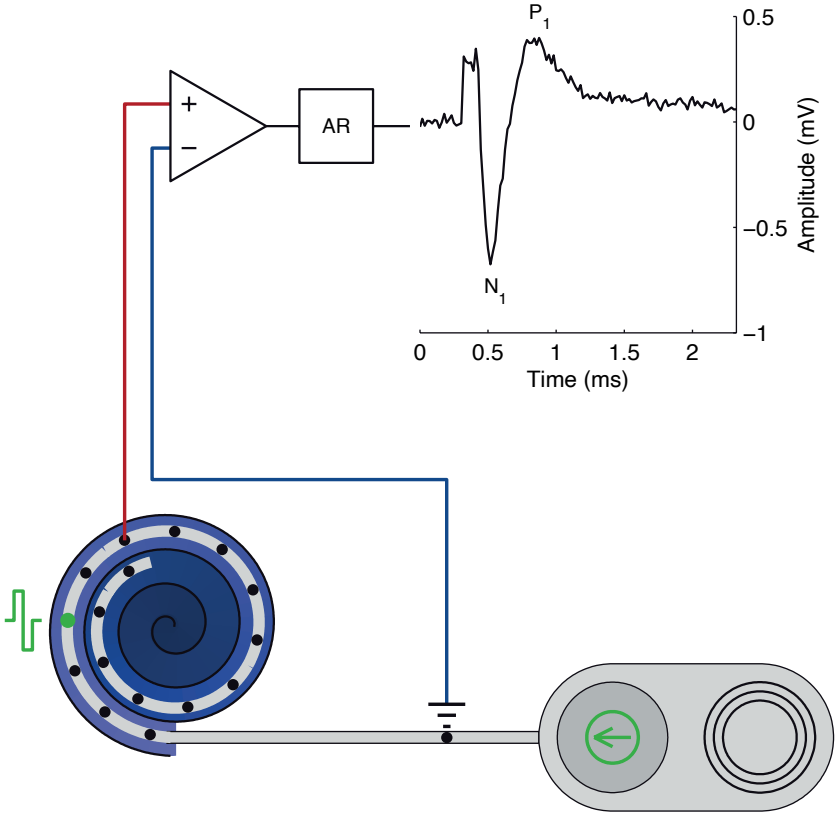

Figure 1.2. Schematic representation of an eCAP measurement. The CI (gray) has a current source (green arrow) that provides electrical stimulation (green pulse) via one of the electrode contacts in the cochlea (blue). Due to electrical stimulation, there arises an eCAP (black signal in the graph) which can be measured using the telemetry function of the CI, including a neural amplifier (represented by the triangle) and an artifact rejection method. CI indicates cochlear implant; eCAP, electrically evoked compound action potential, AR, artifact rejection.

Two different electrical signals play a role in recording eCAPs: the stimulus and the eCAP signal. The stimulus is typically a biphasic pulse with an amplitude of a few hundred microamperes. A biphasic pulse is charge-balanced, which means that the delivered net charge is zero in order to prevent tissue damage due to charge build-up. The stimulus creates a large electrical potential (factor 10,000 greater than the eCAP) which has a disruptive effect on the measurement amplifier and causes an artifact in the eCAP recording. An amplifier is necessary to increase the relatively small eCAP signal in order to make optimal use of the dynamic range of the analog-to-digital converter. However, the stimulus potential exceeds the input range of the amplifier, consequently causing saturation of the amplifier and blocking the signal from passing through. This blocking is temporary and lasts generally a bit longer than the stimulus duration (50-100 μs). After the stimulus artifact has ended, the magnitude of the potential will decrease exponentially and as soon as it is smaller than the input range of the amplifier the amplifier will provide a reliable output again.

1.2.2. Artifact rejection paradigm

The stimulus artifact thus has a disruptive effect on the eCAP recording. To minimize this effect, the recording contact is often chosen at some distance from the stimulating contact. However, a larger distance between the recording contact and the firing nerve fibers negatively affects the amplitude and the shape of the eCAP. In practice, a distance of one or two physical contacts between the stimulating and recording contacts is often chosen as optimum. Another difficulty is that the eCAP already occurs while the amplifier is still in the recovery phase (Figure 1.3). So, the eCAP is (partly) hidden in the stimulus artifact and these two signals must be separated in order to enable a proper eCAP assessment. Over years, several methods have been developed to separate the eCAP signal from the stimulus artifact (Miller et al. 2000; Klop et al. 2004; Hughes et al. 2016; Baudhuin et al. 2016), whereby forward masking (FM) and alternating polarity (AP) were most commonly used.

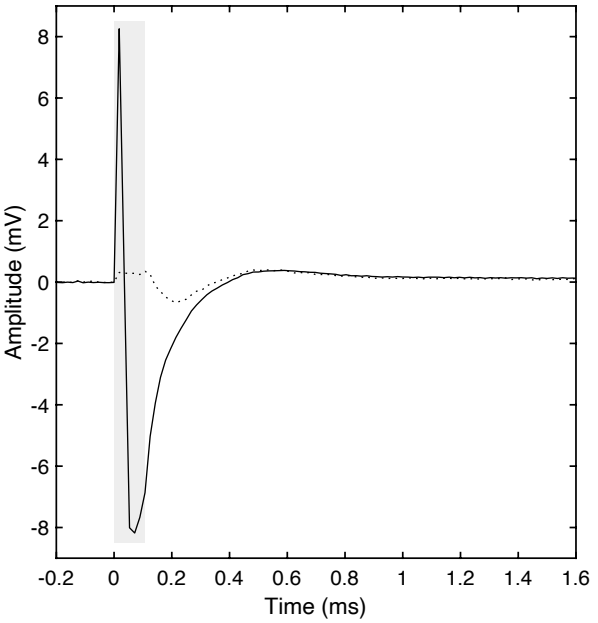

Figure 1.3. As long as the stimulus lasts (gray area) the neural amplifier delivers an unreliable output. The output signal (black line) looks like the stimulus potential, but valuable information about the eCAP is totally blanked. When the stimulus has ended, the stimulus potential decreases exponentially and meanwhile the eCAP (dotted line) occurs. This eCAP can be extracted from the recorded signal using an artifact rejection method. eCAP indicates electrically evoked compound action potential.

The FM paradigm makes use of the refractory properties of the auditory nerve to separate the eCAP from the stimulus artifact. The method used two different stimuli: a masker stimulus and a probe stimulus. Using a combination of these stimuli, four different recordings can be made, which can be subtracted from each other to extract the eCAP (Figure 1.4). First, the masker stimulus (M) is delivered, which results in a stimulus artifact of the masker including an eCAP signal. Then the masker and the probe (MP) are delivered with a masker-probe interval time of typically 300-500 µs. Due to the masker, the nerve fibers are in their absolute refractory state and are insensitive to the probe stimulus. This results in a recording that contains twice a stimulus artifact and one eCAP (after the masker only). When all nerve fibers are recovered from their refractory state, the probe (P) is delivered again resulting in a probe stimulus artifact including an eCAP. The eCAP can now be eliminated from these three recordings by calculating: eCAP = M + P - MP. Finally, a fourth measurement is often subtracted from the measurement signals, the so-called 'system signature'. In this recording, the stimulus levels are set to zero which leads to a recording that contains system properties such as interference and noise, for which can be corrected (Frijns et al. 2002).

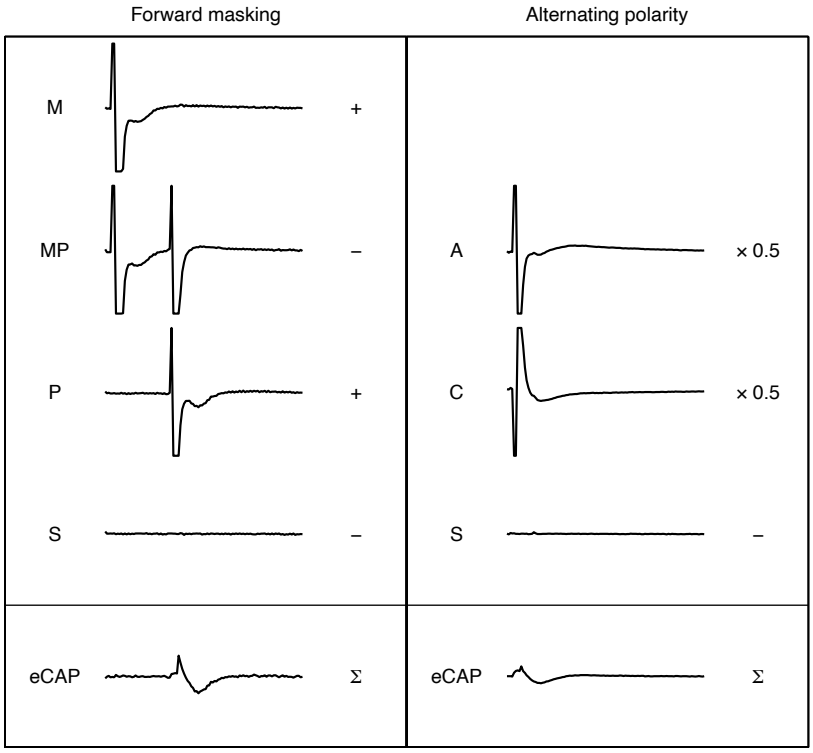

Figure 1.4. Graphical representation of two commonly used artifact rejection paradigms: forward masking (left column) and alternating polarity (right column). The forward masking paradigm consists of four different frames (M, MP, P and S) which can be combined mathematically to extract the eCAP from the stimulus artifact. The AP paradigm consists of three frames (A, C and S) which also can be combined to extract the eCAP. eCAP indicates electrically evoked compound action potential.

The AP paradigm makes use of the eCAP property that the polarity of the eCAP signal does not change when the stimulus polarity is reversed, while the stimulus artifact adopts the polarity of the stimulus. This property can be used to filter the eCAP from the measurement signal (Figure 1.4). For that purpose, two recordings were obtained. First a recording using a biphasic stimulus with a positive phase followed by a negative one (anodic-first, A), and second a recording using a negative phase followed by a positive one (cathodic-first, C). Both stimuli result in an eCAP with the same polarity, while the polarity of the stimulus artifact is opposite. Now the eCAP can be recovered by calculating: eCAP = (A + C) / 2. Lastly, the recording can be corrected for the system signature (S).

1.3. ReaSONS project

Although a rejection paradigm reveals a major part of the eCAP signal, we still do not know what the real shape of the eCAP is in the timespan that the amplifier is saturated and delivers an unreliable output. Considering all difficulties in recording eCAPs, we can conclude that

there is need for a method that enables measuring eCAPs without being bothered by the stimulus artifact. The Real-time Sensing Of Neural Signals project pursues this. The ReaSONS project is funded by the Technological Sciences Foundation under number 11693. The project consists of two parts: (1) developing a new neural amplifier for reliable and accurate eCAP measurements and (2) investigating the clinical applicability and relevance of eCAP measurements. These two components have been elaborated by respectively a PhD student at Technical University Delft and a PhD student at the Leiden University Medical Center. A brief description of the development of the neural amplifier is given below, while the research focusing on the human eCAP measurements will be the content of this thesis.

The new neural amplifier developed at the Technical University Delft uses a compression technique to prevent amplifier saturation. As soon as the recorded signal grows beyond the input dynamic range of the amplifier, the input signal will be corrected (shifted downward) so that it does not exceed the dynamic range of the amplifier. This technique is also called companding. By precise registration of all corrections, the original signal can be reconstructed later, after conversion of the signal to the digital domain by an analog to digital converter. Doing this, the new amplifier has a dynamic range of 126 dB, so that both the stimulus artifact (up to 20V) and the neural response (up to 10μV) can be registered reliably (Bes et al. 2010). After signal reconstruction and artifact rejection, there remains an eCAP signal that has been measured reliably throughout the whole recording time. In addition, the new amplifier is relatively small compared to the electronic components in current CIs. This means that in the future multiple amplifiers will fit into the CI housing, and eCAPs can be measured simultaneously on several electrode contacts. So, the application of the new measuring amplifier seems promising for future research in the field of eCAPs.

1.4. Content of this thesis

This thesis focuses on the clinical applicability and the relevance of eCAP measurements. The goal is to gain more insight into CI functioning and into the effect of electrical stimulation on the auditory nerve. More knowledge about these topics may be useful to further improve CI technology, potentially leading to better CI listening experience.

The first study of this thesis is about the applicability of eCAPs as an objective measure to guide CI fittings. For some CI users, e.g., small children, it can be difficult to find the best CI fitting, because they do not provide adequate feedback to adjustments made by the audiologist. Therefore, it would be valuable if there is an objective tool that helps the audiologist to guide these fittings. With the improvement of the CI telemetry functions, it has been suggested that eCAP measurements may ease this fitting challenge (Brown et

al. 2000). In the last decades, several studies concluded that the eCAP threshold, which is the minimum amount of current required to generate an eCAP, would be a good predictor of the T-level at the same electrode contact (Botros & Psarros 2010; Kaplan-Neeman et al. 2004; Lai et al. 2009; Mittal & Panwar 2009; Morita et al. 2003; Muhaimeed et al. 2010; Pedley et al. 2007; Walkowiak et al. 2011) while others were less conclusive (Franck 2002; Smoorenburg et al. 2002; Potts et al. 2007; Holstad et al. 2009; Jeon et al. 2010; Raghunandhan et al. 2014). Inspired by the contradictory outcomes in the literature, we perform a systematic literature review to clearly state how much evidence there is that eCAPs can be used in fitting CIs **(Chapter 2)**. Another question we have regarding eCAP thresholds is: Why is there often no relationship between the eCAP thresholds and the subjective hearing thresholds of the CI user, while most researchers and clinicians expect this relationship? We may be missing important details of the eCAP because these details are not registered by the current measurement systems. On the other hand, it is also possible that the outcome measures (eCAP thresholds and subjective thresholds) are not precise and accurate enough, as there is a lack of reporting measurement errors in the literature. To further investigate this, we looked at the precision of the eCAP thresholds **(Chapter 3)**.

Besides eCAP thresholds, it is also possible to derive the spread of neural excitation (SOE) from eCAP recordings. SOE is a measure linked to the specificity of the electric-neural interface, and can be estimated objectively from spatial forward masking (SFM) curves (Cohen et al. 2003; Abbas et al. 1999; Hughes & Abbas 2006b; van der Beek et al. 2012). With knowledge about SOE, stimulation strategies can be improved, e.g., by making them more selective and having more control about the induced pitch. The expectation is that selective stimulation is better for the audibility of different sounds and therefore for speech understanding. However, to date, no clear relationships between eCAP-based SOE and speech performance outcomes have been found. In the context of this thesis, we will critically look at the measure of SOE used thus far, that is, the width of the SFM curve. We think that the width of the SFM curve is not an adequate measure of SOE, and we propose a new method to objectively determine the excitation patterns and SOE of individual electrode contacts in CI **(Chapter 4)**. Using that method, we can also study the effect of stimulus level on excitation patterns in more detail **(Chapter 5)**.

The final study of this thesis focuses on a new method for testing pitch discrimination in CI users. Several studies have investigated whether there is a relationship between the eCAP and psychophysical measures such as spatial resolution (Firszt et al. 2007; Koch et al. 2007; Snel-Bongers et al. 2012). In these studies, the pitch discrimination of CI users was often

measured very accurately, but due to time limitations it was collected on a limited number of electrode contacts only. We would like to have a method that tests pitch discrimination on all electrode contacts in a relatively short test time. This knowledge can be used to further improve stimulation strategies and it can be used in studying SOE across the whole electrode array. We develop a new method for testing channel discrimination across all contacts of the electrode array, and we evaluate how well the channel discrimination ability from CI recipients correlate with their speech perception **(Chapter 6)**.

Finally, the thesis ends with a general discussion, wherein we discuss some complexities in recording eCAPs and elaborate on the future perspectives of the eCAP measures **(Chapter 7)**.

CHAPTER

2

Use of electrically evoked compound action potentials for cochlear implant fitting: a systematic review

Johan J. de Vos*, Jan Dirk Biesheuvel*, Jeroen J. Briaire, Pieter S. Boot, Margriet J. van Gendt, Olaf M. Dekkers, Marta Fiocco, Johan H. M. Frijns

* These authors contributed equally to this study

Ear and Hearing, 2018, 39(3):401-411

Objective: The electrically evoked compound action potential (eCAP) is widely used in the clinic as an objective measure to assess cochlear implant functionality. During the past decade, there has been increasing interest in applying eCAPs for fitting of cochlear implants. Several studies have shown that eCAP-based fitting can potentially replace time-consuming behavioral fitting procedures, especially in young children. However, a closer look to all available literature revealed that there is no clear consensus on the validity of this fitting procedure. This study evaluated the validity of eCAP-based fitting of cochlear implant recipients based on a systematic review of the recent literature.

Design: The Preferred Reporting Items for Systematic Reviews and Meta-Analyses (PRISMA) were used to search the PubMed, Web of Science, and Cochrane Library databases. The term 'eCAP' was combined with 'cochlear implants', 'thresholds', and 'levels', in addition to a range of related terms. Finally, 32 studies met the inclusion criteria. These studies were evaluated on the risk of bias and, when possible, compared by meta-analysis.

Results: Almost all assessed studies suffered from some form of risk of bias. Twenty-nine of the studies based their conclusion on a group correlation instead of individual subject correlations (analytical bias); 14 studies were unclear about randomization or blinding (outcome assessment bias); 9 studies provided no clear description of the populations used, for example, prelingually or postlingually implanted subjects (selection bias); and 4 studies had a high rate of loss (>10%) for patients or electrodes (attrition bias). Meta-analysis of these studies revealed a weak pooled correlation between eCAP thresholds and both behavioral T- and C-levels ($r = 0.58$ and $r = 0.61$, respectively).

Conclusions: This review shows that the majority of the assessed studies suffered from substantial shortcomings in study design and statistical analysis. Meta-analysis showed that there is only weak evidence to support the use of eCAP data for cochlear implant fitting purposes; eCAP thresholds are an equally weak predictor for both T- and C-levels. Based on this review, it can be concluded that research on eCAP-based fitting needs a profound reflection on study design and analysis in order to draw well-grounded conclusions about the validity of eCAP-based fitting of cochlear implant recipients.

Abstract

2.1. Introduction

A cochlear implant (CI) is a device that can partially restore hearing in patients who are profoundly deaf or severely hard of hearing. To successfully restore speech perception, the settings of the CI must be optimized for the individual patient, called fitting. When fitting a CI, the behavioral threshold (T) and maximum comfortable hearing levels (C-level/M-level/MCL, terminology varies depending on manufacturer) for each electrode contact of the electrode array are set. In this review, these levels will be denoted as T- and C-levels, respectively. Because of intracochlear changes (e.g., intracochlear fibrosis) and patient adaptation to the implant, the T- and C-levels are prone to change during the first few months after implantation (Hughes et al. 2001), or gradually throughout the life cycle of an implant (Smoorenburg et al. 2002). Therefore, it is necessary to fit the CI periodically. CI fitting is often a time-consuming process, which preferably is conducted by an experienced audiologist. Vaerenberg et al. (2014) showed that the applied fitting method differs between CI-centers and even between audiologists; there is no golden standard for fitting CIs. The actual fitting profile is a product of both the audiologist and the CI patient, whereby the patient must respond to presented stimuli. However, not all CI recipients can respond adequately, especially young children, elderly (e.g., due to cognitive decline) and mentally challenged patients. Consequently, the fit may be suboptimal, resulting in possibly limited speech recognition or a delay in language development in children (Caner et al. 2007).

Since the advent of modern CIs with telemetry function, clinical research has focused on the use of the electrically evoked compound action potential (eCAP) for fitting as an additive or alternative to behavioral fitting (Brown et al. 2000). The eCAP represents the neural response of spiral ganglion cells lining the inner part of the cochlea (Rosenthal's channel) and can be measured in response to electrical stimulation by the telemetry function of a CI. Although all CIs measure the same electrophysiological response, each CI manufacturer has its own measurement method and terminology to depict the measurement of these neural responses: Neural Response Telemetry (NRT) by Cochlear (Sydney, Australia), Neural Response Imaging (NRI) by Advanced Bionics (Valencia, CA), and Auditory Response Telemetry (ART) by MED-EL (Innsbruck, Austria). As all terms denote the same principle, the general term eCAP will be used throughout the paper for this type of measurement. To enable the use of eCAP in clinical practice, CI manufacturers embedded eCAP measurement features in the fitting software. Especially the latest generation fitting software, for example, Custom Sound (Cochlear), Soundwave (Advanced Bionics), and Maestro (MED-EL), have made the use of objective data to obtain direct baseline fitting maps easily accessible. In parallel with this development, objective

fitting of CIs has become of more interest; the feasibility of this approach has been studied extensively in the last decades, however, with contradictory results.

The aim of this systematic review was to assess whether eCAPs can be used for CI fitting purposes. Relevant literature was analyzed using the Preferred Reporting Items for Systematic Reviews and Meta-Analyses (PRISMA) method (Rosenfeld 2010). The studies were assessed on both study design and statistical methodology. Our analyses revealed that the quality of the various studies differs largely and that some conclusions are based on incorrect analysis methods. It is of main importance that the conclusion of most papers about objective fitting is not representative for the individual subjects. In the literature we reviewed, the correlation between eCAP and behavioral thresholds was mostly analyzed using grouped data, while the correlation within individuals is essential to investigate eCAP-based fitting; the group correlation can be qualitatively different from the within-subject association. To clarify, due to the inter-subject variability, individual correlations disappear when the individual threshold values are combined in a grouped data set. This phenomenon, which is better known as Simpsons' Paradox (Julious & Mullee 1994), could lead to an analytical bias. This review will show that the prevention of this bias is of great importance in the research of eCAP thresholds.

2.2. Methods

2.2.1. Literature selection

To ensure that the review included all relevant literature, the initial search included terms encompassing all suitable objective neural response measurements (eCAP, electrically evoked stapedius reflex threshold, and electrically evoked auditory brainstem response). These terms were combined with 'cochlear implants', 'thresholds', and 'levels', and extended with a range of related terms to include all relevant literature. We searched for papers published from 1995 to June 22, 2015. The search strategy (see Supplemental content 2.1) was developed in cooperation with a trained librarian at Leiden University Medical Centre. The PubMed, Web of Science, and Cochrane Library databases were searched at June 22 and 26, 2015. From these papers, all studies concerning eCAPs were manually selected for final analysis using the PRISMA guidelines to minimize publication bias and improve reproducibility.

Consecutively, all papers were screened based on title and abstract to determine whether they met the inclusion criteria: English, Dutch, or German language; measurements conducted in humans; comparison of eCAP and T/C-levels; and the use of Pearson's correlation coefficient for the analysis. We screened on the most commonly used Pearson's

correlation coefficient, because a uniform correlation coefficient was required for proper meta-analysis. Furthermore, the inclusion criteria were applied regardless of study quality, because the quality of the study was assessed in a later stage of the review. Papers from the same author were checked for an overlap of study participants. When two papers used identical populations and similar measurement techniques, the papers were treated as one study. When one of the papers was written based on preliminary data and the follow-up study data were available in the second paper, only the final data were used.

2.2.2. Risk of bias assessment

The study quality was assessed using a risk of bias (ROB) assessment. All included papers were assessed on four types of bias relevant in their field of research: attrition bias, selection bias, outcome assessment bias and analytical bias (Table 2.1).

Table 2.1. Overview of the test conditions to score the different risks of bias.

Design characteristic	Test condition
Attrition bias	Is the loss to follow-up higher than 10%?
Selection bias	Are eligible patients not representative for the population intended to be analyzed?
Outcome assessment bias	Are the researchers not blinded or comparing linked measurements?
Analytical bias	Are the data not analyzed appropriately for answering the research question?

2.2.2.1 Attrition bias

This describes the loss of study participants during follow-up. The ROB was considered high for studies with >10% loss to follow-up (Dumville et al. 2006). We encountered some studies that excluded poor eCAP responders, while other studies considered them as attrition. To be consistent, poor eCAP responders were treated as excluded subjects in this review and not scored as attrition.

2.2.2.2. Selection bias

This is the selection of data in such a way that it is not representative of the population intended to be analyzed. To prevent selection bias, the subjects should be selected on predefined selection criteria in accordance with the research question. Moreover, the subject must be selected randomly. For example, CI recipients are a heterogenic group consisting of prelingually and postlingually deaf subjects with large variation in age of implantation and duration of hearing loss. Depending on these factors, language development and overall performance can differ during fitting (Petersen et al. 2013). When eligible patients were randomly selected from the intended population the risk of selection bias was low.

2.2.2.3. Outcome assessment bias

This is an error made by comparing two measurements which are not independent, or are linked to each other. The following cases were scored as being at risk for outcome assessment bias: (1) when eCAP threshold profiles were adjusted to T- or C-levels using behavioral information, for example, as applied by Willeboer & Smoorenburg (2006); and (2) when the objective and behavioral measurements are performed by the same person, whereby the knowledge of objective performance can severely influence the results of behavioral measurements.

2.2.2.4. Analytical bias

This is an error introduced when data are not analyzed appropriately for answering the research question. For example, when answering the question whether eCAP thresholds could be used to predict fitting levels, correlation analysis of eCAP threshold with T- and C-levels (hereafter denoted as T-eCAP and C-eCAP, respectively) should be performed at the level of individual subjects and not for the population as a whole.

2.2.3. Meta-analysis

A meta-analysis was performed on the studies that provided Pearson's correlation coefficient for T-eCAP or C-eCAP analysis. The analysis was performed in the R software environment (Free Software Foundation's GNU General Public License, version 2.18). The T-eCAP and C-eCAP correlations of each study were pooled in order to estimate their overall correlation and associated confidence interval (c.i.). For studies showing the correlation coefficients of individual patients (Franck & Norton 2001; Franck 2002; Potts et al. 2007; Holstad et al. 2009), the mean of the individual correlations for T-eCAP and C-eCAP was used as study-specific correlation. The study-specific correlations were transformed by using Fisher's *r*-to-*z* transformation (Hedges & Olkin 1985) and, subsequently, a weighted pooled correlation of these transformed scores has been computed (Borenstein 2009). For both T-eCAP and C-eCAP, a fixed and random effects model was estimated. The fixed model assumes that the variation between study results is due to chance alone. The random model also takes into account between study differences, for example, sample size. Additionally, an overall measure of heterogeneity between studies was reported, whereby the I^2 shows the percentage of variance attributable to study heterogeneity and τ^2 is an estimate of the between-study variance in the random effects model (DerSimonian & Laird 1986). A sensitivity analysis was performed to investigate the robustness of the meta-analysis by looking how the results are affected by different types of studies. The tested groups were: studies based on group correlations (n = 11), studies based on individual correlations (n = 3), studies with adequate blinding (n = 10), studies with adults only (n = 6), and studies with children only (n = 2).

2.3. Results

2.3.1. Overview of selected literature

Figure 2.1 shows the flow diagram of our PRISMA analysis. The search strategy provided 1972 papers, 1515 after removing duplicates. A total of 160 papers met our inclusion criteria as defined in the methods section. Assessing the papers for eligibility provided 68 items, 37 of which used eCAP as objective measure (others were electrically evoked stapedius reflex threshold and electrically evoked auditory brainstem response). These 37 papers were finally included in the review (see Table 2.2 for references). Papers from the same author were checked for an overlap of study participants. Ten papers were combined into five studies: Franck & Norton (2001) with Franck (2002); Thai-Van et al. (2001) with Thai-Van et al. (2004); Akin et al. (2006) with Akin et al. (2008); Lorens et al. (2004) with Walkowiak et al. (2011); Gordon et al. (2004a) with Gordon et al. (2004b). This reduced the total of number of unique studies to 32.

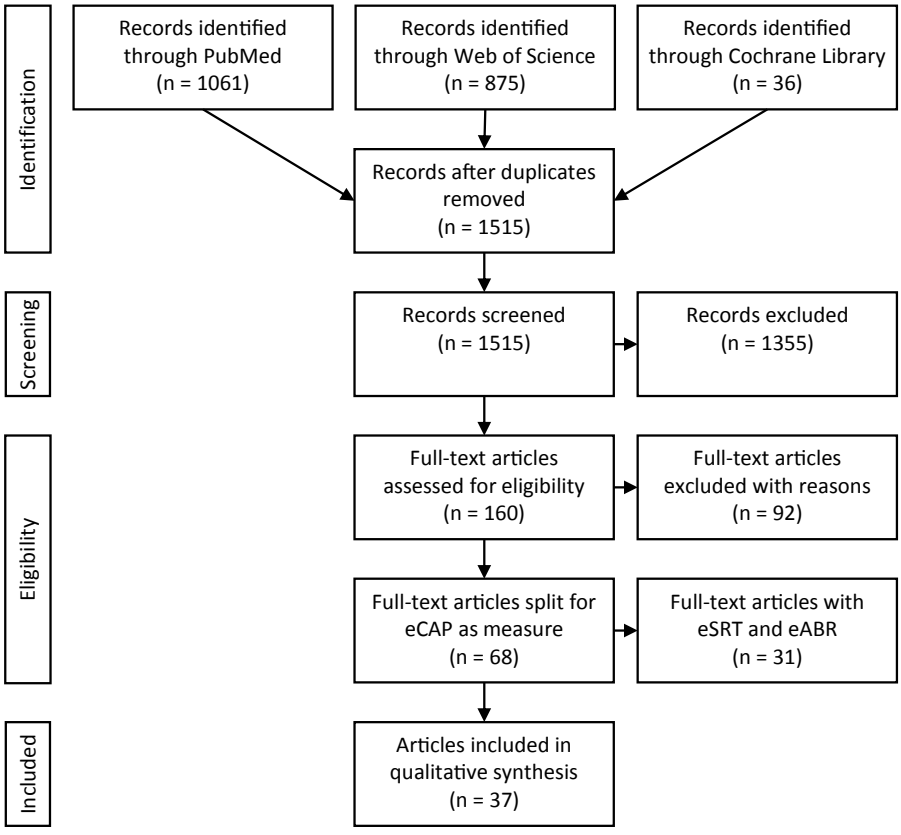

Figure 2.1. PRISMA flow diagram. Adapted from: PLOS Med, 6:e1000097. eCAP indicates electrically evoked compound action potential; eSRT, electrically evoked stapedius reflex threshold; eABR, electrically evoked auditory brainstem response, PRISMA, preferred reporting items for systematic reviews and meta-analyses.

In addition, Supplemental content 2.2 provides an overview of the judgment on eCAP based fitting, study design and used cochlear implants of each study. One study used Ineraid implants (Brown et al. 1996), while all other studies use modern cochlear implants from Cochlear (22 studies), Advanced Bionics (7 studies) and MED-EL (2 studies). Further, most studies have compared eCAP threshold profiles with both T- and C-levels (23 studies), whereas a few studies made the comparison for either T-levels (1 study) or C-levels (8 studies). A total of 11 studies provided a group correlation coefficient for T-eCAP usable for meta-analysis (Figure 2.2, studies without asterisk) and 12 studies for C-ECAP (Figure 2.3, studies without asterisk). In addition, 3 studies provided individual correlations for both T-eCAP and C-eCAP (Franck & Norton 2001; Franck 2002; Potts et al. 2007; Holstad et al. 2009).

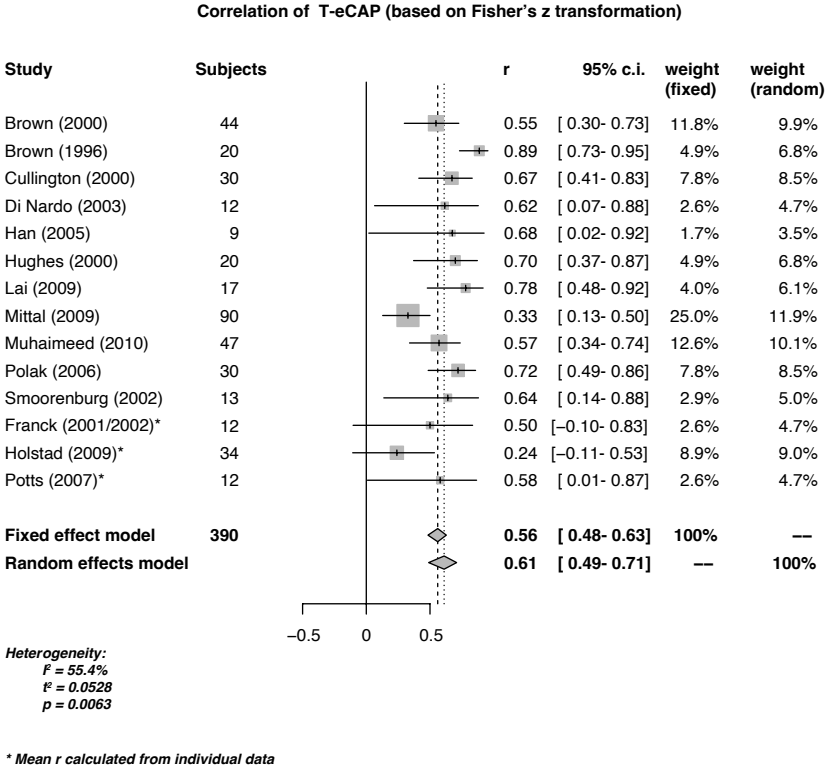

Figure 2.2. Forest plot showing the meta-analysis of T-eCAP. The first and second column shows the included studies and number of subjects, respectively. In the middle, a graphical representation of the study results is depicted, whereby the gray square indicates the group size, the vertical line Pearson's r and the horizontal line the 95% confidence interval of r. The values of r, 95% confidence interval, weight in the fixed model, and weight in the random model can be found in the last columns, respectively. The dark dotted line is the pooled correlation found for the fixed model, and the lighter dotted line is the pooled correlation found for the random model. eCAP indicates electrically evoked compound action potential; c.i., confidence interval.

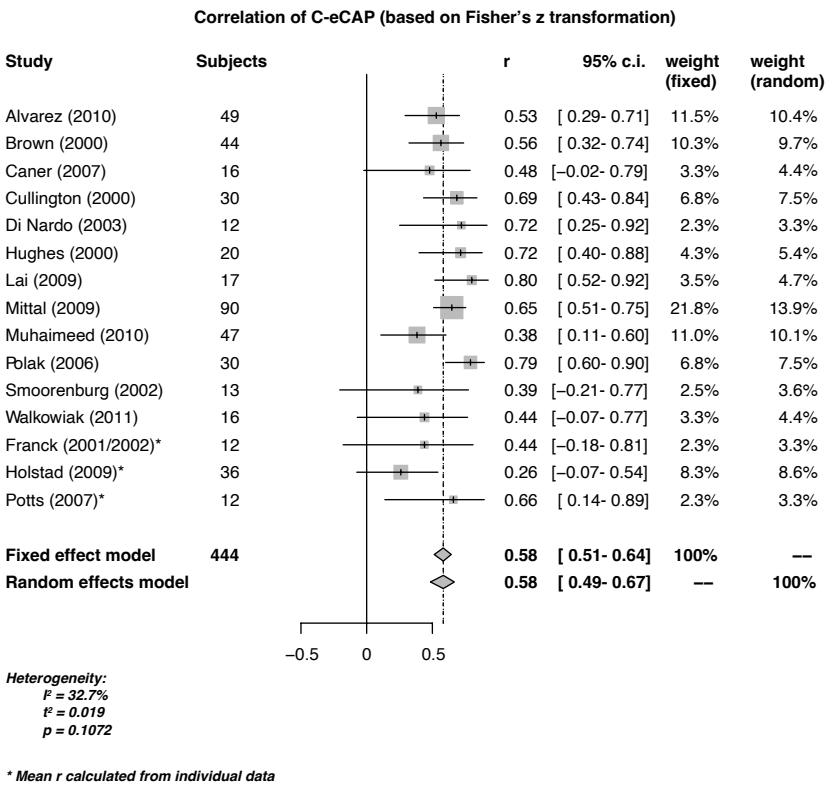

Figure 2.3. Forest plot showing the meta-analysis of C-eCAP. The results were presented similarly as in Figure 2.2. eCAP indicates electrically evoked compound action potential; c.i., confidence interval.

2.3.2. ROB assessment

Table 2.2 shows the ROB scores from the assessment of all 32 studies on attrition bias, selection bias, outcome assessment bias and analytical bias. A black dot indicates a positive score (bias present), a white dot a negative score (bias absent), and a question mark indicates that the paper did not provide enough information to score that bias. To summarize Table 2.2, only four studies had more than 10% attrition (Akin et al. 2006, 2008; Franck & Norton 2001; Franck 2002; Han et al. 2005; Holstad et al. 2009). However, note that most studies screened for available eCAPs before or during their research, because CI subjects without measurable eCAP are unusable. There was no clear evidence for studies suffering from selection bias, however, nine studies did not provide sufficient information about the selection procedure or the randomization (Brown et al. 1996, 2000; Akin et al. 2006; Caner et al. 2007; Pedley et al. 2007; Botros & Psarros 2010; Jeon et al. 2010; Wesarg et al. 2010; Raghunandhan et al. 2014). These studies have an increased risk for selection bias and were scored with a question mark. Concerning outcome selection bias, three provided an inadequate description of the measuring procedure (Kiss et al. 2003; Gordon et al. 2004a,b; Lai et al. 2009). Seven studies used fitting software with embedded eCAP measurement feature, (Soundwave by

Advanced Bionics or Custom Sound by Cochlear), while the use of this feature has not been reported explicitly. These studies have an increased risk of outcome selection bias and are also marked with a question mark (Han et al. 2005; Akin et al. 2006, 2008; Caner et al. 2007; Wolfe & Kasulis 2008; Jeon et al. 2010; Muhaimeed et al. 2010; Raghunandhan et al. 2014).

Table 2.2. Rating of the risk of bias analysis per study. A filled circle indicates a positive score, that is, the bias is present, while an open circle indicates the study did not suffer for that type of bias. When there was uncertainty about the risk of bias in a study by lack of data in the methods section, this was scored with a question mark.

			Bias			
	Study	**Year**	**Attrition**	**Selection**	**Outcome assessment**	**Analytical**
	Potts	2007	○	○	○	○
	Franck	2001/2002	●	○	○	○
	Holstad	2009	●	○	○	○
	Alvarez	2010	○	○	○	●
	Cullington	2000	○	○	○	●
	Di Nardo	2003	○	○	○	●
	Hughes	2000	○	○	○	●
	Kaplan-Neeman	2004	○	○	○	●
	King	2006	○	○	○	●
	Mittal	2009	○	○	○	●
	Morita	2003	○	○	○	●
	Polak	2006	○	○	○	●
	Thai-Van	2001/2004	○	○	○	●
	Van den Abbeele	2012	○	○	○	●
	Lorens/Walkowiak	2004/2011	○	○	○	●
	Brown	1996	○	?	○	●
	Gordon	2004a/2004b	○	○	?	●
	Kiss	2003	○	○	?	●
	Lai	2009	○	○	?	●
	Muhaimeed	2010	○	○	?[c]	●
	Wesarg*	2010	○	?	○	●
	Pedley	2007	○	?	○	●
	Wolfe	2008	○	○	?[s]	●
	Cafarelli Dees	2005	○	○	●	●
	Smoorenburg	2002	○	○	●	●
	Caner	2007	○	?	?[s]	●
	Jeon	2010	○	?	?[s]	●
	Brown	2000	○	?	●	●
	Botros	2010	○	?	●	●
	Raghunandhan	2014	○	?	?[s]	●
	Han	2005	●	○	?[s]	●
	Akin	2006/2008	●	?	?[s]	●
Total	32	37	4	9?	4/10?	29

? At risk; not enough information available
● Positive score (bias present)
○ Negative score (bias absent)
s Use of Soundwave software (Advanced Bionics)
c Use of Custom Sound software (Cochlear)
* Use of three populations

Four studies suffered from inadequate blinding; they adjusted eCAP threshold profiles to match T- and C-levels (Brown et al. 2000; Smoorenburg et al. 2002; Cafarelli Dees et al. 2005; Botros & Psarros 2010). Wesarg et al. (2010) used 3 groups of subjects, with the third group making use of subjective fitting based on eCAP thresholds. Only three studies were not suffering from the analytical bias, providing individual T-eCAP and C-eCAP correlation coefficients (Franck & Norton 2001; Franck 2002; Potts et al. 2007; Holstad et al. 2009). In addition to Table 2.2, a more comprehensive overview for study analysis and assessment of different subject populations can be found in Supplemental content 2.3 and 2.4, respectively.

2.3.4. Meta-analysis

Meta-analyses for T-eCAP and C-eCAP are shown in Figure 2.2 and Figure 2.3, respectively. The figures show study name, population size (subjects), correlation coefficient (*r*) and 95% c.i. for each study. Additionally, the study's weight in the meta-analysis is shown in the last two columns, separately for the fixed and random effects model. Results based on both fixed and random effects model are shown. Because the studies are heterogeneous, results based on the random effects model are more appropriate. A total of 390 subjects from 14 studies were analyzed for T-eCAP (Figure 2.2). Pearson's correlation coefficients varied from $r = 0.24$ (Holstad et al. 2009) to $r = 0.89$ (Brown et al. 2000). The weighted pooled correlation for T-eCAP was weak ($r = 0.56$, c.i. 0.48 to 0.63). The pooled correlation in the random effects model was similar ($r = 0.61$, 95% c.i. 0.49 to 0.71). The percentage of variance in study results attributable to heterogeneity (I^2) was 55.4%. For the C-eCAP (Figure 2.3), a total of 444 subjects from 15 studies were analyzed. The correlation coefficients varied between $r = 0.26$ (Holstad et al. 2009) and $r = 0.80$ (Lai et al. 2009). The pooled correlations in the fixed and random effects models were identical ($r = 0.58$), though the c.i. was slightly broader for the random effects model. The I^2 for C-eCAP was 32.7%. Note that the correlation for Franck (2002), Holstad et al. (2009) and Potts et al. (2007) was calculated based on individual correlations.

Figure 2.4 shows the results of the sensitivity analysis for the meta-analysis of both T-eCAP and C-eCAP. From left to right the outcomes of the meta-analyses are shown based on all studies, studies reporting group correlations, studies reporting individual correlations, studies with adequate blinding, studies with adults only, and studies with children only. The correlation coefficient was slightly lower for the 'individual correlations' group (T-eCAP: $r = 0.36$ and C-eCAP: $r = 0.38$) and the 'Children' group (T-eCAP: $r = 0.42$ and C-eCAP: $r = 0.35$). Notably, the T-eCAP correlation in children had an uninformatively large 95% c.i. due to the small sample size. The pooled average of groups with an adequate

number of studies ('group correlations', 'blinded' and 'adults') showed no significant difference when comparing T-eCAP and C-eCAP (whiskers representing the 95% c.i. do overlap).

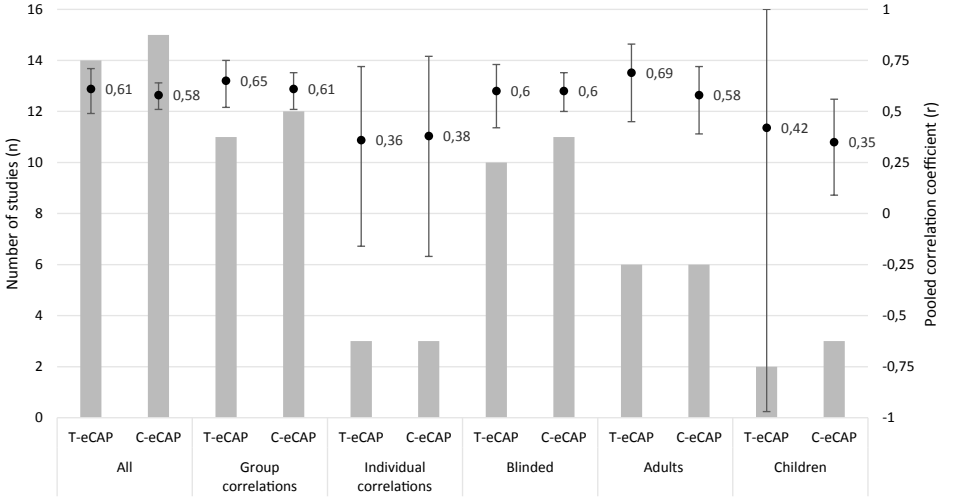

Figure 2.4. Sensitivity analysis graph showing in gray bars the number of studies included (left ordinate) and in black dots the pooled correlation coefficient (right ordinate) for each analyzed group. The whiskers indicate the 95% confidence intervals of the pooled correlation coefficient. From left to right the outcomes of the meta-analyses are shown for: all studies, studies based on group correlations, studies based on individual correlations, studies with adequate blinding, studies with adults only, and studies with children only. eCAP indicates electrically evoked compound action potential.

2.3.5. Individual correlation data

To investigate the use of eCAP for fitting individual subjects, comparison of eCAP and behavioral thresholds within individuals is highly preferable. However, only three studies reported individual T-eCAP and C-eCAP correlations (Franck & Norton 2001; Franck 2002; Potts et al. 2007; Holstad et al. 2009). In Figure 2.5 a histogram is plotted which shows the distribution of the individual correlation coefficients, separately for T-eCAP (top) and C-eCAP (bottom). The correlation coefficients were spread across a wide range. Franck (2002) reported both the T-eCAP and C-eCAP data for 12 subjects, ranging from r = -0.36 to r = 0.97 for T-eCAP and from r = -0.29 to r = 0.86 for C-eCAP. The T-eCAP and C-eCAP data from Potts et al. (2007) (n = 15) revealed individual T-eCAP correlations ranging from r = 0.07 to r = 0.88 and C-eCAP correlations ranged from r = 0.23 to r = 0.95. Holstad et al. (2009) reported the largest group of individual correlation data (n = 36 subjects) for both T-eCAP and C-eCAP. For T-eCAP, correlations varied from r = -0.67 to r = 0.97, while for C-eCAP, the correlations varied from r = -0.63 to r = 0.97.

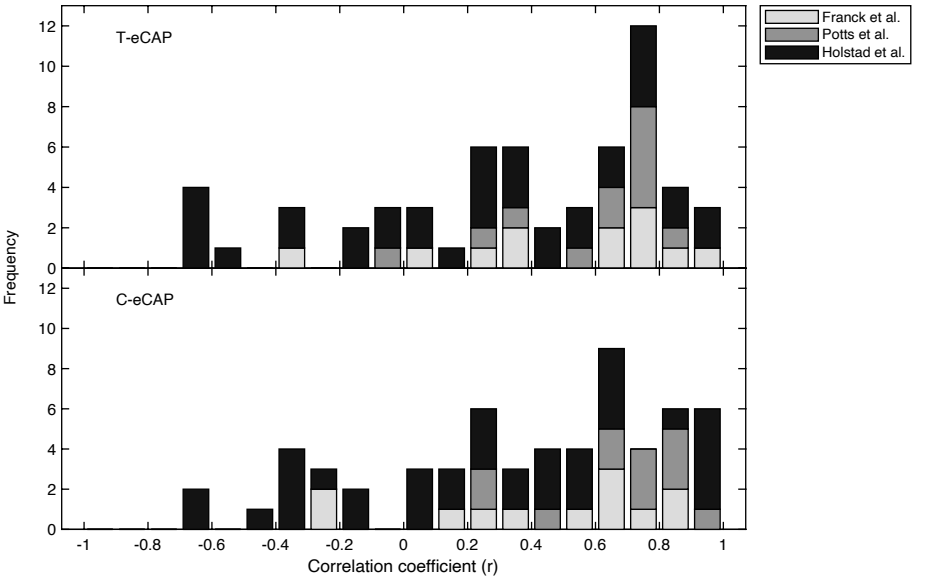

Figure 2.5. Histogram of T-eCAP (top) and C-eCAP (bottom) correlation coefficients (x-axis) from individual subjects as reported by Franck et al. (2001/2002), Potts et al. (2007) and Holstad et al. (2009). Correlation coefficients were grouped in bins with a width of 0.1. Black indicates individuals from the study of Holstad et al., dark gray from the study of Potts et al. and light gray from the study of Franck et al. eCAP indicates electrically evoked compound action potential.

2.4. Discussion

This systematic review evaluated 37 papers describing 32 unique studies for their evidence of eCAP-based fitting of CIs. The studies were reviewed using the PRISMA method and a ROB assessment. The ROB assessment was chosen because the overall study quality did not enable the common screening for level of evidence. The ROB assessment scored overall study quality on attrition bias, selection bias, outcome assessment bias and analytical bias.

2.4.1. ROB assessment

2.4.1.1. Attrition bias

Attrition more than 10% was found in only four studies (Akin et al. 2006, 2008; Franck & Norton 2001; Franck 2002; Han et al. 2005; Holstad et al. 2009). However, there was no clear consensus on reporting CI users with poor eCAPs; some studies exclude poor responders prior to the study, whereas others count these subjects as lost in follow-up. Since the exclusion of subjects with poor or no measurable eCAPs will not necessarily influence the results, it would be valid to exclude these poor eCAP responders. Therefore, we did not count poor responders as attrition in the ROB assessment. On the other hand, it is important to report the amount of poor eCAP responders, because it provides insight

in the success rate and applicability of objective fitting for CI recipients. The exclusion of poor eCAP responders can therefore also be seen as a selection bias.

2.4.1.2. Selection bias

We found that the studied populations differed considerably between studies. Some studies used a heterogenic group of CI recipients, whereas other studies used specific subpopulations, for example, prelinguals, postlinguals, children or adults (see Supplemental content 2.3). Therefore, the selection bias was scored with respect to the intended population. As long as the subjects were selected randomly from within the intended subpopulation and there was a proper representation of the population intended for the conclusion, we scored studies positive for randomization. When the randomization was not described clearly, the study was scored by a question mark indicating that there is an increased risk on selection bias (Table 2.2).

A more hidden form of selection bias is the overrepresentation of one manufacturer (Cochlear) both in literature and the reviewed studies: 24 Cochlear, 7 Advanced Bionics, 1 Ineraid, and 2 MED-EL (see Supplemental content 2.2). Brand-related differences in hardware (e.g., noise floor) and software (e.g., eCAP detection method, linear versus logarithmic current scale) might lead to differences in eCAP thresholds and fitting levels. Consequently, the correlation between these two measures could be (slightly) different for each manufacturer. Therefore, a more balanced representation of all manufacturers is desirable to get a more general answer on the question whether eCAP could be used for objective fitting.

2.4.1.3. Outcome assessment bias

The use of objective measures to set the behavioral fitting parameters was scored as a lack of blinding. Such data cannot be used to investigate the predictive value of eCAP thresholds for fitting levels, because the behavioral data are not independent from objective measurements. The risk for this specific form of bias is especially high in more recent studies, as modern fitting software (Soundwave, ART, and AutoNRT) enables the user to easily adjust the behavioral map by using the objectively measured eCAP data. Unfortunately, it was not feasible to determine the exact influence of this fitting software. To avoid underreporting outcome assessment bias, we scored studies that used modern fitting software while the use of the eCAP feature has not been reported explicitly as 'unknown' for blinding.

Of special interest was the use of behavioral data to adjust the objective threshold profile. Brown et al. (2000) introduced a method to shift the eCAP threshold profile toward hearing level using the behavioral threshold at one electrode contact. The shift does not influence the correlation between the objective and behavioral thresholds as long as it is performed within subjects. For this reason, applying the shift in combination with a within subject correlation, for example as Frank & Norton (2001), was not scored as outcome assessment bias. For group correlation, the shift could increase the correlation dramatically (Franck & Norton 2001). However, group correlation does not provide reliable results for individual patients (see section 2.4.1.4. Analytical bias). Therefore, shifting eCAP threshold prior to a group correlation received a positive score for outcome assessment bias, for example as Brown et al. (2000). In addition to the shift, Smoorenburg et al. (2002) introduced a tilt to further improve the fit between the objective and behavioral profiles, better known as the 'shift and tilt' method. However, the 'shift and tilt' approach provides eCAP threshold profiles which are no longer fully independent from the behavioral profiles. Therefore, the use of the 'shift and tilt' approach was scored as an outcome assessment bias, for example, as in Smoorenburg et al. (2002) and Cafarelli Dees et al. (2005). In the study of Botros & Psarros (2010), shifted eCAP threshold profiles were additionally scaled. This scaling resulted in flatter profiles at higher stimulation level, because the scaling factor was inversely related to the stimulus level. Though less obvious, the eCAP-based profiles were not independent of the behavioral profiles, thus, these studies were scored positive for outcome assessment bias.

2.4.1.4. Analytical bias

Besides properly collected data, a correct (statistical) analysis is also a prerequisite for reliable results and valid conclusions. Therefore, all studies were scored on analytical bias. Van der Beek et al. (2015) showed a great inter-subject variability in both eCAP thresholds and behavioral T/C-levels. The correlation analysis between eCAP thresholds and behavioral fitting levels should therefore ideally be based on subject level. However, only three studies showed the correlation within individual subjects (Franck & Norton 2001; Franck 2002; Potts et al. 2007; Holstad et al. 2009). The correlation coefficients reported in these studies (plotted in a histogram in Figure 2.5) show great variation per individual subjects. Based on their results, Holstad et al. (2009) suggested that the individual variation was too large for reliable objective fitting of children without the use of subjective data. Potts et al. (2007) mentioned that when behavioral measures cannot be obtained consistently, eCAP thresholds can provide valuable information about the level associated with an auditory response on each electrode. However, eCAP thresholds should be used conservatively to create an initial speech processor map. In contrast

to these three studies, all other studies did not take into account the within-subject correlation; they based their conclusion on a grouped correlation only. The problem of a group correlation is that the correlation is driven by the (large) inter-subject variation and can be qualitatively different form the within-subject association. Being not aware of this effect, which is also called the Simpsons' Paradox (Julious & Mullee 1994), will result in a high risk for incorrect conclusions. Given the contradictory outcomes and conclusions of several studies (see Supplemental content 2.2), the suspicion arises that not all studies are calculating the correlations in a proper way. This notion is supported by the fact that studies using grouped correlations were positive about the role of eCAP data in fitting procedures (Morita et al. 2003; Kaplan-Neeman et al. 2004; Pedley et al. 2007; Lai et al. 2009; Mittal & Panwar 2009; Botros & Psarros 2010; Muhaimeed et al. 2010; Walkowiak et al. 2011), whilst Holstad et al. (2009) and Potts et al. (2007), who base their analysis on individual correlations, are dismissive.

2.4.2. Meta-analysis

A meta-analysis on the included studies that reported a Pearson's correlation coefficient revealed that the use of eCAP thresholds is a weak predictor of both T- and C-levels. We found a pooled correlation of $r = 0.61$ for T-eCAP and C-eCAP had a slightly lower pooled correlation of $r = 0.58$. Note that two types of correlation coefficients are included in the analysis: grouped correlations and means of individual correlations (studies with asterisk). Whereas the majority of the reviewed studies reported a group correlation, the individual correlations were included as well, because they provide useful information (see section 2.4.1.4. Analytical bias). The sensitivity analysis showed that including both types of correlation coefficients did not change the results of the meta-analysis significantly (Figure 2.4). Franck & Norton (2001) provided both grouped and individual correlations. Comparing both types of correlation coefficients revealed that the group correlation between eCAP thresholds (visual) and T-levels (80 Hz) was stronger than the mean individual correlation ($r = 0.77$ versus $r = 0.50$, respectively). However, similar comparison for C-eCAP revealed the opposite: a group correlation of $r = 0.03$ and a mean individual correlation of $r = 0.44$. This example clearly demonstrates that: (1) individual correlations can be totally different than a grouped correlation on the same data (Simpson's paradox), and (2) the choice of analysis method has major consequences for the results and conclusion.

The majority of the studies included in the T-eCAP and C-eCAP meta-analysis used Cochlear devices. From the 15 studies, only 2 studies used implants of Advanced Bionics (Han et al. 2005; Caner et al. 2007) and 2 studies of MED-EL (Alvarez et al. 2010; Walkowiak et al. 2011). Due to the low number of Advanced Bionics and MED-EL studies, we could not

statistically test the effect of manufacturer on the pooled correlation coefficients. However, based on the distribution of the correlation coefficients of the Cochlear studies, we might conclude that the results of the meta-analysis are representative for Cochlear. Further, the sensitivity analysis did not show any significant difference when a meta-analysis performed on all studies was compared with the meta-analysis performed by selectively incorporating studies with adequate blinding, studies with children only, and studies with adults only (Figure 2.4). This indicates that the meta-analysis was robust for all subpopulations.

2.4.3. Towards eCAP based fitting

This review revealed several issues with respect to study design and statistical analysis, as well as contradictory outcomes between different studies (see Supplemental content 2.2) and a large variation in individual correlations (Figure 2.5). Hence, we must conclude that there is currently no evidence for the validity of eCAP based fitting of CIs. To be able to answer the question whether eCAP thresholds can predict fitting levels, at least the biases reported in this study must be avoided. In other words, the subjects must be selected randomly and the exclusion of poor eCAP responders should be reported, because this affects the success rate of eCAP based fitting. Further, the behavioral levels must be measured blinded from the eCAP measurements, and both the eCAP and behavioral measurements should be described in detail. Finally, the correlation between eCAP and behavioral levels must be investigated within individual subjects to draw valid conclusions for eCAP-based fitting of individuals.

In addition, we want to highlight the following considerations in eCAP threshold research:

2.4.3.1. Measurement data

Review of the applied fitting strategies showed that most of the studies did not elaborate in detail on the applied strategy. This challenges the systematic review of eCAP-based fitting, because it is unknown whether the different study results are based on comparable data. Three studies reported that the T-levels were set as 10% of the C-level (default in the SoundWave fitting software of Advanced Bionics), but these levels were not used in a correlation analysis (Caner et al. 2007; Akin et al. 2008; Raghunandhan et al. 2014). One study reported that the C-level was typically set a predefined number of programming units above T-level, because they are dealing with children (Hughes et al. 2000). All other studies reported that the behavioral levels were measured, fitted by an audiologist, or they only mentioned that the fitting levels were collected. When reviewing the fitting strategies, we found many differences due to manufacturer, used software, measurement properties, audiologist experience and CI-center. A few studies used comparable fitting

strategies, for example, the default fitting method recommended by the manufacturer, or a fitting method based on the Hughson-Westlake approach (Thai-Van et al. 2004; Pedley et al. 2007; Jeon et al. 2010).

It is likely that the encountered methodological differences affect the actual fitting levels and thus the correlation. However, it was not possible to include the applied methods in the ROB- and meta-analysis; they could not be classified and the number of available studies was too low for statistical analysis. Additionally, one might wonder whether current CI devices and fitting software do a better job than previous versions thereby improving the correlation. However, the Figures 2.2 and 2.3 do not support this; more recent studies did not show a better correlation between eCAP and behavioral measures. For example, Figure 2.2 shows that the highest correlation coefficients originate from the oldest study (Brown et al. 1996).

2.4.3.2. Stimulation rate

Another factor possibly affecting the correlation is the applied stimulation rate. Behavioral fitting levels are routinely measured at high-rate pulse trains (250 to 3500 Hz) (Arora et al. 2012), while eCAP-based telemetry is performed at much lower rates (35 to 80 Hz). Brown et al. (1998) and Franck & Norton (2001) found that the correlation between behavioral and eCAP thresholds is best at equal stimulation rate for behavioral and eCAP stimulation. Based on these findings, we can conclude that, if the eCAP would be used to predict fitting levels, the pulse rate for eCAP measurements ideally should be close to the (high) rate used for behavioral measurements. However, Charasse et al. (2004) showed that increasing the stimulus frequency for the measurement of eCAP responses saves time during measurements but has a degrading effect on the quality and amplitude of the eCAP response. Further, McKay et al. (2013) investigated whether high rate behavioral thresholds can be predicted by eCAP thresholds combined with rate-dependent eCAP characteristics (e.g., loudness growth and temporal integration). However, they still conclude that it is unlikely that the lower rate eCAP thresholds can be combined with the high-rate behavioral fitting levels.

2.4.3.3. Measurement error

When comparing measurements, the measurement error should be considered in order to correctly interpret the differences. However, we encountered no study that included a measurement error for the eCAP and behavioral measurements. eCAP thresholds and fitting levels were handled as fixed data points, even though they have an uncertainty depending on the measurement properties and conditions. Therefore, the precision of the

measurements probably differs between studies and affects the presented correlations. Potentially, including the measurement error will lead to better measurements and could enhance the usability of eCAPs in clinical practice.

2.4.3.4. Speech perception

Several papers were encountered that used speech perception as outcome measure for eCAP-based fitting rather than the behavioral fitting levels (Frijns et al. 2002; Sun et al. 2004; Guedes et al. 2007; Cosetti et al. 2010; D'Elia et al. 2012; Zhang et al. 2013; Bournique et al. 2014; Scheperle & Abbas 2015). Seyle & Brown (2002) even used different types of eCAP based fitting maps to investigate objective fitting with speech perception as outcome measure. These studies propose that speech perception, though it is subjective, is more directly related to the quality of hearing in CI recipients than the fitting levels. Consequently, speech performance potentially is a better outcome measure for assessing eCAP-based fitting than behavioral T/C-levels (Seyle & Brown 2002; Guedes et al. 2007; Zhang et al. 2013). Although it is an interesting topic, it is beyond the scope of this paper to review the objective fitting based on speech perception, for example, whether and, if so, which speech perception test is best suited for this purpose.

2.5. Conclusions

This systematic review shows that many of the included studies dealt with methodological shortcomings in randomization, blinding, population etiology and statistical analysis. Considering statistical analysis, studies building their conclusions on group analysis, thereby negating within subject variation, have a high risk on analytical bias whereby the conclusion is not representative for individual subjects. We conclude that most of the reviewed studies are not optimal to answer the research question whether the eCAP could be used to predict fitting levels of individual CI recipients. Additionally, the three studies which applied appropriate statistical analyses do not support the use of eCAP threshold data only for CI fitting purposes. In future studies, we recommend emphasizing correct blinding, a well-defined study design and the use of appropriate statistical analyses. Finally, we point out to multiple studies which suggest speech perception as potentially better outcome measure for assessing eCAP-based fitting, rather than comparing objective eCAP thresholds to behavioral fitting levels.

Supplemental

Supplemental Table 2.1. Literature search

Database	Search strategy	Date and time	No. hits
PubMed	("Cochlear Implants"[Mesh] OR "Cochlear Implantation"[Mesh] OR "cochlear implants"[all fields] OR "cochlear implant"[all fields] OR "cochlear implantation"[all fields] OR "Cochlear Prosthesis Implantation"[all fields] OR "Cochlear Prosthesis Implantations"[all fields]) AND ("electric stimulation"[All Fields] OR "electrical stimulation"[All Fields] OR "electric stimulation"[MeSH] OR "electrically evoked compound action potential"[all fields] OR "ECAP"[all fields] OR "EAP"[all fields] OR "evoked potentials"[All Fields] OR "evoked potential"[All Fields] OR "evoked potentials"[MeSH] OR "evoked potentials, auditory"[MeSH] OR "Cochlear Microphonic Potentials"[Mesh] OR "neural response telemetry"[all fields] OR "neural response imaging"[all fields] OR "NRT"[all fields] OR "NRI"[all fields] OR "eSRT"[All Fields] OR "SRT"[all fields] OR "Stapedius reflex"[all fields] OR "Auditory Nerve Response Telemetry"[all fields] OR "ART"[all fields] OR "electrically evoked auditory brainstem response"[All Fields] OR "eABR"[All Fields] OR "ABR"[All Fields] OR "eBAER"[All Fields] OR "eBERA"[all fields] OR "BAER"[All Fields] OR "BERA"[all fields]) AND ("thresholds"[all fields] OR "threshold"[all fields] OR "level"[all fields] OR "levels"[all fields]) AND ("1995/01/01"[PDAT] : "3000/12/31"[PDAT])	22 June 2015 10:00	1061 results
Web of Science	TS=("Cochlear Implants" OR "Cochlear Implantation" OR "cochlear implant" OR "Cochlear Prosthesis Implantation" OR "Cochlear Prosthesis Implantations") AND TS=("electric stimulation" OR "electrical stimulation" OR "electrically evoked compound action potential" OR "ECAP" OR "EAP" OR "evoked potentials" OR "evoked potential" OR "Cochlear Microphonic Potentials" OR "neural response telemetry" OR "neural response imaging" OR "NRT" OR "NRI" OR "eSRT" OR "SRT" OR "Stapedius reflex" OR "Auditory Nerve Response Telemetry" OR "ART" OR "electrically evoked auditory brainstem response" OR "eABR" OR "ABR" OR "eBAER" OR "eBERA" OR "BAER" OR "BERA") AND TS=("thresholds" OR "threshold" OR "level" OR "levels")	26 June 2015 11:00	875 results (418 after deduplication with PubMed search)
Cochrane Library	(cochlear implant* OR Cochlear Prosthesis Implantation*) AND ("electric stimulation" OR "electrical stimulation" OR "electrically evoked compound action potential" OR "ECAP" OR "EAP" OR "evoked potential*" OR "Cochlear Microphonic Potentials" OR "neural response telemetry" OR "neural response imaging" OR "NRT" OR "NRI" OR "eSRT" OR "SRT" OR "Stapedius reflex" OR "electrically evoked auditory brainstem response" OR "eABR" OR "ABR" OR "eBAER" OR "eBERA" OR "BAER" OR "BERA") AND ("threshold*" OR "level*")	26 June 2015 11:00	36 results

Supplemental Table 2.2. Study overview

	Study			Judgement on eCAP based fitting					Study type		Control		Manufacturer			
	Author	n (papers)	Year	Negative (1)	Dismissive (2)	Neutral (3)	Optimistic (4)	Positive (5)	Prospective	Retrospective	T-level	C-level	Cochlear	Advanced Bionics	MED-EL	Other
	Akin	2	2006/2008	○	○	○	●	○	●	○	○	●	○	●	○	○
	Alvarez	1	2010	○	○	○	●	○	●	○	●	●	○	○	●	○
	Botros	1	2010	○	○	○	○	●	●	○	●	●	●	○	○	○
	Brown	1	2000	○	○	○	●	○	●	○	●	●	●	○	○	○
	Brown	1	1996	○	○	○	●	○	●	○	●	●	○	○	○	●
	Caner	1	2007	○	○	○	●	○	●	○	○	●	○	●	○	○
	Cullington	1	2000	○	○	●	○	○	●	○	●	●	●	○	○	○
	Cafarelli Dees	1	2005	○	○	○	●	○	●	○	●	●	●	○	○	○
	Di Nardo	1	2003	○	○	●	○	○	●	○	●	●	●	○	○	○
	Franck	2	2001/2002	○	●*	○	○	●*	●	●	●	●	●	○	○	○
	Gordon	2	2004/2004	○	○	○	●	○	●	○	●	●	●	○	○	○
	Han	1	2005	○	○	○	●	○	●	○	○	●	○	●	○	○
	Holstad	1	2009	●	○	○	○	○	●	○	●	●	●	○	○	○
	Hughes	1	2000	○	●	○	○	○	●	○	●	●	●	○	○	○
	Jeon	1	2010	○	●	○	○	○	●	○	●	●	○	●	○	○
	Kaplan-Neeman	1	2004	○	○	○	○	●	●	○	●	●	●	○	○	○
	King	1	2006	○	○	○	●	○	●	○	○	●	●	○	○	○
	Kiss	1	2003	○	○	○	●	○	●	○	●	○	●	○	○	○
	Lai	1	2009	○	○	○	○	●	●	○	●	●	●	○	○	○
	Mittal	1	2009	○	○	○	○	●	●	○	●	●	●	○	○	○
	Morita	1	2003	○	○	○	○	●	●	○	●	●	●	○	○	○
	Muhaimeed	1	2010	○	○	○	○	●	●	○	●	●	●	○	○	○
	Pedley	1	2007	○	○	○	○	●	●	○	●	●	●	○	○	○
	Polak	1	2006	○	○	○	●	○	●	○	●	●	●	○	○	○
	Potts	1	2007	○	●	○	○	○	●	○	●	●	●	○	○	○
	Raghunandhan	1	2014	○	●	○	○	○	●	○	○	●	○	●	○	○
	Smoorenburg	1	2002	●	○	○	○	○	●	○	●	●	●	○	○	○
	Thai-Van	2	2001/2004	○	●*	○	●*	○	●	○	●	●	●	○	○	○
	Van den Abbeele	1	2012	○	○	○	●	○	●	○	○	●	○	●	○	○
	Lorens/Walkowiak	2	2004/2011	○	○	○	○	●	●	○	○	●	○	○	●	○
	Wesarg	1	2010	○	○	●	○	○	●	○	●	●	●	○	○	○
	Wolfe	1	2008	○	○	●	○	○	●	○	○	●	○	●	○	○
Total	32	37		2	6	4	13	9	32	1	24	31	22	7	2	1

● Positive score.
○ Negative score.
* Studies consist of multiple papers, resulting in multiple judgments.

Supplemental Table 2.3. Study analysis

	Study		Quality			Population					Methods		Loss		
	Author	Year	Blinding	Individual correlation	Random selection	n (subjects)	Children	Adults	Prelingual	Postlingual	Confounders	Non-verbal T C levels	Attrition bias <10% loss	n	%
	Akin	2006/2008	?[s]	○	?	19	●	●	●	●	○	○	●	10	53
	Alvarez	2010	●	○	●	49	●	●	●	●	○	●	○		
	Botros	2010	●	○	?	13	○	●	?	?	○	○	○		
	Brown	2000	●	○	?	44	○	●	○	●	○	○	○		
	Brown	1996	●	○	?	20	○	●	○	●	○	○	○		
	Caner	2007	?[s]	○	?	16	●	○	●	○	○	●	○	1	7
	Cullington	2000	●	○	●	30	●	●	?	?	○	●	○		
	Cafarelli Dees	2005	●	○	●	74	●	●	○	●	○	○	○		
	Di Nardo	2003	●	○	●	12	●	●	●	●	○	○	○		
	Franck	2001/2002	●	○	●	15	○	●	○	●	○	○	●	3	20
	Gordon	2004a/2004b	?	○	●	68	●	○	?	?	○	●	○	5	7
	Han	2005	?[s]	○	●	9	●	●	?	?	○	○	●	1	11
	Holstad	2009	●	●	●	41	●	○	●	○	○	○	●	5	12
	Hughes*	2000	●	○	●	20	○	●	?	?	○	●	○		
	Jeon	2010	?[s]	●	?	12	○	●	○	●	○	○	○		
	Kaplan-Neeman	2004	●	○	●	10	●	○	●	○	○	●	○		
	King	2006	●	○	●	21	○	●	?	?	○	○	○	1	4
	Kiss	2003	?	○	●	27	●	●	?	?	○	○	○		
	Lai	2009	?	○	●	17	○	●	○	●	○	○	○		
	Mittal	2009	●	○	●	90	●	●	?	?	○	○	○		
	Morita	2003	●	○	●	12	●	●	●	●	○	○	○		
	Muhaimeed	2010	?[s]	○	●	47	●	○	●	○	○	●	○		
	Pedley	2007	●	○	?	8	○	●	○	●	○	○	○		
	Polak	2006	●	○	●	30	○	●	●	●	○	○	○	1	3
	Potts	2007	●	●	●	12	○	●	○	●	○	○	○		
	Raghunandhan	2014	?[s]	○	?	10	●	○	●	○	○	●	○		
	Smoorenburg	2002	●	○	●	13	○	●	○	●	○	○	○		
	Thai-Van	2001/2004	●	○	●	49	●	○	?	?	○	●	○		
	Van den Abbeele	2012	●	○	●	73	●	●	?	?	○	○	○		
	Lorens/Walkowiak	2004/2011	●	○	●	16	○	●	○	●	○	○	○		
			●			29									
	Wesarg**	2010	●	○	?	22	○	●	○	●	○	○	○		
			○			20									
	Wolfe	2008	?[s]	○	●	19	?	?	●	●	○	○	○	1	5
Total	32	37	19/10?	3	23/9?		17/1?	24/1?	11/10?	17/10?	0	9	4		

s Use of Soundwave software (Advanced Bionics).
c Use of Custom Sound software (Cochlear).
? Unknown, not described in the paper.
* Hughes et al. use of 2 groups, unknown blinding for Cochlear subjects, adequate blinding for Advanced Bionics subjects.
** Wesarg et al. use of 3 groups.
● Positive score.
○ Negative score.

Supplemental Table 2.4. Study polulations.

	Study			Judgment					T/C		Manufacturer				Bias					
	Author	Year	Number of subjects	Negative (1)	Dismissive (2)	Neutral (3)	Optimistic (4)	Positive (5)	T-level	C-level	Cochlear	Advanced Bionics	MED-EL	Other	Outcome assessment bias	Analytical bias	Selection bias	Attrition bias (>10% loss)	n	%
Prelingual children	Caner	2007	16	○	○	○	●	○	○	●	○	●	○	○	?[s]	●	?	○	1	7
	Holstad	2009	41	●	○	○	○	○	●	●	●	○	○	○	○	○	○	●	5	12
	Kaplan-Neeman	2004	10	○	○	○	○	●	●	●	●	○	○	○	○	●	○	○		
	Muhaimeed	2010	47	○	○	○	○	●	●	●	●	○	○	○	?[c]	●	○	○		
	Raghunandhan	2014	10	○	●	○	○	○	○	●	○	●	○	○	?[s]	●	?	○		
Total	5		124	1	1	0	1	2	3	5	3	2	0	0	3?	4	0	1		
Postlingual adults	Brown	2000	44	○	○	○	●	○	●	●	●	○	○	○	○	●	?	○		
	Brown	1996	20	○	○	○	●	○	●	●	○	○	○	●	○	●	?	○		
	Franck	2001/2002	15	○	●	○	○	○	●	●	●	○	○	○	○	○	○	●	3	20
	Jeon	2010	12	○	●	○	○	○	●	●	○	●	○	○	?[s]	○	?	○		
	Lai	2009	17	○	○	○	○	●	●	●	●	○	○	○	?	●	○	○		
	Pedley	2007	8	○	○	○	○	●	●	●	●	○	○	○	○	●	?	○		
	Potts	2007	12	○	●	○	○	○	●	●	●	○	○	○	○	○	○	○		
	Smoorenburg	2002	13	●	○	○	○	○	●	●	●	○	○	○	●	●	○	○		
	Lorens/Walkowiak	2004/2011	16	○	○	○	○	●	○	●	○	○	●	○	○	●	○	○		
	Wesarg**	2010	71	○	○	●	○	○	●	●	●	○	○	○	○	●	?	○		
Total	10		228	1	3	1	2	3	9	10	7	1	1	1	1/1?	7	5?	1		
Mixed	Akin	2006/2008	19	○	○	○	●	○	○	●	○	●	○	○	?[s]	●	?	●	10	53
	Alvarez	2010	49	○	○	○	●	○	●	●	○	○	●	○	○	●	○	○		
	Di Nardo	2003	12	○	○	●	○	○	●	●	●	○	○	○	○	●	○	○		
	Morita	2003	12	○	○	○	○	●	●	●	●	○	○	○	○	●	○	○		
Total	4		92	0	0	1	2	1	3	4	○	○	1	0	1?	4	1?	1		

s Use of Soundwave software (Advanced Bionics).
c Use of Custom Sound software (Cochlear).
? Unknown, not described in the paper.
● Positive score.
○ Negative score.
** Wesarg et al. use of 3 groups.

CHAPTER

3

The precision of eCAP thresholds derived from amplitude growth functions

Jan Dirk Biesheuvel, Jeroen J. Briaire, Johan H.M. Frijns

Ear and Hearing, 2018, 39(4):701-711

Abstract

Objective: An amplitude growth function (AGF) shows the amplitude of an electrically evoked compound action potential (eCAP) as a function of the stimulation current. AGFs can be used to derive the eCAP threshold, which represents the minimum amount of current needed to elicit a measurable eCAP. eCAP thresholds have been widely used clinically to, for example, assist with sound processor programming. However, no eCAP precision has been included to date. The aim of this study was to investigate the precision of eCAP thresholds and determine whether they are precise enough for clinical use.

Design: The study is retrospective and the data comprised 826 AGFs, intra-operatively measured in 111 patients implanted with a HiRes90K cochlear implant (Advanced Bionics). For each AGF, the eCAP threshold was determined using two commonly used methods: linear extrapolation (LE) toward the x-axis and detection of the last visible (LV) eCAP. Subsequently, the threshold confidence interval (TCI) of each eCAP threshold was calculated to serve as a metric for precision, whereby a larger TCI means a lower precision or reliability. Additionally, the eCAP thresholds results were compared with most recent behavioral fitting thresholds (T profile) to put the eCAP threshold analysis in clinical context. Thereby, the association between eCAP and behavioral thresholds was calculated, both for all subjects together (group analysis) and, in contrast to previous studies, within individual subjects.

Results: Our data show that the TCIs were larger with the LE method than with the LV method. The eCAP thresholds estimated by the LE method were systematically smaller than those estimated by the LV method, while the LE thresholds with the smallest TCIs correlated best with the LV thresholds. Correlation analysis between eCAP and behavioral thresholds revealed correlation coefficients of $r = 0.44$ and $r = 0.54$ for the group analysis of LE and LV thresholds, respectively. Within individual subjects, however, the correlation coefficients varied from approximately –1 to +1 for both LE and LV thresholds. Further analysis showed that across subjects the behavioral thresholds fell within the TCIs of the eCAP threshold profiles.

Conclusion: This study shows that eCAP thresholds have an uncertainty that can be estimated using TCIs. The size of the TCI depends on several factors, for example, the threshold estimation method and measurement conditions, but it is often larger than one would expect when just looking at the threshold values. Given these large TCIs, future research on eCAP thresholds should be accompanied by a measure of precision to correctly apply eCAP thresholds in clinical practice. Comparing our eCAP threshold results with T profiles indicates that the eCAP thresholds are possibly not precise enough to predict T profiles.

3.1. Introduction

The electrically evoked compound action potential (eCAP) of the auditory nerve can be measured using the telemetry function of a cochlear implant (CI). The eCAP is a synchronous response from multiple auditory nerve fibers evoked by electrical stimulation. An eCAP is typically recorded as a negative peak (N_1) followed by a positive peak or plateau (P_1). The amplitude of the response is measured from peak to peak and reaches values of several hundred microvolts (Abbas et al. 1999). Since the eCAP amplitude depends on the applied current, plotting the amplitude as function of stimulus level will result in an amplitude growth function (AGF) (Figure 3.1A). From this AGF, the eCAP threshold can be derived, representing the minimum amount of current needed to evoke a measurable neural response (Hughes 2013). These thresholds can be used to assist with sound processor programming predicting behavioral threshold levels (T profiles) and maximum comfort levels (C/M level). However, no clear correlations between eCAP thresholds and fitting levels have been found (Franck & Norton 2001; Franck 2002; Potts et al. 2007; Holstad et al. 2009). Possibly the mismatch between eCAP thresholds and T profiles can be explained by an error analysis of eCAP thresholds. Two commonly used terms in error analysis are 'accuracy' and 'precision'. Accuracy describes the difference between the estimated and the true value, whereas the precision describes the error around the estimated value. Since the eCAP threshold is a (best) estimate, we do not know the true value, and the accuracy can hardly be determined. Therefore, the focus of this study is on the precision of the eCAP thresholds as derived using standard (clinical) methodologies and the consequences for clinical practice.

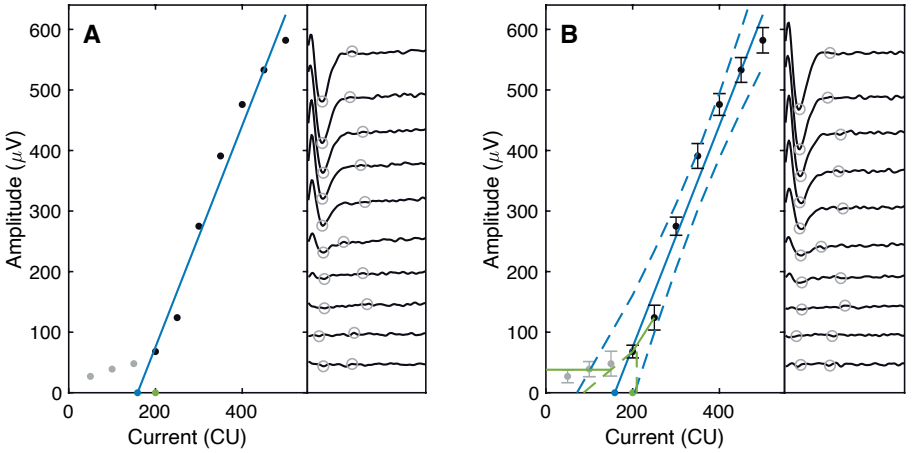

Figure 3.1. Example of an AGF shown as commonly used (A), and with additional information about the precision of eCAP and eCAP threshold (B). The AGF shows the eCAP amplitude as function of stimulus level, whereby corresponding eCAPs are shown at the right side, plotted from high (top) to low (bottom) stimulus level. Data points not representing true eCAPs are shown in gray and points reflecting eCAP responses (black) were used to estimate the eCAP thresholds for the LE (blue dot) and LV (green dot) methods. In B, error bars are added reflecting the variation in eCAP amplitude. The guides were used to estimate the precision of the LE (blue) and LV (green) thresholds, whereby the dashed lines represent the threshold confidence interval. AGF indicates amplitude growth function; eCAP, electrically evoked compound action potential; LE, linear extrapolation; LV, last visible.

Two methods are commonly used to estimate eCAP thresholds (Figure 3.1A). The simplest method is detection of the last visible (LV) eCAP. This method tracks all recordings of the AGF from high to low current while detecting whether the recording still contains an eCAP. The current level where the eCAP was last visible is defined as the eCAP threshold. The LV threshold (green dot) of the AGF shown in Figure 3.1A is 200 clinical units (CU). Because eCAP amplitudes below noise level cannot be detected, the LV threshold reflects the eCAP threshold at noise level. The second method is called linear extrapolation (LE). This method uses a linear regression line (Figure 3.1A, blue line) through data points representing a true neural response (black dots) to estimate the eCAP threshold at zero amplitude. The intercept of the line with the x-axis is defined as the eCAP threshold (blue dot at 159 CU). In general, eCAP thresholds are determined automatically using smart algorithms followed by visual inspection by an expert (clinician and audiologist). Visual inspection is necessary to verify whether the algorithm has not been misguided by, for example, (stimulus) artifacts or noise. Moreover, one should be aware of bias (e.g., systematically over- or underestimation of threshold) because of methodology or observer (Glassman & Hughes 2013; Akhoun et al. 2015).

Thus far, AGFs have been measured without any precision analysis; eCAP amplitudes have been used as data points without measurement error (Figure 3.1A). However, the eCAP amplitude has a measurement error that can easily be included, and it would be worthwhile to include also a measure of the precision of eCAP thresholds. For example, the measurement error of the eCAP amplitude can be derived from a measurement without stimulation or from a section of the recording in which no neural response is expected (e.g., the last samples of the recording). In Figure 3.1B, the measurement error is added to the eCAP amplitude, as shown by the error bars. The method of threshold estimation itself also has uncertainty. Unfortunately, standard clinical AGFs do not contain the required information to calculate the measurement error of the eCAP threshold itself. Alternatively, we defined the threshold confidence interval (TCI) as a metric of threshold precision. The blue and green lines in Figure 3.1B show how the precision of the LE and LV methods can be determined, and this is explained below in the methods section.

The aim of this study was to investigate the precision of the eCAP threshold and the consequences on clinical practice. The study was retrospective, and we made use of large data set of eCAP recordings, which were measured regularly during surgery. Further, the LV and LE methods were evaluated as commonly done in the literature and clinic. The LV threshold was identified by a human observer rather than using an automated computer algorithm. The LE method was based on a linear fit toward the zero-intercept,

though a nonlinear fit or the intercept just above noise level would be better. To put the eCAP threshold precision in clinical context, we additionally compared the eCAP threshold analyses to behavioral T profiles, and the association between both measures was calculated as well. To the best of our knowledge, this study is the first to perform this analysis for such a large population of CI recipients using an Advanced Bionics (AB) implant. In contrast to previous studies, the correlation analysis was not only performed for all subjects together (group analysis), but also performed within individual subjects. This makes present study one of the few studies examining the association between eCAP and behavioral thresholds within individual subjects (de Vos et al. 2017).

3.2. Methods

3.2.1. Patients and data

The AGFs used in this study originate from intraoperative eCAP measurements sequentially recorded in our hospital from January 2010 to December 2015. AGFs were available from 191 patients. All patients were implanted with a HiRes90K device (Advanced Bionics, Sylmar, CA), either with a 1J or Mid-Scala electrode array, both consisting of 16 electrode contacts (1 to 16 in an apical to basal order). The AGFs were collected as part of our standard clinical eCAP recordings using forward masking and the Research Studies Platform Objective Measures (RSPOM) software from AB. This allowed us to compare the AGF data with the other eCAP recordings, including spread of excitation (Biesheuvel et al. 2016) and refractoriness. The AGFs were measured on all odd electrode contacts using the following parameters: monopolar cathodic first biphasic pulses; pulse duration, 32 µs/phase; masker probe interval, 400 µs; sweep rate, 25 Hz; masker offset, 0%; sampling rate, 56 kHz; gain, 300; 32 averages; recording electrode two electrodes apical to stimulus (except electrode 1, where the recording electrode was two electrodes basal to the stimulus).

The eCAP analysis was performed automatically by RSPOM using the default settings. Raw eCAP recordings were filtered using a low-pass filter with a cut-off frequency of 8 kHz. Peak N_1 was detected as the minimum over the time period between 180 and 490 µs and peak P_1 as the maximum between 470 and 980 µs after the end of stimulation. The eCAP amplitude was calculated as the peak-to-peak voltage between P_1 and N_1. After the automatic analysis, all peak detections and data points were verified. If necessary, corrections were made manually. In addition, the signal-to-noise ratio (SNR) and measurement error of each eCAP were calculated using MATLAB (Mathworks, Inc., Natick, MA). The SNR of the eCAP was calculated as the eCAP amplitude divided by the noise amplitude, which in turn was defined as the maximal amplitude difference in the last 30 samples of the response.

We assumed that no possible remaining artifact or neural response would occur over this section. The measurement error of the eCAP was set to the noise amplitude.

The total batch of AGF measurements comprised AGFs measured with six and ten current steps. The functions with six current steps were measured when a full AGF with ten current steps could not be recorded because of time limitations during surgery. These six-point curves were measured in 56 patients and were, unfortunately, not reliable enough for the purpose of this study. Therefore, only the 10-point AGFs, measured in 135 patients, were analyzed. Each AGF was visually inspected for inclusion; an AGF was included when at least one clear eCAP response was available and the AGF was not disrupted, such as because of a stimulus artifact. Finally, a total of 826 AGFs originating from a heterogenic group of 111 patients were included for further analysis (Table 3.1).

Table 3.1. Patient demographics.

Number of patients	111
Gender (n)	
Male	45
Female	66
Implant type (n)	
HiRes90K 1J	16
HiRes90K Mid-Scala	95
Age (years)	
Children (< 12)	38
Adults	73
Mean ± SD	39 ± 30
Etiology (n)	
Medication	1
Meniere	0
Meningitis	5
Otosclerosis	3
Trauma	3
Usher	3
Rubella	3
Congenital/Hereditary	37
Enlarged vestibular aqueduct	1
Cytomegalovirus	4
Other/Unknown	51

To put the eCAP threshold analysis in clinical context, we additionally compared the eCAP threshold results with behavioral T profiles. Most recent fitting thresholds were extracted from the SoundWave fitting software, assuming that these T profiles were stable and most optimal. To ensure the reliability of the T profiles, we only included profiles measured in subjects with an age above 4 years, resulting in T profiles from 73 subjects. The threshold levels were measured either for each electrode contact separately or by using streamlined programming (Plant et al. 2005). For these measurements we used tone bursts of biphasic

pulse trains of 200 ms, as provided by the clinical speech program of the CI user. The measurement started at a subthreshold stimulus level, and the level was increased until the patient heard the sound. After a clearly audible percept was achieved, the stimulus level was decreased to reach a subthreshold level again. Subsequently, the stimulus level was raised to find the final threshold level. The behavioral T profiles were never set automatically using 10% of most comfortable level (optional in SoundWave).

3.2.2. eCAP thresholds and precision

The eCAP thresholds were calculated using a semi-automatic method programmed in MATLAB. The method automatically detects which recordings contain an eCAP using two conditions: the eCAP amplitude exceeds 20 μV and the SNR of the eCAP exceeds +13 dB Subsequently, all eCAPs and AGFs were visually inspected and, if necessary, corrections made manually.

The LE method was based on a linear least square fit through all data points containing a neural response. Data points at the top of the AGF which clearly deviate from linear amplitude growth were excluded from the fit, as common in clinical practice. At least three data points were required because confidence intervals cannot be determined if the number or observations is equal to the number of coefficients. The precision of the LE threshold was calculated using the 95% confidence interval of the linear fit (Figure 3.1B, blue dashed line); there is a 95% probability that the true best-fit line for the AGF lies within this confidence interval. The confidence interval was extrapolated toward the x-axis to estimate the interval at zero amplitude. For this purpose, the steepest and least steep linear fits within the confidence interval were calculated, and the intercepts of these lines with the x-axis were used to extrapolate the lower and upper boundaries of the confidence interval, respectively. Next, the distance between the two intercepts of the confidence interval with the x-axis was defined as the TCI. This TCI will be used as a measure of precision of the eCAP threshold estimated by the LE method.

For the LV method, the eCAP threshold was set to the current level where the smallest true eCAP could be detected. This threshold can be found by tracking all recordings of the AGF from high to low current. The lowest current whereby an eCAP could be detected was defined as the eCAP threshold. Estimating the precision of LV thresholds was less straightforward than with the LE method because the LV method does not have any mathematical clues. In our opinion, a good method was to use several guides as depicted in green in Figure 3.1B. The noise level (horizontal solid line) was estimated using data points not representing an eCAP (gray dots). Subsequently, a guide was drawn from the

data point representing the LV (abscissa: 200 CU, ordinate: 68 μV) through the calculated noise level (abscissa: eCAP threshold minus one current step = 150 CU, ordinate: 38 μV). This guide (dashed line) represents the precision of the eCAP threshold toward the left side. If the noise level is zero, the size of the confidence interval at the left side of the threshold will be equal to the step size in current; the true zero-amplitude threshold will be between the estimate threshold and lower current. A high noise level, which is close to the smallest detectable eCAP amplitude, will result in a large(r) left confidence interval. Thus, because of the high noise level, it is uncertain where the zero-amplitude threshold exactly is. In addition, there is a high chance that the detected amplitude is not an eCAP, but still noise. In principle, the zero-amplitude threshold is at a lower current than the LV threshold, and consequently, the confidence interval at the right side could be set to zero. However, it is important to also include the eCAP measurement error, especially in cases in which the noise level is close to the smallest detectable eCAP amplitude. Therefore, the amplitude variation (error bar) in the LV eCAP was translated into CU using a guideline between the LV and next eCAP (solid green line). Projecting the top of the error bar on this guide led to the precision at the right side of the threshold, expressed in CU (vertical dashed line). Finally, the total TCI of LV thresholds was calculated as the distance between the two dashed lines at zero-amplitude. Importantly, the TCIs are not the true errors of the eCAP thresholds, but a best estimate of their precision.

3.2.3. Analysis

When investigating the predictive value of eCAP thresholds for fitting behavioral levels, thresholds are frequently processed according to the method of Brown et al. (2000), matching the eCAP threshold profile with the T profile using the threshold data at one electrode contact. This method overcomes the offset difference between the objective and subjective profiles induced by the effect that a small stimulus may be audible though the eCAP is still too small to measure. This method was applied in our study as well. It is important to realize that the study of Brown included Nucleus patients, in which the currents are presented along a logarithmic scale, while the HiRes90K as used in the present study applies linear current units. From a mathematical point of view, a scaling factor was required to replicate the shift as described by Brown. In addition, the scaling was also required to take the pulse width into account when comparing behavioral thresholds (measured in microampere) to the objective thresholds (measured in CU). The profiles were matched on the electrode providing the least square error between the two profiles.

Exploration of the TCI values estimated with the LE and LV methods revealed non-normally distributed TCI values and unequal variances for both methods. Therefore, the difference

in TCI size between the two methods was investigated using Student's t-tests for unequal variances in combination with a logarithmic transformation of the TCI values. Assuming that within the LE and LV methods the TCIs are equally distributed across the electrode array, we applied a linear mixed model to test the effect of electrode contact on the TCI size for each method separately. The model included electrode as fixed effect and subject as random effect. Straightforward correlation analysis was used to compare the eCAP thresholds obtained by the LE and LV methods.

In addition, the association between eCAP thresholds for behavioral T profiles was examined using a linear regression model. Pearson's correlation coefficient was calculated within individual subjects and for all thresholds together (group analysis). Fisher's z-transformation was used to summarize the individual correlation coefficients and to enable further analyses on the correlation coefficients.

3.3. Results

Figure 3.2 shows four illustrative examples of AGFs to demonstrate the effect of AGF morphology on the eCAP threshold and TCI. In Figure 3.2A, the AGF measured at electrode 7 in patient S124 is shown. The AGF contains clear and large eCAPs, leading to a clear distinction of measurements containing an eCAP. Consequently, the TCI is small for both LE and LV methods, and the thresholds of both methods are close to each other. In Figure 3.2B, an AGF with much smaller eCAPs is shown. Because the eCAPs are closer to the noise level, it is more difficult to distinguish eCAPs from noise. Because of the lower SNR, the precision of eCAP amplitudes is less, resulting in a less reliable fit for the LE method and larger TCIs for both LE and LV methods. The examples in Figure 3.2A and C clearly show that an AGF is not necessarily linear; a shoulder near the noise level or a rollover at the top of the AGF was observed frequently. When data points at the top of the AGF clearly deviated from the linear amplitude growth, they were excluded from the linear fit (Figure 3.2C), considerably improving the precision of the eCAP threshold. The AGF in figure 3.2D illustrates the effect of using a weighted linear fit (red) instead of the default normal fit (blue). The weighted fit took into account the measurement error of the eCAP amplitude. Consequently, the fit best reflects the most precise data points. In this example, weighting the measurement errors in the fit did not markedly affect the eCAP threshold itself, but the TCI became smaller. Finally, all AGFs were classified on eCAP amplitude to indicate how many AGFs will be represented by the examples shown. It turned out that 11% of the AGFs have an amplitude larger than 900 μV (Figure 3.2A), 62% between 300 μV and 900 μV (Figure 3.2C), 23% between 150 μV and 300 μV (Figure 3.2D) and 5% smaller than 150 μV (Figure 3.2B).

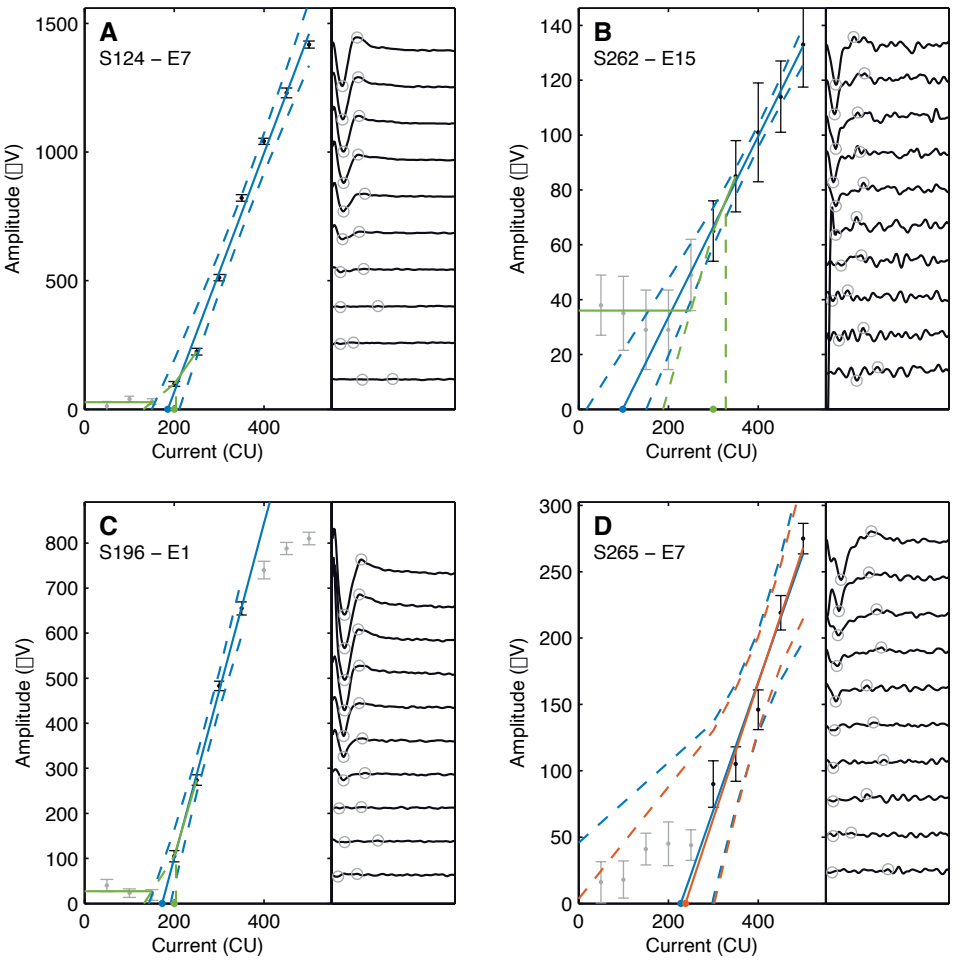

Figure 3.2. Four examples of AGFs, illustrating different curve morphologies and their consequences for eCAP threshold and precision. The AGFs were plotted in the same way as in Figure 3.1. In addition, the LE method based on a weighted linear fit was drawn in D (red), while the LV threshold was omitted for the sake of visibility. AGF indicates amplitude growth function; eCAP, electrically evoked compound action potential; LE, linear extrapolation; LV, last visible.

The boxplots in Figure 3.3 show the absolute TCIs grouped per electrode contact for the LE (Figure 3.3A) and LV (Figure 3.3B) methods. For each AGF, the absolute size of the confidence interval with respect to the corresponding eCAP threshold was calculated separately for the left and right side. The intervals of all subjects were grouped per electrode contact and they are shown in boxplots. For visibility, the limits of the current axis were set to –750 and 250 CU. Consequently, for the LE method 13 outliers fell outside the axes limits of the figure: 11 on the left side (< –750 CU) and 2 on the right side (> 250 CU). For the LV method, all data points were within the axes limits. Comparing the TCIs of both methods revealed that the TCIs of the LE method were significantly larger at the contacts 3-15 ($p < 0.005$ for

contact 5, $p < 0.001$ for all other contacts), while no difference in TCI size was found for the most apical contact 1 ($p = 0.28$). Further analysis of the effect of electrode contact on the TCI size revealed that for both the LE and LV methods, the TCI is significantly larger ($p < 0.001$) at the base than at the apex. Across the electrode array, larger eCAP amplitudes were observed at the apex than at the base.

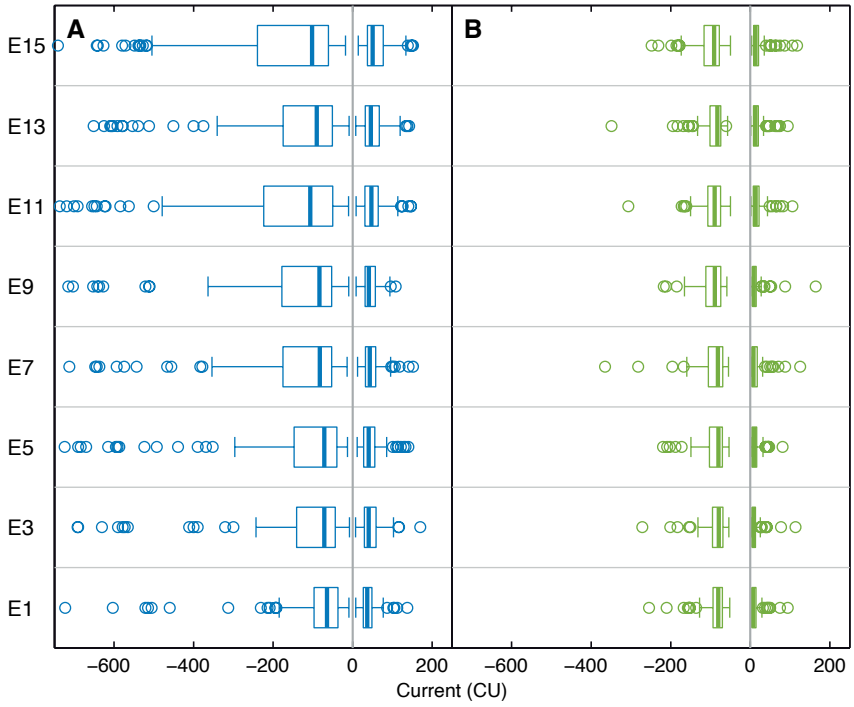

Figure 3.3. Illustration of the absolute TCI size (expressed in CU) across all subjects. The TCIs are grouped per electrode contact for the LE (A, blue) and LV (B, green) methods separately. Box boundaries represent the 25th and 75th percentiles, whiskers represent the most extreme data points not considered outliers, open circles represent outliers, and solid line within the box represent median. CU indicates clinical units; TCI, threshold confidence interval; LE, linear extrapolation; LV, last visible.

In Figure 3.4A, the absolute difference between the LE and LV thresholds was plotted as a function of TCI size for the LE method. The LE thresholds are divided into four groups, each containing 25% of the sorted TCIs. The figure shows that the LV thresholds are larger than the corresponding LE thresholds and that the difference between the LV and LE threshold tends to increase with increasing TCI for the LE method. In addition, for each category, the LE thresholds were plotted against the LV thresholds using the same colors (Figure 3.4B). Significant correlations were found between the LE and LV thresholds for all groups ($p < 0.001$). The group with the most reliable LE threshold correlated best with the LV thresholds ($r = 0.91$ versus $r = 0.71$ for the most extreme pairs).

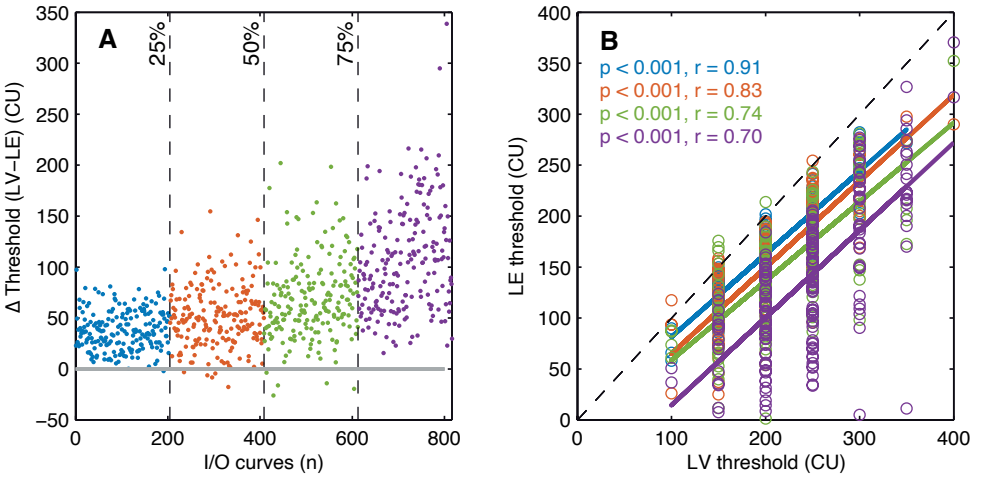

Figure 3.4. Difference between thresholds estimated using the LE and LV methods. The LE thresholds are sort from small to large TCI and divided in four groups, each group containing 25% of the AGFs (blue, red, green, purple). Panel A shows the absolute difference between LV and LE thresholds for each group separately. In panel B, a scatterplot between LV and LE thresholds is shown for the same groups. TCI indicates threshold confidence interval; LE, linear extrapolation; LV, last visible; AGF, amplitude growth function.

The scatterplots in Figure 3.5A and B show the relationship between eCAP thresholds and behavioral thresholds for the LE and the LV methods, respectively. Only subjects who had a complete eCAP threshold profile were included in the analysis. This resulted in 48 subjects for the LE method and 50 for the LV method, whereby only 5 subjects had an 1J array and the others a Mid-Scalar. The thresholds are plotted in gray, and the correlations within individual subjects are illustrated by the black regression lines. Below the scatterplots, accompanying individual correlation coefficients are presented rank-ordered from low to high (Figure 3.5C and D). The coefficients vary from –0.96 to 0.82 for the LE thresholds and from –0.81 to 0.92 for the LV thresholds. Mean individual Pearson's correlation coefficients (calculated using Fisher's z-transformation) for the LE and LV methods were $r = 0.16$ and $r = 0.34$, respectively. When analyzing all threshold values as one data set, significant correlations were found between T profiles and LE threshold profiles ($p < 0.001$, $r = 0.44$) and between T profiles and LV threshold profiles ($p < 0.001$, $r = 0.54$). Additionally, Figure 3.6 compares the behavioral thresholds with the eCAP thresholds and their TCIs. The TCIs are visualized as in Figure 3.3 but rotated 90 degrees clockwise. Remember from Figure 3.3 that the (normalized) eCAP thresholds are represented by the line at 0 CU. In Figure 3.6A, the data are shown for the LE method (blue) and in Figure 3.6B for the LV method (green). The behavioral thresholds (T, red) were plotted relative to the eCAP threshold profiles, showing the absolute difference between the eCAP and behavioral thresholds per electrode contact. Across all patients, the behavioral thresholds fell within the TCIs of the eCAP thresholds.

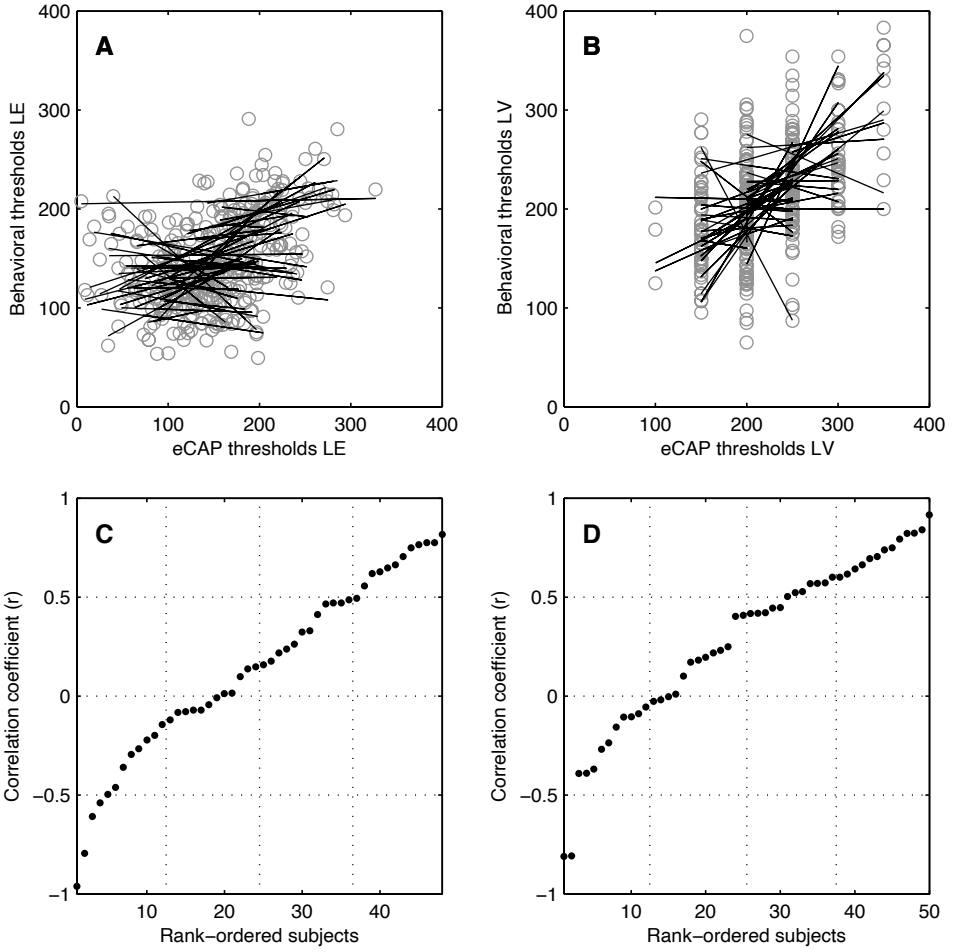

Figure 3.5. Scatterplots showing the correlation between eCAP thresholds (x-axis) and behavioral thresholds (y-axis) for the LE method (A) and the LV method (B). The thresholds are plotted in gray and the correlations within individual subjects are depicted by the black lines. Below the scatterplots (C and D), accompanying Pearson's correlation coefficients were presented rank-ordered from low to high (black line). eCAP indicates electrically evoked compound action potential, LE, linear extrapolation; LV, last visible.

3.4. Discussion

This study focuses on the precision of eCAP thresholds. To estimate precision, TCIs were assigned to eCAP thresholds estimated using the LE and LV method. eCAP thresholds estimated by the LE method were systematically smaller than the thresholds estimated by the LV method. The TCIs of the LE method were larger than those of the LV method, whereas the LE thresholds with the smallest TCIs correlated best with the LV threshold. Comparing the eCAP threshold profiles to optimally scaled T profiles, we found that the T profiles fell within the TCIs of the eCAP threshold profiles. This finding is one of the

potential explanations why the literature provides mixed results for correlations between behavioral and objective profiles; the eCAP threshold precision is too low.

3.4.1. Correlation between eCAP and behavioral thresholds

The correlation between eCAP thresholds and behavioral T and C/M levels has frequently been investigated to determine whether eCAP can be used to assist with sound processor programming and verify questionable behavioral responses. However, the outcomes have been moderate at best (Brown et al. 2000; Hughes et al. 2000; Franck & Norton 2001; Smoorenburg et al. 2002; Franck 2002; Di Nardo et al. 2003; Polak et al. 2006; Potts et al. 2007; Holstad et al. 2009; Mittal & Panwar 2009; Botros & Psarros 2010; Muhaimeed et al. 2010). There are several possible causes of the mismatch between objective and behavioral thresholds.

First, there is an offset difference between behavioral and objective thresholds; a small stimulus may be audible though the eCAP is still too small to measure. This offset is patient dependent and can even vary between electrode contacts, for example, because of the electrode impedances. The difference between eCAP thresholds and behavioral levels can be reduced by matching the two profiles using the threshold data at one electrode contact (Brown et al. 2000), which was applied in this study as well. Additionally, there are known variations, between clinics and brands, in the way T profiles are set in clinical routine. Next to the commonly used 10% of M level for AB recipients, there are various ways to determine the threshold levels (e.g., first hearing thresholds, counted thresholds, single-electrode stimulation, interleaved bursts). Up till now, there has been no consensus which of these approaches lead to the best subjective map and should serve as the reference for eCAP-based fitting. The actual way of determining thresholds across the various studies using eCAP-based fittings is highly underreported (de Vos et al. 2017), making it difficult to determine the best methods. Further, it is well known that pulse rate and duration of the stimulus affect both eCAP and behavioral thresholds, for example, because of temporal integration (McKay et al. 2005; Lai & Dillier 2007; McKay et al. 2013; Hughes et al. 2014). Previous research found that the relationship between eCAP and behavioral thresholds becomes stronger when associated stimulation rates were equal or close to each other (Brown et al. 1998; Franck & Norton 2001). However, equalizing the stimulation rates of eCAP and behavioral measurements, routinely measured with single pulses (30 Hz) and pulse trains (>500 Hz), respectively, is not ideal. Lowering the stimulation rate for behavioral measurements makes the thresholds inadequate with respect to the high-rate speech strategy, while increasing the rate of eCAP measurements has a degrading effect on the quality and amplitude of the eCAP response (Charasse et al. 2004; Hughes

et al. 2014). Therefore, the correlation between eCAP and behavioral thresholds is likely affected by differences in stimulation rate. This is probably also the case in this study.

Because our study was retrospective, there were some nonideal conditions for comparing the eCAP outcomes to behavioral data. First, there was a time lag between the intraoperative eCAP measurements and the T profiles obtained from regular fitting sessions. We decided to use most recent T profiles because we assumed that these were stable and most optimal. However, because of physiologic changes within the cochlea in the first months after surgery (Hughes et al. 2001; Spivak et al. 2011), it is likely that the association between eCAP thresholds and T profile presented in this paper is affected by the time lag between the two measurements. To evaluate this potential effect on our results, we reanalyzed the correlation using T profiles from the first regular fitting after surgery, which were available in our SoundWave database as well. Using the Fisher r-to-z transformation, we tested whether the correlation changes if first fitting data (on average 2 months after surgery) was used instead of the most recent fitting profiles (on average 11 months after surgery). However, no significant differences were found, neither for all threshold data together (LE thresholds: $p = 0.94$, LV thresholds: $p = 0.56$) nor for the individual correlations (LE thresholds: $p = 0.79$, LV thresholds: $p = 0.50$).

Further, our eCAPs were measured using RSPOM with the forward masking artifact rejection method, because they were a part of our clinical eCAP recording protocol. In contrast, eCAPs for fitting AB recipients will likely be measured via the clinical SoundWave software which by default uses alternating polarity. This difference in artifact rejection method potentially affects the clinical applicability of our results as some studies observed an effect of method on the eCAP (Frijns et al. 2002; Baudhuin et al. 2016). However, Hughes et al. (2016) thoroughly investigated the effect of artifact rejection on eCAP and they found no significant difference between forward masking and alternating polarity for the amplitude and threshold of the eCAPs measured in AB recipients. For Cochlear devices, they conclude that the forward masking paradigm was even advantageous over alternating polarity. Finally, the majority of the available AGF literature is based on the Cochlear system in which the forward masking technique is the default (de Vos et al. 2017). Considering these aspects, we think that the effect of these measurement settings is negligible in light of the TCI size, the main topic of the study.

Looking at the methods for calculating the correlation between objective and behavioral thresholds, only four studies perform correlation analysis on individual eCAP and T profiles (Holstad et al. 2009; Franck 2002; Franck & Norton 2001; Potts et al. 2007), while

the majority of the studies perform the analyses on grouped data (Brown et al. 2000; Cullington 2000; Smoorenburg et al. 2002; Di Nardo et al. 2003; Kiss et al. 2003; Morita et al. 2003; Kaplan-Neeman et al. 2004; Cafarelli Dees et al. 2005; King et al. 2006; Polak et al. 2006; Pedley et al. 2007; Lai et al. 2009; Mittal & Panwar 2009; Alvarez et al. 2010; Botros & Psarros 2010; Hughes & Stille 2010; Muhaimeed et al. 2010). However, group analysis does not provide any information about the correlation between profiles of individual subjects. The group correlation will be driven by the interpatient variation, especially when the eCAP thresholds were matched to the T profiles using one behavioral point (Brown et al. 2000; Smoorenburg et al. 2002; Willeboer & Smoorenburg 2006). Group analyses of our data revealed moderate correlation coefficients of $r = 0.44$ for T profiles versus LE thresholds and $r = 0.54$ for T profiles versus LV thresholds. Despite the nonideal conditions for comparing eCAP and behavioral thresholds, these correlation coefficients were in accordance with other (large) studies in which the grouped correlation coefficient was calculated for T profiles versus eCAP. Mittal & Panwar (2009) found $r = 0.33$ based on 90 subjects, Brown et al. (2000) found $r = 0.55$ with 44 subjects and Muhaimeed et al. (2010) found $r = 0.57$ with 47 subjects. However, to examine the predictive value of eCAP thresholds for the fitting of individual subjects, it is preferable to compare the eCAP and behavioral thresholds for individual patients (de Vos et al. 2017). Calculating the correlation within individuals resulted in correlation coefficients varying from strongly negative to strongly positive (Figure 3.5C and D). Compared to the three studies reporting within-subject correlation coefficients, our results were comparable with these of Holstad et al. (2000). The study of Holstad reported coefficients ranging from –0.67 to 0.99 with a mean of 0.24. Note that these results were obtained in children using Cochlear devices. In the studies of Franck et al. (2001/2002) and Potts et al. (2007), the individual correlation coefficients ranged between 0 and +1. Together with the finding that the behavioral threshold levels fell within the (relative large) TCIs of the eCAP thresholds (Figure 3.6), these results indicate that the eCAP thresholds are possibly not precise enough to predict T profiles at the level of individual subjects.

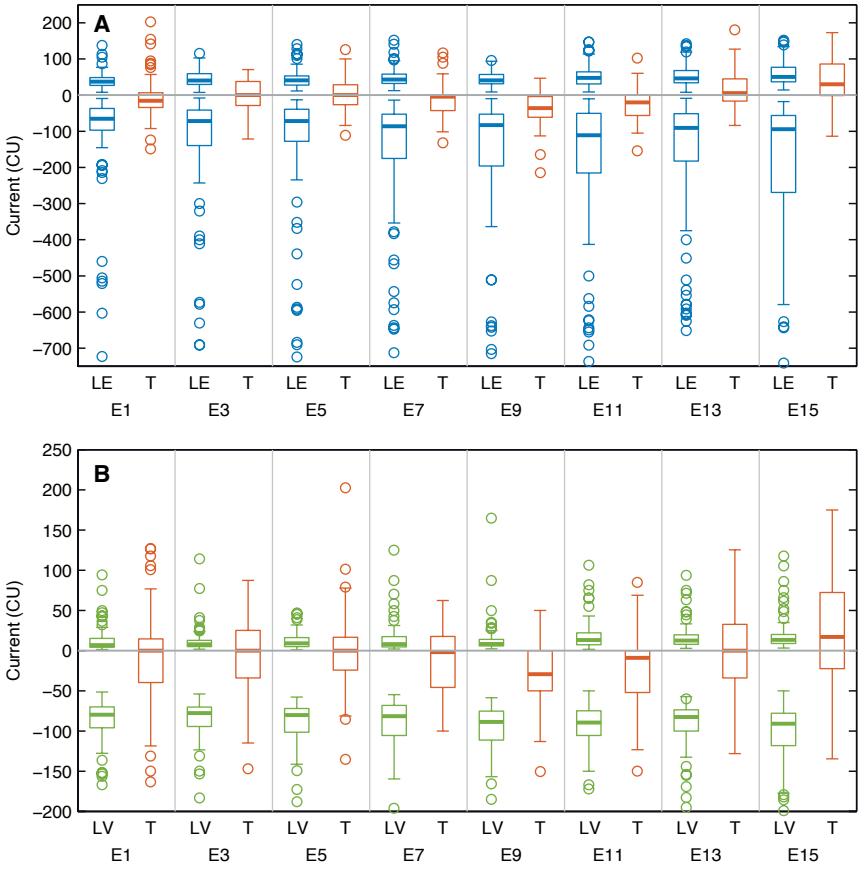

Figure 3.6. Comparison of the behavioral threshold profiles (T, red) with the objective eCAP thresholds and TCIs obtained with the LE (A, blue) and LV (B, green) methods. The eCAP thresholds and TCIs are presented as in Figure 3.3, whereby the (normalized) eCAP thresholds are represented by the line at 0 CU. The threshold values are grouped per electrode (horizontal) and expressed in CU (vertical). Box boundaries represent the 25th and 75th percentiles, whiskers represent the most extreme data points not considered outliers, open circles represent outliers, and solid line within the box represent median. CU indicates clinical units; eCAP, electrically evoked compound action potential, LE, linear extrapolation; LV, last visible; TCI, threshold confidence interval.

3.4.2. eCAP threshold precision

To the best of our knowledge, no study on eCAP thresholds has included error analysis for the eCAP amplitude. The data points of AGFs are commonly processed without error bar, and the estimated eCAP threshold is assumed to be good enough for application. However, to ensure that measurements are providing data that actually is clinical applicable, its precision should be evaluated. For the LE method, eCAP amplitudes have a measurement error that can be used to improve the reliability of the linear fit. Data points with a small measurement error will have a higher weight, contributing more to the fit than points with a larger error. The effect of including the measurement error is shown in Figure 3.2D. Here, the TCI becomes smaller when a weighted linear fit is used. To investigate how a weighted

fit influences the eCAP threshold and its TCI on group level, a correlation analysis was performed on both thresholds and TCIs estimated by LE and weighted LE. This post-hoc analysis revealed no significant difference between both LE and weighted LE thresholds ($p < 0.001$, $r = 0.99$) and between corresponding TCIs ($p < 0.001$, $r = 0.97$). Nevertheless, including the measurement error increases the reliability of the eCAP threshold and TCI, because the weighted linear fit better reflects the measured data points.

In addition, the goodness of fit (GOF) could be evaluated to estimate the reliability of the LE threshold. A worse fit would lead to a less reliable eCAP threshold and vice versa. Concerning the GOF, the question arose whether the linear fit is ideal because we recurrently observed nonlinear AGFs (e.g., Figure 3.2C). Therefore, we are working on a follow-up-study whereby we investigate the shape of the AGF and the GOF of several mathematical functions, for example, a sigmoid fit (Ramekers et al. 2014). Because the GOF is an indicator for the error of the linear fit (expressed as R^2), it does not provide a valid measure of precision for the extrapolated threshold value (expressed in CU). Therefore, the TCI was developed to estimate the eCAP threshold precision in CU. Note, that the TCI is strongly associated with the GOF ($p < 0.001$, $r = -0.79$), because TCI of the LE method is based on 95% confidence bounds which also is measure of GOF.

It would be worthwhile to (re)consider what is actually measured by the LE and LV methods. For example, what kind of information is in an AGF, and how precisely can eCAPs and their thresholds be measured? Figure 3.4 shows that there is a systematic difference in the eCAP thresholds estimated by the two commonly used methods, thresholds estimated by LE being systematically lower than those estimated by the LV method. This difference can be explained by the fact that LE thresholds are estimated at zero amplitude, where LV thresholds are estimated just above noise level. Consequently, the LV thresholds are probably overestimated compared to the real eCAP threshold. Furthermore, the success rate of the LV method is higher than that of LE. To estimate the eCAP threshold, one eCAP response is sufficient for the LV method, while at least two responses are required for the LE method. This explains why 48 subjects were included in Figure 3.5A compared to 50 in Figure 3.5B. To estimate threshold precision, one additional data point at a higher current is required for the LV method. For the LE method, at least three data points are required because the TCI cannot be computed if the number of data points is equal to the number of coefficients in the linear fit. The size of the TCI considerably reduces when four, or even more, data points are used. The step size or applied current scale affects the TCI as well, for example, using a logarithmic current scale (Nucleus) would result in different TCIs than using a linear scale (this study). When relatively large current steps are used, the LV

threshold can be estimated less precisely, probably resulting in a larger overestimation of the threshold. In this study, a default step size of 50 CU was used, which was not ideal for the LV method. Generally, the LV method is performed with smaller current steps, especially around the threshold level (Botros et al. 2007; Glassman & Hughes 2013; Baudhuin et al. 2016). The use of smaller current steps in this study would have led to lower LV thresholds and, possibly, smaller TCIs. The measure of how well the LV threshold represents the real eCAP threshold also depends on the noise level. The higher the noise level, the larger the eCAP must be to be visible and, in turn, the larger the deviation from the true eCAP threshold. Thus, when a measurement system has a relatively high noise floor, the LE method provides a better approximation of the eCAP threshold than the LV method. For our data, a mean systemic noise of 31.4 µV with a standard deviation of 14.4 µV was found. Compared to other studies, this noise level is relatively high (Glassman & Hughes 2013). Therefore, performing the analysis on an AGF measured by a CI with lower systemic noise would reduce the eCAP thresholds and TCIs, especially with the LV method. Finally, note that presented method of estimating eCAP precision using TCIs is generally applicable, but the presented quantities are specific for our data. Interpretation of eCAP thresholds and their precision should always be performed in light of the measurement conditions. Furthermore, the TCI reflects a best guess of the eCAP threshold precision rather than the true threshold error. In the follow-up-study, we want to investigate the error of the eCAP threshold induced by methodology or the random noise component as well. This error could be estimated using a varying number of averages or repeated measures.

In addition to high Glassman & Hughes (2013), who already comprehensively compared the LE and LV methods, we wanted to highlight that the relationship between these two methods depends on the threshold precision. Figure 3.4 shows that the correlation between LE and LV thresholds is best if the TCI is small, originating from clear, that is, relatively large eCAPs with a low measurement error (e.g., Figure 3.2A). Considering the points of the most precise thresholds (blue and red points), the correlation is close to that found by Glassman & Hughes (2013), suggesting that the eCAPs and AGFs used by Glassman et al. in their analysis were very clear. Additionally, we found that the TCIs were smaller at the apex than at the base of the cochlea, and that the TCIs of the LE and LV methods did not differ for the most apical electrode contact (Figure 3.3). This can be explained by the larger eCAPs at the apex than at the base of the cochlea.

3.5. Conclusions

This study showed that eCAP thresholds estimated by LE and LV have an uncertainty that can be estimated using TCIs as measure of precision. The size of the TCI depends on several

factors, for example, the threshold estimation method and measurement conditions, but it is often larger than one would expect when just looking at the threshold values. Given the relatively large TCIs, we recommend that future research on eCAP thresholds should be accompanied by a measure of precision to correctly apply eCAP thresholds in clinical practice. Comparing our eCAP outcomes with behavioral fitting levels, we found that the T profiles fell within the TCI of the LE and LV thresholds. Further, although our conditions for comparing eCAP and behavioral thresholds were nonideal, our findings were in line with the literature: significant correlations between the two parameters at the level of grouped data and correlation coefficients almost homogeneously ranging from −1 to +1 for individual subjects. Therefore, not only the relative large TCIs, but also the poor individual correlations of eCAP and behavioral thresholds indicate that the eCAP thresholds are possibly not precise enough to predict T profiles.

CHAPTER

4

A novel algorithm to derive spread of excitation based on deconvolution

Jan Dirk Biesheuvel, Jeroen J. Briaire, Johan H.M. Frijns

Ear and Hearing, 2016, 37(5):572-581

Abstract

Objective: The width of the spread of excitation (SOE) curve has been widely thought to represent an estimate of SOE. Therefore, correlates between psychophysical parameters, such as pitch discrimination and speech perception, and the width of SOE curves, have long been investigated. However, to date, no relationships between these objective and subjective measurements have yet been determined. In a departure from the current thinking, the authors now propose that the SOE curve, recorded with forward masking, is the equivalent of a convolution operation. As such, deconvolution would be expected to retrieve the excitation areas attributable to either masker or probe, potentially more closely revealing the actual neural SOE. This study aimed to develop a new analytical tool with which to derive SOE using this principle.

Design: Intraoperative SOE curve measurements of 16 subjects, implanted with an Advanced Bionics implant were analyzed. Electrically evoked compound action potential (eCAP)-based SOE curves were recorded on electrodes 3 to 16, using the forward masker paradigm, with variable masker. The measured SOE curves were then compared with predicted SOE curves, built by the convolution of basic excitation density profiles (EDPs). Predicted SOE curves were fitted to the measured SOE curves by iterative adjustment of the EDPs for the masker and the probe.

Results: It was possible to generate a good fit between the predicted and measured SOE curves, inclusive of their asymmetry. The rectangular EDP was of least value in terms of its ability to generate a good fit; smoother SOE curves were modeled using the exponential or Gaussian EDPs. In most subjects, the EDP width (i.e., the size of the excitation area) gradually changed from wide at the apex of the electrode array, to narrow at the base. A comparison of EDP widths to SOE curve widths, as calculated in the literature, revealed that the EDPs now provide a measure of the SOE that is qualitatively distinct from that provided using conventional methods.

Conclusions: This study shows that an eCAP based SOE curve, measured with forward masking, can be treated as a convolution of EDPs for masker and probe. The poor fit achieved for the measured and modeled data using the rectangular EDP, emphasizes the requirement for a sloping excitation area to mimic actual SOE recordings. Our deconvolution method provides an explanation for the frequently observed asymmetry of SOE curves measured along the electrode array, as this is a consequence of a wider excitation area in the apical part of the cochlea, in the absence of any asymmetry in the actual EDP. In addition, broader apical EDPs underlie the higher eCAP amplitudes found for apical stimulation.

4.1. Introduction

Modern cochlear implants (CIs) have an in-built telemetry function, which allows them to record the physiological response of auditory nerve fibers to electrical stimulation, the so-called electrically evoked compound action potential (eCAP). Typically, the eCAP response is recorded as a waveform with a negative peak (N_1), followed by a positive peak or plateau (P_1). The amplitude of this response is measured from N_1 to P_1, and can reach a value of several hundred microvolts (Abbas et al. 1999). Various aspects of neural function can be interrogated using specific eCAP measurement paradigms. A common example is the measurement of spread of excitation (SOE) (Cohen et al. 2003; Abbas et al. 1999; Hughes & Abbas 2006b; van der Beek et al. 2012). SOE curves have been used to measure the longitudinal SOE along the auditory nerve. There has been much interest as to whether the width of the SOE curve can be correlated with subjective psychophysical parameters such as pitch discrimination, and speech perception. However, to date, no convincing correlates for SOE width and these criteria have yet been established (Hughes & Abbas 2006b; Snel-Bongers et al. 2012; van der Beek et al. 2012; Cohen et al. 2003). In this article, we will demonstrate that the width of the SOE curve is, of itself, an insufficient measure of the SOE. Instead, the SOE curve must be subject to a post-processing algorithm to retrieve the novel measure of SOE. We developed this analytical tool using SOE data collated from a cohort of 16 subjects. Our data now provides a new and improved measurement for the SOE, and provides insight into the actual SOE.

SOE curves are measured using the forward masking (FM) subtraction paradigm (Abbas et al. 2004; Cohen et al. 2003; Hughes & Abbas 2006b). Basically, FM is used to un-mix the eCAP from the stimulus artifact taking advantage of neural refractory properties. The basic principle of this artifact rejection methodology is depicted in Figure 4.1. Application of the masker and probe at different electrode contacts generates a SOE curve. Ordinarily, the SOE curve is measured using a fixed probe and roving masker, with a recording contact set two electrodes apical to the probe. The resultant SOE curve shows the eCAP, derived from the overlap of neural populations recruited by masker and probe, as a function of masker position. The SOE curve typically has its maximum amplitude around the location of maximum stimulation (where masker and probe coincide). Ordinarily, the amplitude then decreases with increasing distance between the masker and probe. However, in practice, various SOE curves have been observed: symmetric and asymmetric, wide and narrow, large in the apex and small in the base.

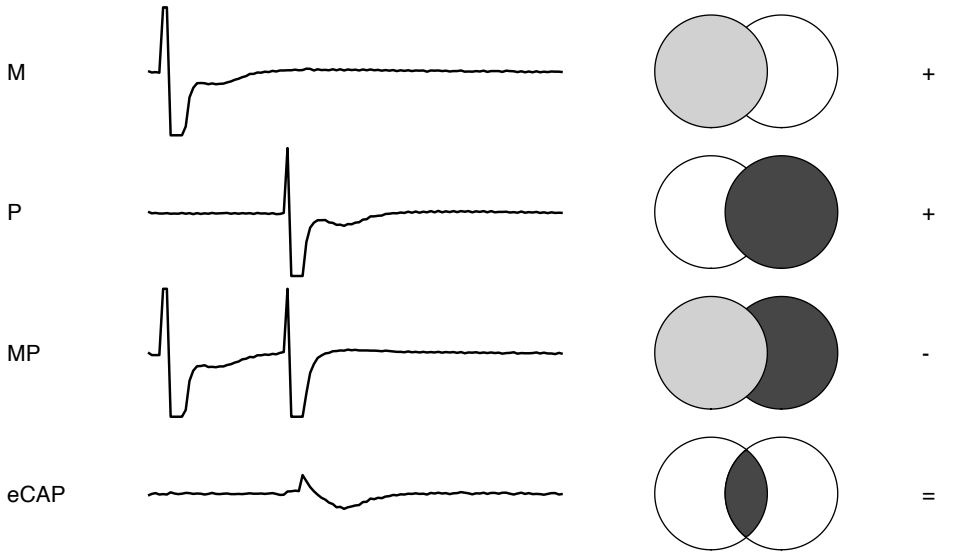

Figure 4.1. Forward masking paradigm, which takes advantage of neural refractory properties to un-mix the eCAP and stimulus artifact. The paradigm comprises a M, P, and combined MP frame. The traces on the left-hand side show the recording; the Venn diagrams, shown to the right, designate the response areas of the masker and the probe. Light or dark gray areas indicate excitation in the masker or probe frame, respectively. The eCAP is calculated by adding frames M and P, and subtracting the MP frame. The result is the response of the region of overlap, while eliminating stimulus artifacts. eCAP indicates electrically evoked compound action potential; M, masker; P, probe, MP, masker-probe.

The underlying reasons for only some of these SOE curve irregularities have been explained. For example, the measurement technique used can influence the shape of the SOE curve, whereas the location of the recording electrode can alter eCAP amplitude (van der Beek et al. 2012; Hughes & Stille 2010; Frijns et al. 2002; Cohen et al. 2004). To date, there has been no convincing explanation for the frequently reported asymmetry of the SOE curve along the electrode array (Cohen 2009; Cohen et al. 2003; Hughes & Stille 2010; Hughes & Abbas 2006b). Our previous data leads us to suggest that asymmetric SOE curves may indicate a nonuniform excitation of nerve fibers along the electrode array. A wider excitation pattern at the apex versus the base, would, because of FM, result in SOE curves that steadily become asymmetric towards the apex (van der Beek et al. 2012). A theoretical illustration is provided in Figure 4.2. Initially, with the masker positioned at electrode 1, and the probe fixed at electrode 8, there is no overlap in the areas excited by either. As the masker tracks towards electrode 16, the first overlap between excitation areas occurs at electrode 4, resulting in an eCAP. This overlap, and the accompanying eCAP, will peak as the masker and probe coincide at electrode 8. As the masker continues on towards electrode 16, the area overlap and, as a consequence, the eCAP shrink. The measured SOE (mSOE) curve is therefore a result of excitation areas of masker and probe. As a consequence, the real SOE, generated by neural populations recruited by either the masker or probe, cannot be estimated directly from the width of the SOE curve.

From a mathematical point of view, the movement of the masker, with respect to the fixed probe, can be seen as a convolution operation. A convolution is defined as a mathematical operation that expresses the amount of overlap of one function as it is shifted over another function, in formula:

$$(f * g)[n] = \sum_{m=-\infty}^{\infty} f[m]g[n-m] \qquad [4.1]$$

Applied to the measurement of a SOE curve, *f* represents the excitation density profile (EDP) of the fixed probe and *g* the EDP of the roving masker, whereby the position of probe and masker is denoted by *n* and *m* respectively. An EDP reflects the percentage of neurons that are excited as a function of their distance along the basilar membrane. Conversely, if we assume that the SOE curve is a convolution of masker and probe, then its deconvolution would yield the excitation areas for the masker and probe respectively, and thus the actual SOE at electrode level.

This study aimed to develop a new analytical tool with which to transform SOE curves into a new measure of SOE using deconvolution. To directly deconvolve the SOE curve, the overlap function (SOE curve) is required, together with the EDP of the masker or probe. However, as neither excitation area is known, direct deconvolution is not feasible. Instead, we decided to create a model whereby we convolve basic EDPs for masker and probe to generate a predicted SOE curve (pSOE) that, with iterative adjustment of the EDPs, could most closely approximate mSOE curves.

4.2. Methods

4.2.1. Subjects and data

The SOE curves used in this study were measured intraoperatively in the period from January to December 2006. All subjects were implanted with a HiRes90k device with HiFocus1J electrode array (Advanced Bionics, Sylmar, CA). This electrode array consists of 16 electrode contacts (1 to 16, numbered from apex to base), each 1.1 mm apart (measured from the center of each electrode). Data were collected using the Bionic Ear Data Collection System (BEDCS) research software from Advanced Bionics (Sylmar, CA). The following measurement parameters were used: monopolar biphasic pulses, anodic first; pulse duration: 32 µs/phase; masker-probe interval: 500 µs; sampling rate: 56 kHz; gain: 100; 16 averages; measurement paradigm: FM, variable masker, recording two electrodes apical to probe stimulus. In total 41 measurements were available, comprising 14 SOE curves measured at electrodes 3 to 16.

Signal-to-noise ratio (SNR) and eCAP amplitude were calculated automatically using MATLAB (Mathworks, Inc., Natick, MA). Raw eCAP recordings were filtered using a zero-phase shift filtering based on a fourth order Butterworth low-pass filter with a cut-off frequency of 8.4 kHz. Peak N_1 was detected as the minimum over the time period between 150 and 400 μs and peak P_2 between 350 and 900 μs after the end of stimulation. The eCAP amplitude was calculated as peak- to-peak voltage between P_2 and N_1 in millivolt (mV). The SNR of the eCAP was calculated as the root mean square of the signal divided by the root mean square of the noise. Signal was defined as the part of the response between N_1 and P_1. Noise was defined as the last 30 samples of the response; it was assumed that no possible remaining artifact or neural response would still happen over this section. The measurement error of the eCAP was defined as the standard deviation of its noise section.

SOE curve measurements were included when, for a minimum of 10 SOE curves, the center electrode, and at least 2 electrodes on either side, had an eCAP amplitude larger than 0.15 mV, with SNR exceeding 6 dB. Based on these criteria, 16 of 41 measurements were included in this study. The corresponding subject demographics are shown in Table 4.1. For S5, S7, and S9, certain electrodes were excluded given their presumptive inability to record or to stimulate, as suggested by their SOE curve data (Table 4.1).

Table 4.1. Subject demographics.

				Excluded	
	Gender	**Age (y)**	**Etiology**	**Electrodes**	**SOE**
S1	F	6	Unknown	-	-
S2	F	37	Progressive	-	-
S3	M	1	Meningitis	-	-
S4	M	1	Meningitis	-	-
S5	F	54	Progressive	11,12,13[1]	11,12,13
S6	M	44	Unknown	-	16[3]
S7	F	3	Unknown	2[1]	1
S8	M	27	Congenital	1	1
S9	M	26	Congenital	11[2]	11,13
S10	F	60	Congenital	-	-
S11	F	84	Ménière's disease	-	-
S12	F	3	Familiar congenital	-	13[3]
S13	M	66	Progressive	-	-
S14	M	2	Unknown	-	-
S15	M	1	Meningitis	-	-
S16	M	1	Meningitis	-	-
Average		26			

[1] Not able to stimulate
[2] Not able to stimulate and to measure
[3] Insufficient data points
SOE indicates spread of excitation

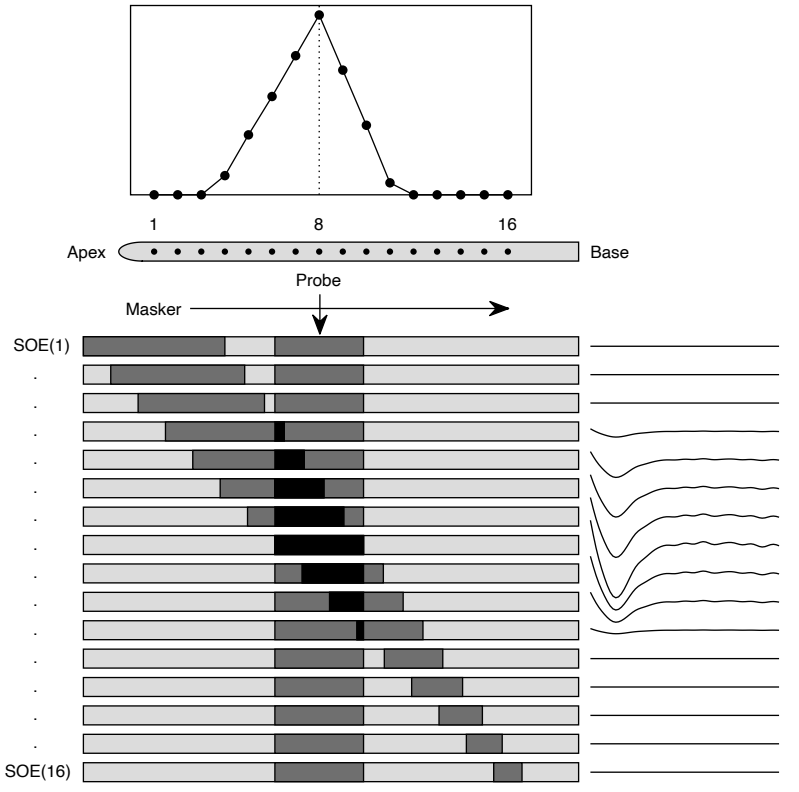

Figure 4.2. The SOE curve measured with forward masking (top panel) reflects the relative overlap (black areas in lower panel) of neural populations, as they are recruited by the fixed probe, and variable masker (dark gray), along the electrode array. The corresponding eCAPs are depicted in the right panel. eCAP indicates evoked compound action potential; SOE, spread of excitation.

4.2.2. Deconvolution

Deconvolution of SOE curves was performed using MATLAB. Initially, we modeled a basic EDP for each electrode. In total, three basic EDP shapes were evaluated; these are depicted in Figure 4.3. The first EDP we tested was rectangular; this was used to investigate whether a straight and simple EDP could predict a physiological SOE curve. The designs of the other two EDP shapes were based on literature. One expressed a symmetric and exponential decay in excitation density (Cohen et al. 2003; Smit et al. 2009; Vanpoucke et al. 2004) and the other was shaped as a Gaussian function (Kalkman et al. 2015; Cohen 2009). The design of these latter two EDP shapes was to help us evaluate the expectation that decay in excitation density along the basilar membrane would contribute to the SOE curve. Henceforth in this article, these EDPs are denoted rectangular (R), exponential (E), and Gaussian (G), respectively. Since the excitation area was not restricted to the limits of the electrode array, EDPs were modeled across an extended virtual range from electrode –19

to electrode 36. It turned out that this broad range was more than adequate to prevent truncation errors. Small incremental step sizes of 0.05 enabled us to create smooth EDPs.

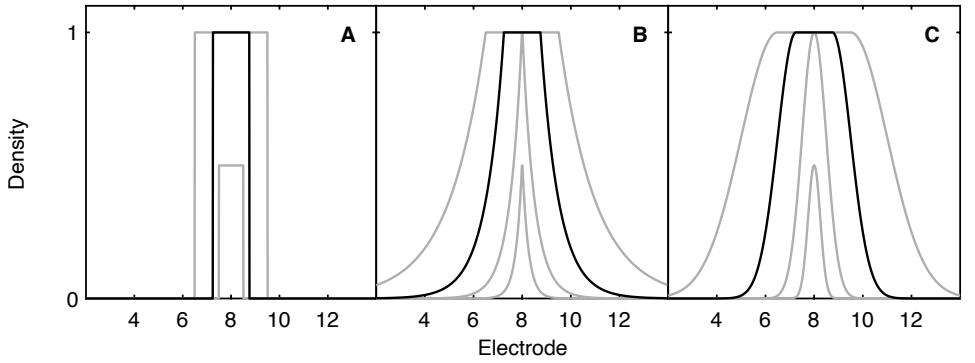

Figure 4.3. The three evaluated EDPs: rectangular (A), exponential (B), and Gaussian (C). Each EDP indicates the percentage of neurons that are excited, as a function of distance along the basilar membrane. The black lines represent the basic EDPs, with gray lines showing possible excitation patterns after varying width and slope parameters. The width parameter represents the width at top of the EDP, also called plateau width. The density scale of the EDP is shown on the left. EDP indicates excitation density profile.

The pSOE curves for electrodes 3 to 16 were modeled by convolving the basic EDPs according to the following formula:

$$SOE_p(m) = Scale \times \sum_{i=apical}^{basal} EDP_m(i) \times EDP_p(i) + Noise_{offset} \qquad [4.2]$$

where *p* is the position of the (fixed) probe and *m* is the location of the (moving) masker, both expressed in electrode number. The summation is across the sample (*i*) of the EDPs. Subsequently, pSOE curves were fitted to mSOE curves by optimizing the EDP variables, and then determining the most optimal EDP shape. The method contained as few parameters as possible still providing reliable pSOEs. In total, 19 variables were optimized: 16 variables for the EDP plateau width (unit: number of electrodes) at each electrode, 1 variable for longitudinal density decay (for all EDPs, no unit), 1 scaling variable (for all EDPs, no unit) to scale pSOE curves to mSOE curves, and 1 variable as offset (unit: mV) for the pSOE curve representing the noise floor. Scaling the pSOE curves to the mSOE curves was required , because EDPs were dimensionless while pSOEs were expressed in mV. The start parameters of the optimization routine were chosen in such a way that the Gaussian EDP looked like Kalkmans' profile for maximum comfortable loudness (Kalkman et al. 2015). The domain of variables was set so as not to restrict the optimization routine: width [–1, 15], slope [0.1, 6], offset [0, 1], and scale [0, 1]. All variables had to be positive, except width, which could be negative from –1 to 0. When the width parameter for the exponential and

Gaussian EDP were negative, the EDP had a width of zero, and amplitude of 1+width, resulting in an amplitude of between 0 and 1 (depicted by the gray lines in Figure 4.3B and C). Since the rectangular EDP could not have a width of 0, the minimal width was set to 0.5. When the width parameter for the rectangular EDP was between –1 and 0.5, the EDP had a minimal width of 0.5 and the amplitude was scaled between 0 and 1. The density decay of the exponential and Gaussian EDPs can be calculated by $\exp\left(\frac{x-E}{\sigma}\right)$ and $\frac{1}{\sigma\sqrt{2\pi}}\exp\left(-0.5\left(\frac{x-E}{\sigma}\right)^2\right)$ respectively, where σ is the slope parameter, *x* the samples and *E* the electrode contact. Hence, an EDP was modeled using two parameters; one parameter for the slope and one parameter for the plateau width, which automatically scales the amplitude when the plateau width becomes too small. The optimization procedure was performed using a minimization routine, whereby the root mean square error (RMSE) between the pSOE curves and the mSOE curves served as our optimization parameter.

The three different EDP shapes were evaluated for three variants of (preprocessed) SOE curves: raw SOE curves, normalized SOE curves, and SOE curves based on data points exceeding the noise threshold. These SOE curve variants were termed raw, normalized, and denoised respectively. For the normalized curves, each SOE curve was normalized to its maximum. For the denoised SOE curves, eCAPs with an amplitude of less than 0.15 mV, or a SNR lower than +6 dB, were neglected. These analyses were performed to investigate the effect of normalizing SOE curves, as reported in previous studies (Hughes et al. 2013; Snel-Bongers et al. 2012; van der Beek et al. 2012), and to investigate the influence of noise level on the deconvolution method.

4.2.3. Statistical analysis

The effect of EDP shape and SOE preprocessing were evaluated using two-way analysis of variance. Linear regression analyses were used to compare our new measures of SOE with those generated using conventional methodologies (Abbas et al. 2004; Cohen et al. 2003; van der Beek et al. 2012). To enable this comparison, SOE curves were fitted with a double-sided exponential function, across an extended range from –19 to 36 electrode contacts. The EDP width was calculated at the 80% density level, and the SOE curve width at the 80% amplitude level. All calculations and statistic operations were performed using MATLAB.

4.3. Results

4.3.1. Typical case of deconvolution

Figure 4.4 shows the deconvolution of a set of raw SOE curves (error bars) measured for subject 10. The SOE curve measured at electrode 3 (apex) had the greatest magnitude, with the overall amplitude of the SOE curves declining toward electrode 16 (base). This deconvolution was performed using Gaussian EDPs. The calculated EDPs (Figure 4.4, gray lines) showed that the excitation areas were nonuniform across the electrode array. In this subject, the EDPs were broad apically and became narrower toward the base of the electrode array. The pSOE curves are presented in the same graph (black lines), and match the mSOE curves (RMSE = 0.045 mV), including their apical asymmetry.

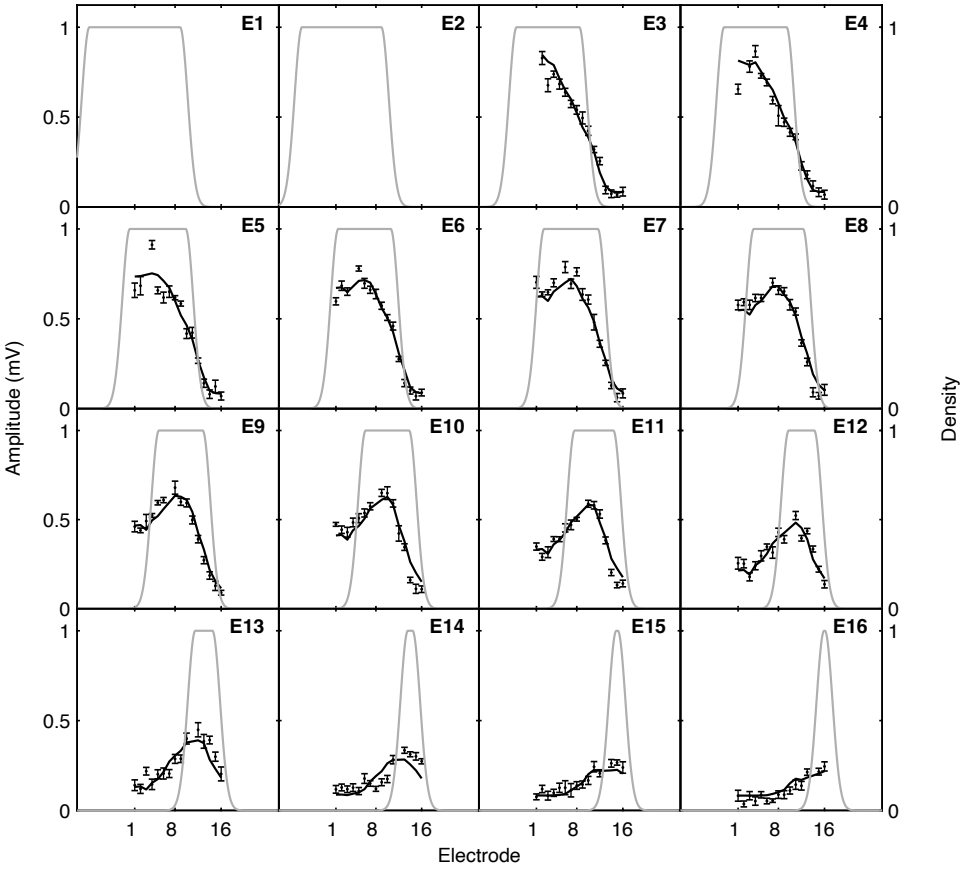

Figure 4.4. Deconvolution of 14 SOE curves, measured at electrodes 3 to 16. The curves for electrode 1 to 16 are shown from top left to bottom right. The black dots represent the measured SOE curves including measurement error, and the black solid lines represent the modeled SOE curves. The optimized EDP for each electrode is shown in gray. To the left-hand side, is the amplitude scale of the SOE. The EDP density scale is shown to the right. EDP indicates excitation density profile; SOE, spread of excitation.

4.3.2. Effect of EDP shape and SOE preprocessing

The boxplots in Figure 4.5 show the RMSEs grouped per combination of EDP and SOE variant. Two-way analysis of variance revealed a significant effect of SOE curve preprocessing [F (2, 135) = 99.04, p < 0.001]. The deconvolution (or prediction) of normalized SOE curves generated a significantly higher RMSE than the deconvolution of raw (p < 0.001, asterisk), or denoised SOE curves (p < 0.001, triangle). The deconvolution model worked equally well for raw and denoised SOE curves (p = 0.74). Of major influence in our analyses was the basic EDP used [F (2, 135) = 3.41, p < 0.05]. Figure 4.5 shows that, in general, the rectangular EDP provided the highest RMSEs followed by the exponential. The Gaussian EDP generated the lowest RMSEs. Statistical analyses revealed a significant difference between the rectangular and Gaussian EDP only (p < 0.05, dot). Figure 4.6 zooms to one electrode to demonstrate the increased RMSE using the rectangular EDP. To place the examples in perspective to Figure 4.5, both the total RMSE across the SOE curves of all electrodes ($RMSE_T$) and the RMSE of the shown curves ($RMSE_S$) are provided. The angular pSOE curves based on the rectangular EDP (Figure 4.6A) resulted in a poorer fit between the pSOE and mSOE ($RMSE_T$ = 0.048 mV, $RMSE_S$ = 0.088 mV), compared to those generated using the exponential (Figure 4.6B; $RMSE_T$ = 0.044 mV, $RMSE_S$ = 0.054 mV) or the Gaussian EDP (Figure 4.6C; $RMSE_T$ = 0.042 mV, $RMSE_S$ = 0.076 mV).

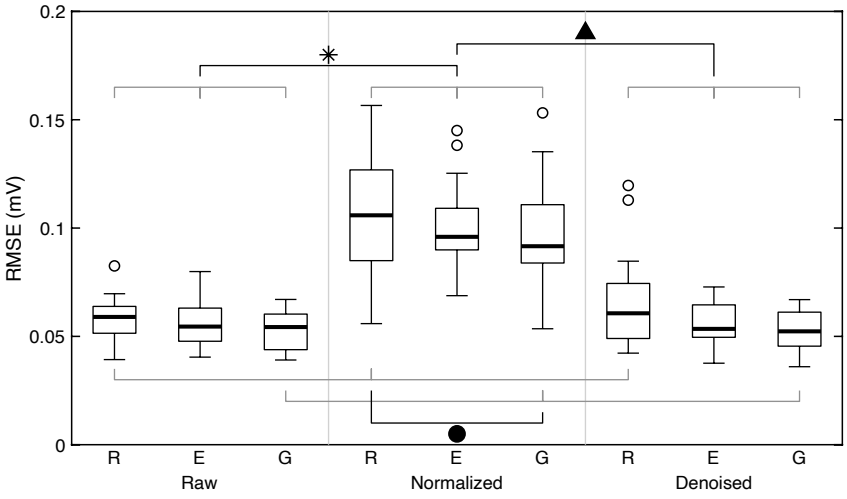

Figure 4.5. RMSEs obtained with the three different EDPs (R, E, G), separated by SOE preprocessing methodology (raw, normalized, denoised). Box boundaries represent the 25th and 75th percentiles, whiskers represent the most extreme data points not considered outliers, open circles represent outliers, and horizontal solid line within the box represent median. The symbols indicate a significance difference between the denoted groups. E indicates exponential; EDP, excitation density profile; G, Gaussian; R, rectangular; RMSEs, root mean square errors; SOE, SOE, spread of excitation.

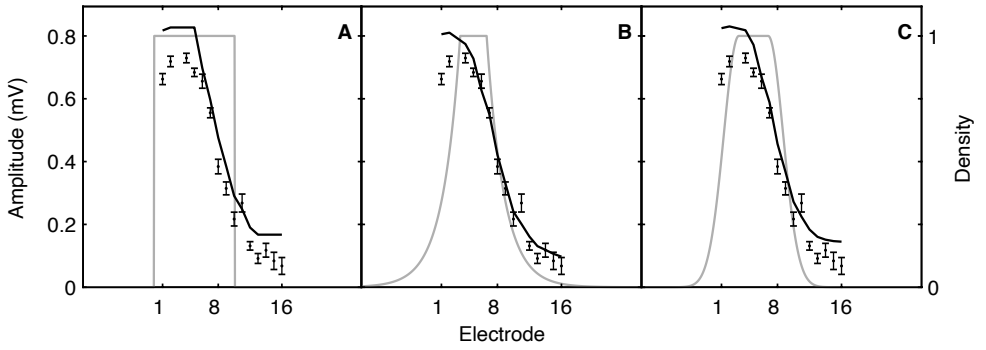

Figure 4.6. The effect of different EDPs (gray) on modeled SOE curves (black solid line). The SOE curve modeled using the rectangle EDP (A) is rougher than the SOE curves generated using the exponential (B) and the Gaussian EDP (C). The result is a poorer fit between the predicted and measured SOE curves (black dots with error bar, identical for A, B and C). The amplitude scale of the SOE curves is shown on the left side, and the density scale for the EDPs, to the right. EDP indicates excitation density profile; SOE, spread of excitation.

4.3.3. Size of excitation area

Figure 4.7 shows the widths of the optimized rectangular (square), exponential (dot), and Gaussian (triangle) EDPs. The EDPs originate from the deconvolution of raw SOE curves and are shown for all individual subjects (S1 to S16). The widths, which represent the size of the excitation area, were calculated at the 80% density level of the EDPs, and plotted as a function of the electrode number. It was evident that in multiple subjects, the EDP width decreased in a direction of travel from apex to base. The corresponding SOE curves (in this article, shown only for S10 (Figure 4.4)) show that the larger the difference between EDP width, apical to basal, the greater the asymmetry of the SOE curves. Conversely, the SOE curves of S7 and S16 are symmetric, with EDP widths largely stable across the electrode array. A comparison of the eCAP amplitudes, measured with masker and probe at the same electrode, with corresponding EDP widths, revealed the following relationship; higher eCAP amplitudes correlated with larger excitation areas, and vice versa. For all 16 subjects, a significant correlation ($p < 0.05$) was found between these eCAP amplitudes and the surface under the corresponding Gaussian EDPs. The scatterplots of these correlations are shown in Figure 4.8. In this figure, the eCAP amplitude is plotted versus the area under the corresponding EDP, represented by the density summation of all samples of that EDP. Except for S6, S9 and S12, these correlates remained significant ($p < 0.05$) after applying a Bonferroni correction (for performing the same correlation on multiple data sets). Within a single subject, the widths of the three different EDPs follow, to a large extent, the same pattern. In general, the rectangular EDPs were widest, followed by the Gaussian, and then exponential.

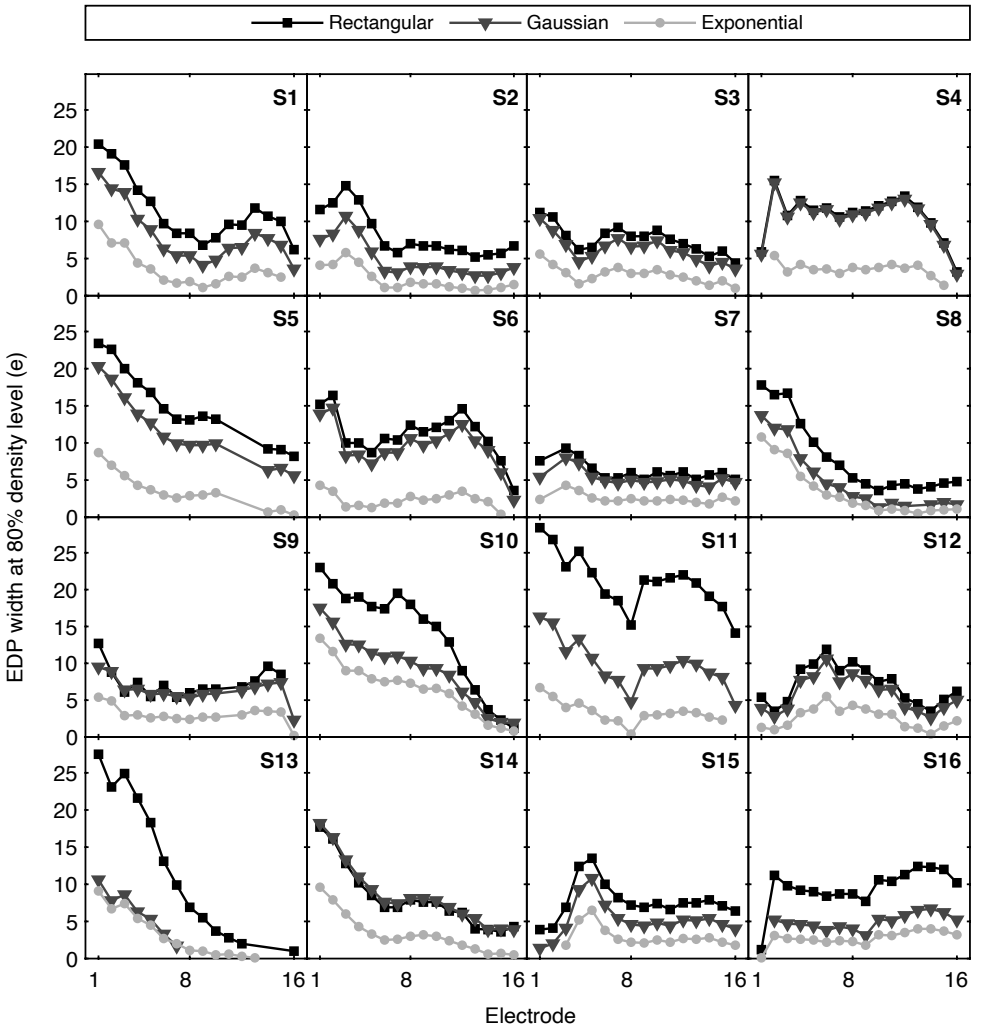

Figure 4.7. Optimized widths of the rectangular (black square), exponential (gray dot) and Gaussian (light gray triangle) EDPs generated by deconvolution of raw SOE curves. The widths, expressed in number of electrode contacts (y-axis), are plotted as a function of the electrode number (x-axis), for subject 1 (top left), through to subject 16 (bottom right). EDP indicates excitation density profile; SOE, spread of excitation.

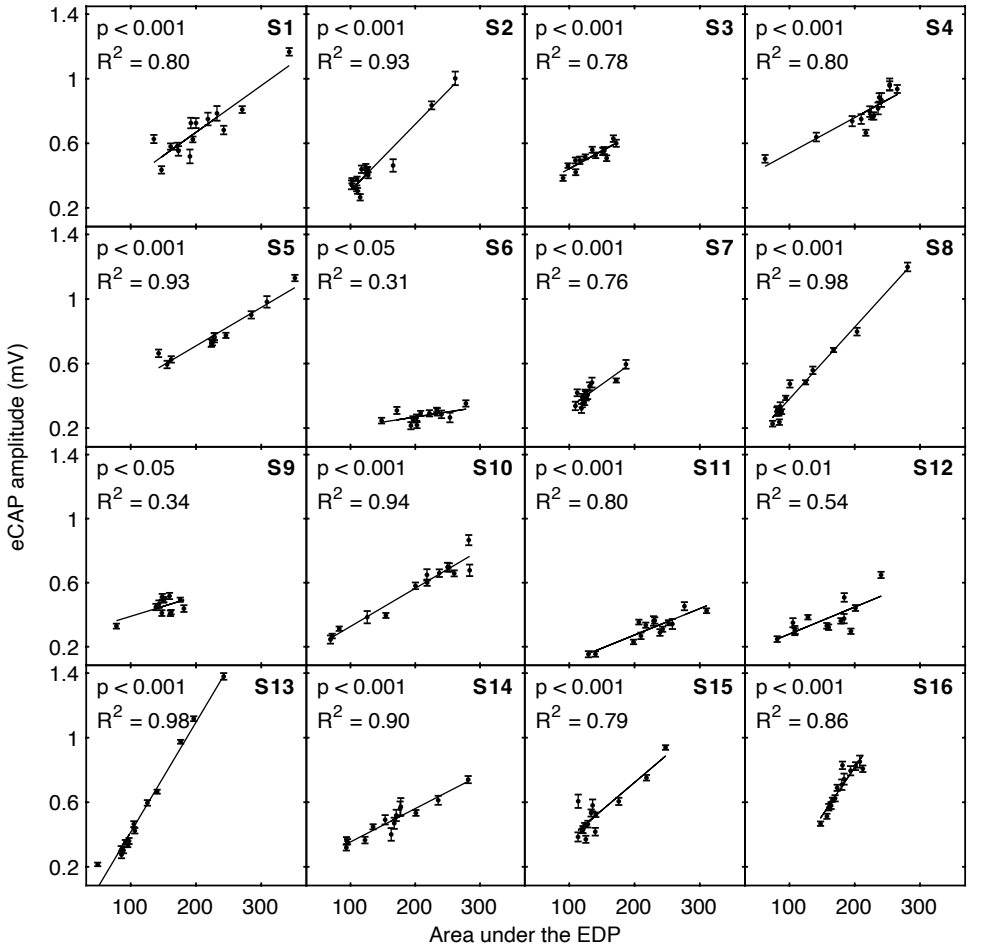

Figure 4.8. Scatterplots showing the correlation between eCAP amplitude (ordinate) and area under the Gaussian EDP (abscissa), for subject 1 (top left) to subject 16 (bottom right). The eCAP amplitude is expressed in millivolt (mV). The area under the EDP is represented by the density summation of all samples of that EDP. eCAP indicates evoked compound action potential; EDP, excitation density profile.

4.3.4. EDP width versus the SOE curve width

The scatterplots in Figure 4.9 show how the width of the EDP correlates with the width of the SOE curve. For this correlation analysis, we used the widths of the Gaussian EDP estimated by the deconvolution of raw SOE curves. In the first scatterplot (Figure 4.9A), the EDP width (y-axis) was plotted against the SOE curve width (x-axis), both expressed as electrode number. Data points were not drawn where the sides of the EDP failed to attain the 80% density level, or the sides of the exponential fit to the SOE curve failed to drop to the 80% amplitude level. For this plot, no significant correlation was found between the two measures of SOE. In the second scatterplot (Figure 4.9B), the EDP width was again plotted against the SOE curve width for the identical electrode. However, in this case,

where a side of the exponential fit to the SOE curve did not drop to the 80% amplitude level (within the limit of the array), the width was set to the limit of the array in the apical or basal direction (Abbas et al. 2004). In this comparison, a significant correlation between the EDP width and SOE curve width ($p < 0.001$), with a low explained variance ($R^2 = 0.07$), was found.

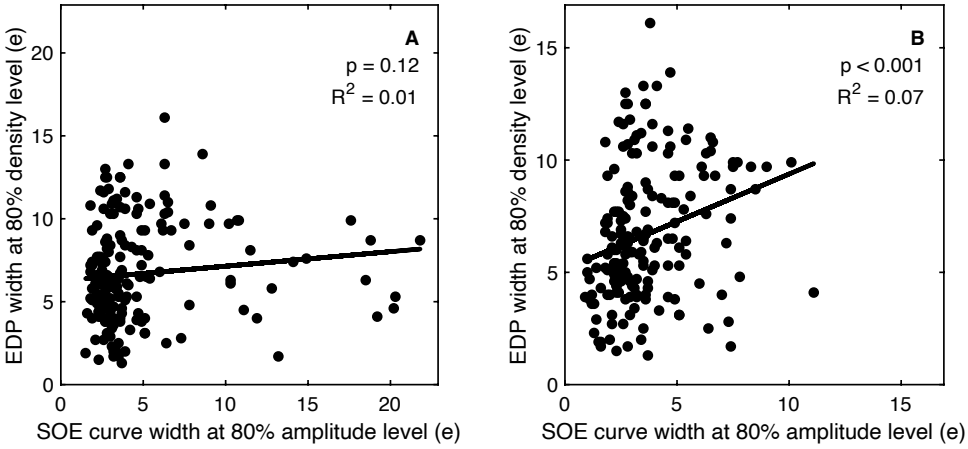

Figure 4.9. Scatterplots showing the correlation between the width of the EDP and the width of the SOE curve. In the left-hand scatterplot (A), the EDP width (y-axis) was plotted against the SOE curve width (x-axis) of the identical electrode contact. The SOE curve width was based on the exponential fit to both sides of the SOE curve. For the scatterplot shown in (B), when a side of the exponential fit to the SOE curve did not drop to the 80% amplitude level, within the limit of the array, the width was set to the limit of the array in either the apical or basal direction. EDP indicates excitation density profile; SOE, spread of excitation.

4.4. Discussion

In a departure from the current thinking about SOE curves, we show that the SOE curve represents a convolution of two excitation areas, one originating from the masker and the other from the probe. It was suggested that deconvolution of the SOE curve would therefore yield the neural excitation areas at the electrode level. Since the SOE curve could not provide all the requisite information for direct deconvolution, we opted to use a modeling approach to solve this problem. Our deconvolution paradigm for SOE curves showed that the EDP at electrode level should, preferably, have a sloped side (Figures 4.5 and 4.6), and express a nonuniform pattern along the electrode array. In most cases, the EDP was broad in the apex and narrower at the base (Figure 4.7), especially if the mSOE curves are asymmetrical. The broader apical EDPs now provide an explanation for the asymmetry in SOE curve toward the apex, as well as the higher eCAP amplitudes found for apical stimulation (Figure 4.4).

4.4.1. Processing of SOE curves

Our provision of an explanation for the asymmetry in SOE recordings is a breakthrough in the field of objective measurements using CIs. So far, the asymmetry in the SOE curve along the electrode array has been frequently noted, but never quantified in detail (Cohen 2009; Cohen et al. 2003; Hughes & Stille 2010; Hughes & Abbas 2006b). This asymmetry has presented a major obstacle in the clinical application of SOE curves, where the width of the curve is used to estimate longitudinal neural excitation spread in the cochlea (Hughes & Abbas 2006b; Snel-Bongers et al. 2012; van der Beek et al. 2012; Cohen et al. 2003). The asymmetry of the SOE curve has led to obvious confusion in estimating its width. To counter this, multiple groups have chosen to estimate SOE width at a set percentage of peak amplitude, ranging from 50% (Cohen et al. 2003), to 60% (van der Beek et al. 2012) and 75% (Abbas et al. 2004; Hughes & Abbas 2006a; Snel-Bongers et al. 2012; Busby et al. 2008). To confuse matters further, SOE curve widths have been calculated using different methods, using linear interpolation between the data points (Abbas et al. 2004; Hughes & Abbas 2006b), an exponential fit to the sides of the SOE curve (Cohen et al. 2003) or a polynomial fit to the SOE curve (van der Beek et al. 2012). In cases where the minimum value of the SOE curve did not drop to the defined percentage of peak amplitude, the width could not be calculated. Alternatively the width was set to the limit of the array in the apical or basal direction (Abbas et al. 2004; van der Beek et al. 2012), or it was calculated using a virtual range outside of the limit of the electrode array (Cohen et al. 2003; Cohen 2009). Taken together, research in this field over the last decade has adopted multiple methodologies with which to estimate the SOE curve width, and therewith SOE. In contrast, the deconvolution method that we present, can handle any SOE curve, the method does not require preprocessing of the SOE curve, and the EDP can even be calculated in the absence of an SOE curve for a particular electrode.

4.4.2. EDP shape and SOE preprocessing

The results in Figures 4.5 and 4.6 show that when the EDP has sloped sides the pSOE is more accurate. This confirms our expectations that proximity to the electrode contact maximizes excitation density, which then declines to zero at larger distances. In addition, previous research has suggested the importance of sloped sides in deriving SOE curves or excitation areas (Cohen et al. 2003; Vanpoucke et al. 2004; Smit et al. 2009; Kalkman et al. 2015). Sloped sides are major contributors to the total excitation area and, due to convolution, to the SOE curve. We found that a shallower decay could be compensated for by a smaller plateau width (Figure 4.7). The absence of sloped sides (as with rectangular EDPs) resulted in a poorer fit of pSOE to mSOE recordings (Figure 4.6).

Although supplemental parameters will make the fit more accurate, the method will become less intuitive, the outcome less valid and the calculations more time consuming. Therefore, we explicitly chose for as few parameters as possible but still providing reliable pSOEs. To reduce the parameter set, we opted to only use symmetric EDPs, based on the model findings of Kalkman et al. (2015) who showed that asymmetry in the EDPs is not evident. Using symmetric EDPs, we can now explain that asymmetric SOE curves do not necessarily also imply asymmetric EDPs, although it is still possible that the actual EDPs will show asymmetry.

Evaluating the effect of the different preprocessing methods for SOE curves, it became clear that the deconvolution of normalized SOE curves provided less reliable EDPs (Figure 4.5). In other words, eCAP amplitude information is required for calculating the EDP. This result indicates that there is a link between eCAP amplitude and EDP, which is confirmed by our finding of a significant correlation between eCAP amplitude and area under the EDP. Assuming that our method is correct, our results show that SOE curves should not be normalized, which is frequently done (Hughes & Abbas 2006b; van der Beek et al. 2012; Abbas et al. 2004). Deconvolution of denoised SOE curves did not lead to smaller RMSEs and therefore more reliable EDPs, which can be explained by the noise-offset parameters (see Equation 4.2) that have already corrected for noise level.

4.4.3. Size of EDP

The width of the EDPs provides a novel, potentially more authentic, measure of SOE. One of the main results of this study is that the size of the EDP is not uniform along the electrode array. In multiple subjects, the EDP width decreased in the apical to basal trajectory (Figure 4.7). The described relationship between EDP size and asymmetry, indicates that asymmetry along the electrode array (with a shoulder at the apical side) can be explained by broader excitation areas in the apical versus basal part of the cochlea. This explanation has been suggested earlier (van der Beek et al. 2012; Hughes & Abbas 2006b), and is now confirmed here. The broader EDPs in the apical part of the cochlea could also be explained by the geometry of the cochlea, which tapers from the base to apex, reducing the distance to the modiolus, and reducing the volume in the apex (Cohen et al. 2003; Hughes & Abbas 2006b; van der Beek et al. 2012; Frijns et al. 2001). Because we are not able to distinguish cross-turn stimulation, it is also possible that a larger SOE, and broader EDPs apically, could be caused by cross-turn stimulation, which is known to be more likely at the apex where the cochlea is more tightly coiled (Frijns et al. 2001). In Addition, residual hearing could generate larger eCAPs and broader EDPs in the apex.

4.4.4. EDP width versus SOE curve width

To evaluate our measure of SOE in the light of more conventional methodologies, we compared the width of the EDP with two different SOE curve widths (Figure 4.9). Only the scatter plot in Figure 4.9B showed a significant correlation. However, it should be noted that the method for estimating the SOE curve widths mixed two measures of SOE (Abbas et al. 2004; van der Beek et al. 2012). The setting of the SOE curve width to the limit of the array (in either the apical or basal direction) where one side of the exponential fit to the SOE curve fails to drop to the 80% amplitude level (within the limit of the array), results in an underestimate of SOE curve widths. These underestimates have, hitherto, been assumed to represent the real SOE curve widths. So, taking into account the low explained variance of this correlation, we conclude that the EDPs we provide constitute a qualitatively different measure of SOE compared to those generated previously.

4.4.5. Deconvolution of SOE curves for clinical practice

Current results indicate that the deconvolution of SOE curves into EDPs has potential for clinical practice. The EDPs provide a measure of neural excitation at the electrode level and thereby provides new insights into eCAP and spatial selectivity. An additional benefit is that the deconvolution method can provide a measure of SOE, even when the SOE curve of that electrode is unavailable. In principle, it is possible to derive the EDPs for all electrodes by the deconvolution of one SOE curve. However, the reliability of derived EDPs increases considerably when multiple SOE curves are analyzed. Increasing the data set reduces noise and including SOE curves measured across the full range (apical, middle, basal) of the electrode array will better reflect the EDPs with respect to location. The measurement of a whole SOE curve for each electrode can be time consuming. To reduce measuring time, duplicate recordings of identical stimulus conditions can be avoided. For instance, when measuring a SOE curve with variable masker, the probe frame is independent from the masker location and can be reused for all eCAPs measurements. To reduce the amount of noise in the recordings, the reused frames can be measured with twice the number of averages. Using this option, we are able to measure 16 SOE curves intraoperatively in 10 minutes.

4.4.6. Future directions

Thus far, our simple deconvolution method has fulfilled its purpose as a proof of principle function. In future study, the model can be improved to increase reliability. An obvious start point is to correct for the recording contact. This would be a major step forward as it was found that apical recordings shift the flank of the SOE curve apically, and basal recordings, basally (van der Beek et al. 2012). Alternatively, the EDPs can be optimized

to better reflect the authentic SOE; for instance, taking into account asymmetry, neural survival and current spread in the scala tympani. Furthermore, we will extend our dataset using intra- and postoperative measurements. The addition of data for speech perception and postoperative imaging in the same subjects will enable us to evaluate the clinical relevance of our deconvolution methodology.

4.5. Conclusions

This study shows that eCAP based SOE curves, measured with FM, can be seen as a convolution of the EDPs of masker and probe. The poor fit achieved for the measured and modeled data using the rectangular EDP, emphasizes the requirement for a sloping excitation area to mimic actual SOE recordings. The deconvolution method explains the frequently observed asymmetric SOE curves along the electrode array; these are a consequence of a wider excitation area in the apical part of the cochlea. In other words, it demonstrates that asymmetric SOE curves do not necessarily also imply asymmetric EDPs, although it is still possible that the actual EDPs show asymmetry. In addition, the broader EDPs in the apex can explain the higher eCAP amplitudes found for apical stimulation.

CHAPTER

5

The effect of stimulus level on excitation patterns of individual electrode contacts in cochlear implants

Jan Dirk Biesheuvel, Jeroen J. Briaire, Randy K. Kalkman, Johan H. M. Frijns

Hearing Research, 2022, volume 420, 108490

Objective: Spread of excitation (SOE) in cochlear implants (CI) is a measure linked to the specificity of the electrode-neuron interface. The SOE can be estimated objectively by electrically evoked compound action potential (eCAP) measurements, recorded with the forward-masking paradigm in CI recipients. The eCAP amplitude can be plotted as a function of the roving masker, resulting in a spatial forward masking (SFM) curve. The eCAP amplitudes presented in the SFM curves, however, reflect an interaction between a masker and probe stimulus, making the SFM curves less reliable for examining SOE effects at the level of individual electrode contacts. To counter this, our previously published deconvolution method estimates the SOE at the electrode level by deconvolving the SFM curves (Biesheuvel et al., 2016). The aim of this study was to investigate the effect of stimulus level on the SOE of individual electrode contacts by using SFM curves analyzed with our deconvolution method.

Design: Following the deconvolution method, theoretical SFM curves were calculated by the convolution of parameterized excitation density profiles (EDP) attributable to masker and probe stimuli. These SFM curves were subsequently fitted to SFM curves from CI recipients by iteratively adjusting the EDPs. We first improved the EDP parameterization to account for stimulus-level effects and validated this updated parameterization by comparing the EDPs to simulated excitation density profiles (sEDP) from our computational model of the human cochlea. Secondly, we analyzed SFM curves recorded with varying probe stimulus level in 24 patients, all implanted with a HiFocus Mid-Scala electrode array. With the deconvolution method extended to account for stimulus level effects, the SFM curves measured with varying probe stimulus levels were converted into EDPs to elucidate the effects of stimulus level on the SOE.

Results: The updated EDP parameterization was in good agreement with the sEDPs from the computational model. Using the extended deconvolution method, we found that higher stimulus levels caused significant widening of EDPs ($p < 0.001$). The stimulus level also affected the EDP amplitude ($p < 0.001$) and the center of excitation ($p < 0.05$). Concerning the raw SFM curves, an increase in current level led to higher SFM curve amplitudes ($p < 0.001$), while the width of the SFM curves did not change significantly ($p = 0.62$).

Conclusion: The extended deconvolution method enabled us to study the effect of stimulus level on excitation areas in an objective way, as the EDP parameterization was in good agreement with sEDPs from our computational model. The analysis of SFM curves provided new insights into the effect of the stimulus level on SOE. We found that the EDPs, and therefore the SOE, mainly became wider when the stimulus level increased. Lastly, the comparison of the EDP parameterization with simulations in our computation model provided new insights about the validity of the deconvolution method.

Abstract

5.1. Introduction

Modern cochlear implants (CI) are multi-channel devices with multiple electrode contacts on the electrode array. Taking advantage of the tonotopic organization of the cochlea, these different electrode contacts can provide different pitch percepts to the CI recipient (Bonham & Litvak 2008). In practice, however, it can be difficult or even impossible to discriminate sounds produced by two adjacent electrode contacts (Biesheuvel et al. 2019a). A likely explanation for this phenomenon is the relatively large overlap between excitation areas of adjacent electrode contacts (Bierer & Litvak 2016). Previous research has shown that the overlap in excitation areas can be estimated objectively using electrically evoked compound action potentials (eCAP) generated by the auditory neurons (Abbas et al. 1999). When measured via the forward-masking paradigm with fixed probe and roving masker stimulus contacts, the eCAP amplitude can be plotted as a function of the position of the masker contact, leading to the well-known spatial forward-masking (SFM) curve (Abbas et al., 1999; Cohen et al., 2003; Hughes and Abbas, 2006; van der Beek et al., 2012). However, the eCAP amplitudes presented in the SFM curve reflect an interaction between a masker and probe stimulus, making the SFM curve less reliable for examining excitation patterns or spread of excitation (SOE) attributable to individual electrode contacts. To overcome this problem, we developed a deconvolution method that translated SFM curves into excitation patterns attributable to the individual masker and probe stimuli (Biesheuvel et al. 2016). The aim of this study was to investigate the effect of stimulus level on the SOE of individual electrode contacts.

Several studies have investigated the effects of current level on SFM curves. Cohen et al. (2004) reported that the widths of the SFM curves did not vary significantly with probe stimulus current, while the amplitudes of the curves varied systematically with stimulus level. Van der Beek et al. (2012) also did not find a statistically significant effect of stimulus level on the width of the SFM curves. Although some subjects showed a change in curve width with changing stimulus level, the majority of their subjects had SFM curves of similar widths at different stimulus levels. Looking at individual subjects, Hughes & Stille (2010) concluded that stimulus level has a significant effect on the width of the SFM curve. However, across all subjects, significant stimulus level effects were observed in only 34% of the cases. Lastly, Abbas et al. (2004) presented SFM curves with, in most subjects, a clear growth in eCAP amplitude and a tendency to become wider at higher stimulus levels. They suggested that the higher amplitudes were caused by more overlap in neurons excited by the masker and probe and that the increased width of the SFM curve could be partially attributed to an increased SOE. However, it is still unknown whether this increase in SOE is reflected by a higher excitation density (i.e., more excited nerve fibers locally) or

by a wider spread along the electrode array, nor it is known whether it comes from the masker or the probe.

Most studies estimated SOE by determining the width of the SFM curve at a specific amplitude level (Cohen et al. 2003; Abbas et al. 2004; Hughes & Abbas 2006a; Snel-Bongers et al. 2012; van der Beek et al. 2012). However, the width of a SFM curve is difficult to analyze if the curve is not complete, especially at the apical and basal ends of the electrode array (Biesheuvel et al. 2016). Furthermore, a SFM curve reflects the interaction between a probe and masker stimulus, but the width of such a curve cannot reveal the individual contribution of each of the two stimuli. We developed a method to process SFM curves into so-called excitation density profiles (EDP) for individual electrode contacts using mathematical convolution (Biesheuvel et al. 2016). An EDP, depicted in Figure 5.1A, reflects the proportion of excited neurons as a function of location along the electrode array. The deconvolution is performed using an iterative process. In the basis, parameterized EDPs (reflecting masker and probe excitation areas) are convolved to generate predicted SFM curves. Next, the predicted SFM curves are fitted to measured SFM curves (in CI recipients) by iteratively adjusting the EDPs. After many iterations, the method results in EDPs and SFM curves that predict the measured SFM curves quite well. A similar method has been presented by Cosentino et al. (2016, 2015), who analyzed SFM curves using matrix algebra and Gaussian functions, also called the panoramic eCAP method. In our previous study, the EDPs were kept as simple as possible to clearly demonstrate the principle of (de) convolution (Biesheuvel et al. 2016). When using the deconvolution method to study stimulus-level effects on SOE, we have to verify whether our EDP parameterization is suitable for that purpose. As in most parameterizations, defining the optimal number of EDP parameters is a challenging task; too few parameters could lead to a suboptimal representation of the excitation area, while too many parameters likely result in a good fit between the predicted and measured SFM curves but produce non-physiological EDPs. We have considered which EDP parameterizations were relevant for studying stimulus-level effects. First of all, we think that the EDPs must be able to get smaller and narrower with lower stimulus levels. This property has already been realized in the original parameterization, where the EDP width can be adjusted at the top of the Gaussian and the EDP amplitude is linked to the width parameter (Biesheuvel et al. 2016). Based on the literature, we think there are two other useful parameterizations: (1) allowing variation in the center of excitation, and (2) allowing a gradual change in the slopes of the excitation pattern. The rationale for allowing some variation in the center of excitation is that studies have found an effect of stimulation level on perceived pitch (Shannon 1983; Townshend et al. 1987; Arnoldner et al. 2006; Carlyon et al. 2010), and that pitch might be determined

by the centroid of the excitation area (McKay et al. 1999; Laneau et al. 2004; McDermott & McKay 2005). Kalkman et al. (2014) studied place pitch versus electrode location in a computational model of the implanted human cochlea; they found that the elicited pitch of electrode contacts after the first turn decreases as stimulus level increases. So, the above-mentioned studies indicate that an extra parameter that allows a shift in the center of the EDP might be useful. In a subsequent study, Kalkman et al. (2015) added spatial variability of the auditory nerve fibers' cell bodies to the model and examined neural excitation using excitation density curves. They found that the excitation density was lower at lower stimulus levels and spanned a shorter length along the cochlea. Their simulations further showed that the sides or edges of the excitation areas changed slightly with changing stimulus level: the density decay may be steeper or shallower. To include these effects in the EDP parameterization, we wanted to allow a gradual change in the sides of the EDPs.

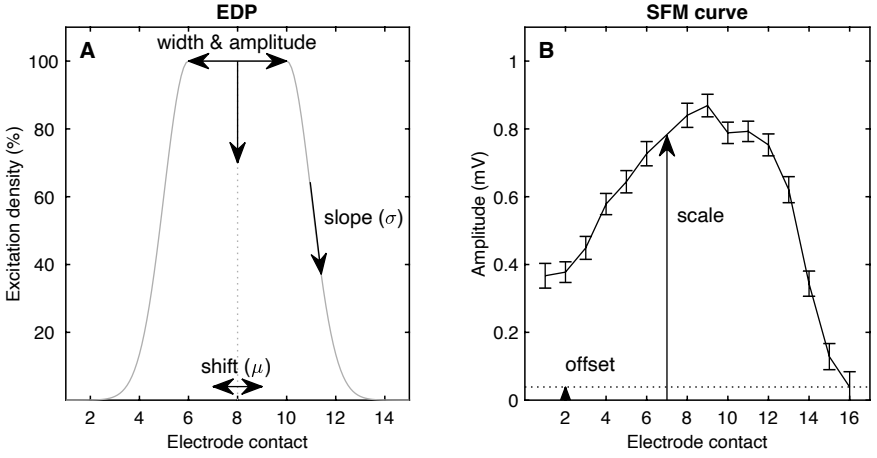

Figure 5.1. Overview of the parameters included in the deconvolution method. The panel left shows an EDP and the panel right shows an SFM curve including the measurement error of the eCAP amplitudes. EDP indicates excitation density profile; SFM, spatial forward masking; eCAP, electrically evoked compound action potential.

The main goal of this study was to examine the effect of stimulus level on SOE by using the deconvolution method (Biesheuvel et al. 2016). Our hypothesis was that the SOE is narrower at lower stimulus levels. The rationale for this hypothesis was that excitation density simulations in our computational model showed narrower SOE at lower current level (Kalkman et al. 2015). Furthermore, the cell bodies are approximately positioned in a row in Rosenthal's canal. In that case, we expect using the physics of current spread that less stimulation would lead to narrower excitation areas, followed by less excitation density. We needed two stages to study our hypothesis. In the first stage, we had to improve the EDP parameterization to account for stimulus level effects. In the absence of exact

information on real neural excitation patterns, we used the output of our computational model to validate the EDP parameterization (Kalkman et al. 2014; Kalkman et al. 2015). In this model, we can study the effect of stimulus level with the simulated excitation density, which strongly resembles the EDP from the deconvolution method (conceptually both describe the proportion of excited neurons along the electrode array). Henceforth the simulated excitation densities from the computational model were indicated with sEDP. In the second stage of this study, we measured SFM curves in human subjects and applied the deconvolution method to these SFM curves. For each subject, two sets of SFM curves were collected. The first set consisted of SFM curves measured at electrode contact 3 through 16 with both masker and probe stimulus levels at 1200 μA, henceforth indicated as SFM_{1200}. The second set consists of SFM curves measured at electrode contact 3 (apex), 9 (middle) and 15 (base), with a masker level of 1200 μA and probe levels ranging from 600 to 1100 μA, indicated as $SFM_{600\text{-}1100}$. Subsequently, the SFM curves of each subject were all together deconvolved into EDPs, revealing the SOE at individual electrode contacts and at different current levels of that subject.

5.2. Updating the EDP parameterization

5.2.1. Materials and methods

5.2.1.1. Parameterization of EDPs

Essentially, an EDP is a Gaussian function extended with other parameters to reflect excitation density. The original deconvolution method included 19 variables to estimate the EDPs across the electrode array of a subject; 16 variables for the EDP plateau width and amplitude at each electrode contact, one variable for the EDP slope at all contacts (the slope depicts the density decay represented by the σ of the Gaussian function), one scaling variable to scale all predicted SFM curves to the measured SFM curves, and one variable as offset for the predicted SFM curves representing the noise floor (see also Figure 5.1) (Biesheuvel et al. 2016).

For studying stimulus level effects, the parameterization of the EDP width, the scaling factor and the offset parameter remained unchanged. The EDP slope was implemented slightly differently and a shift in the center of the EDPs (represented by the μ of the Gaussian function) was added. The shift and slope parametrization accounting for stimulus level effects was only applied on contact 3, 9 and 15, for which $SFM_{600\text{-}1100}$ curves were collected as well. The slope and shift parameters were estimated at probe stimulus levels of 600 μA and 1200 μA and the intermediate stimulus levels were estimated using linear interpolation. Interpolation between the most extreme values 600 μA and 1200 μA is most robust. The interpolation limited the number of additional EDP parameters, and

we did not expect large differences in slope and shift of EDPs obtained with succeeding stimulus levels at fixed electrode sites.

In more detail, we defined two EDP slope parameters: (1) $slope_{1200}$, which estimated the slope at 1200 μA for all EDPs across the electrode array, and (2) $slope_{600}$, which estimated the slope of the EDPs at 600 μA. The fitting range of both slope parameters was [0.1 to 6] and it had no unit. Subsequently, the EDP slope at the current levels between 600 μA and 1200 μA was estimated using linear interpolation. Regarding the relative shift in the center of excitation caused by the stimulus level, we assumed that the shift occurs at the higher stimulus levels because of deeper excitation in the spiral ganglion, while there is no shift at the lower current levels. The shift was represented by two parameters: (1) $threshold_{shift}$, which estimated the current level where the shift was zero, and (2) $shift_{1200}$, which estimated the shift of the EDP at the 1200 μA level. The fitting range of $threshold_{shift}$ was [0 to 600] μA and the range of $shift_{1200}$ was [−1 to +1] electrode contacts. Subsequently, the shift as a function of stimulus level was defined as a linear relationship between the points ($threshold_{shift}$ μA; 0 electrode contacts) and (1200 μA; $shift_{1200}$ electrode contacts). To avoid unrealistic shift in the EDPs across the electrode array, for example, a +1 shift at contact 9 and no shift at contact 10, the shift in the EDPs across the electrode array was estimated using a polynomial function. Given that the degree of the polynomial is limited by the number of data points, we could fit first- and second-order polynomials using the three $shift_{1200}$ values at contacts 3, 9, and 15. An overview of the final EDP parameterizations is shown in Table 5.1.

Table 5.1. Summary of the EDP-parameters per subject. EDP indicates excitation density profile.

	Parameterizations	
	EDP_{1200}	**$EDP_{600\text{-}1100}$**
Width	16 *	6 #
Offset	1	-
Scale	1	-
Density decay (σ)	1	1
Shift (μ)	3	1
Total	22	8 ‡

* Equal to the number of involved electrode contacts across the array.
\# Equal to the number of involved current levels.
‡ Per electrode contact. For example, if $EDP_{600\text{-}1100}$ estimations were obtained at all contacts of interest (3, 9, 15), a total of $22 + 3 \times 8 = 46$ parameters had to be optimized.

5.2.1.2. Computational model of the human cochlea

The updated EDP parameterization was validated using excitation density simulations in our computational model of the implanted human cochlea, developed at the Leiden

University Medical Centre (J.J. Briaire and Frijns, 2000; J.J. Briaire and Frijns, 2000; Frijns et al., 2000, 1995; Kalkman et al., 2020, 2015, 2014). The model consists of two parts: a volume conduction model and a deterministic active nerve fiber model. The volume conduction model uses the boundary element method to simulate electrical potential distributions in a realistic three-dimensional geometry of a human cochlea implanted with a CI electrode array. Next, electrical potentials are determined along nerve fiber trajectories that have been defined in the cochlear geometry with the help of histological data. The nerve fiber model then simulates neural responses resulting from the electrical potential fields generated by the volume conduction model, by modeling each auditory neuron as an active double-cable electrical network using the human-based Schwarz-Reid-Bostock neural kinetics scheme (Schwarz et al. 1995; Kalkman et al. 2022).

In humans, there is a high variability in neural responses. The actual eCAP-data to be measured depend on both the electric potential distribution and the neural activity. The electric potential distribution in the scala tympany is quite broad but uniform across subjects, while the neural activity is highly variable across subjects, depending on the neural survival and neural interactions (Tang et al. 2011). To create a realistic validation model, we simulated excitation density profiles, denoted as sEDPs, at different probe current levels using five different cochlear geometries each modeled with three different states of neural health. Each cochlear geometry contained a representation of a HiFocus Mid-Scala electrode array with sixteen electrode contacts in ideal mid-scalar position. Three sets of 3200 auditory neurons were modeled for each geometry, each representing a different state of neural health: one set of intact nerve fibers, one set of fibers where the lengths of the unmyelinated peripheral terminal nodes were shortened from 10 µm to 1 µm, and one set of fibers from which the peripheral processes were completely removed. The peripheral processes of the intact neurons were spread out evenly along the basilar membrane (BM) and their cell bodies were spatially distributed along Rosenthal's canal in the manner described by Kalkman et al. (2015). The stimuli used in the neural simulations were anodic-first biphasic pulses with 32 µs phase duration. At electrode contact 3, 9 and 15, the stimulus amplitude ranged from 600 µA to 1200 µA in steps of 100 µA, and at the other contacts across the electrode array the stimulus amplitude was 1200 µA. The excitation density results from the neural model were processed into sEDPs, which show the excitation density as a function of cochlear position along the BM. Excitation density was defined as the percentage of excited neurons along 1 mm segments of the BM, centered at the positions of the tips of the peripheral processes of each modeled neuron. For the degenerated nerve fibers, excitation densities were determined as if the neurons still retained their peripheral processes. Further details of the computational model are discussed by Kalkman et al. (2015, 2014).

5.2.1.3. Analysis

In order to validate the EDP parameterization, we analyzed how well the EDPs could fit the sEDPs using the updated parameterization. To increase the sEDP variability and to strengthen the validation, the sEDPs were simulated in five different cochleae, each modeled with three neural states. The sEDPs at electrode contact 1, 2 and 16 were excluded from the analysis, because these sEDPs at the distal electrode contacts were often irregular (contact 1 and 2) or incomplete (contact 16) and fitting the EDPs to these sEDPs would lead to large fitting errors. The irregularities in sEDPs at contact 1 and 2 are likely caused by cross-turn stimulation in the apex and the sEDPs at contact 16 were often incomplete, as their simulation was hindered by the boundaries of the cochlea model, which basally ends at the round window. Moreover, the sEDPs at contact 1, 2 and 16 were strictly not necessary for validating the EDP parameterization to account for stimulus level effects on contact 3, 9 and 15. On the remaining electrode contacts (3 to 15), still 43 sEDPs (9%) were incomplete, e.g., at contact 14 or 15, and 43 sEDPs (9%) at lower stimulus levels did not show any excitation. These sEDPs did not lead to a unique solution and they were also excluded in the validation. We fitted EDPs to the remaining 379 sEDPs and calculated the similarity between each EDP and sEDP using the Jaccard index, which was defined as:

$$J(sEDP, EDP) = \frac{|sEDP \cap EDP|}{|sEDP \cup EDP|} \quad [5.1]$$

The symbols ∩ and ∪ represent, respectively, the intersection and union of the sEDP and EDP. We compared the sEDPs and EDPs with respect to their slope (density decay at the sides of the EDP), full width at half maximum (FWHM), and the shift in excitation center using Bland-Altman plots and mountain plots (Giavarina 2015). In a Bland-Altman plot, the difference between two variables is plotted as function of their average. A mountain plot is a complementary representation of the difference plot. It shows the distribution of the differences by computing a percentile (p) for each ranked difference. The difference is plotted as function of p while $p < 50$, and otherwise as 100–p. Based on the outcomes from the Jaccard index, the Bland-Altman plots, and the mountain plots, we improved the EDP parameterization step by step, resulting in the parameterization as described in section 5.2.1.1.

5.2.2. Results

Figure 5.2 shows an example of sEDPs from the computational model using different current levels (gray lines). The sEDPs originated from electrode contact 9 in cochlea model 4 with completely degenerated dendrites. When we fitted the EDP as parametrized conform our 2016 paper to these sEDPs, it turned out that there was a clear mismatch between the sEDPs and EDPs (panel A). This showed that an EDP parameterization update was

necessary. After optimizing the EDP parametrization, we calculated the similarity between the sEDPs and fitted EDPs using equation 5.1. Across all cochlea models, the similarity between the sEDPs and fitted EDPs increased from an 84.0% median (10th percentile: 69.1%, 90th percentile: 95.0%) using the 2016 parameterization, to a 92.2% median (10th percentile: 82.3%, 90th percentile: 96.5%) when using the new parameterization. Figure 5.2B shows that with the new parameterization the EDPs fitted much better to the sEDPs than in Figure 5.2A.

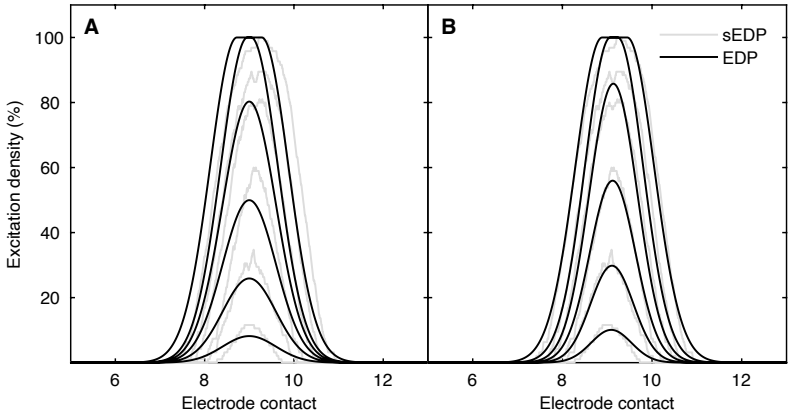

Figure 5.2. Example of sEDPs (gray) and EDPs (black), both showing the excitation density along the basilar membrane. Panel A shows that the original EDPs, which were parameterized conform our 2016 paper, did not optimally fit to the sEDPs obtained at different current levels. Panel B shows that the updated EDPs, which account for stimulus level effects, fitted the sEDPs much better. EDP indicates excitation density profile; sEDP, simulated excitation density profile.

In Figure 5.3, we evaluated the updated EDP parametrization by comparing the EDPs with the sEDPs. We fitted EDPs to the sEDPs and explored the differences with respect to the slope (i.e., density decay at the sides of the EDP), full width at half maximum (FWHM), and the shift in excitation center. Each data point represents a single EDP comparison modelled in a specific cochlea and neural condition. Note that the differences on the y-axes were calculated as sEDP minus EDP and that data presented in this figure are the final results after optimizing the EDP parameterization. None of the differences plotted in panel A, C and E came from a normal distribution, as revealed by the Anderson-Darling test for normal distribution. Therefore, percentiles rather than the regular means and 95% confidence bounds are shown in the Bland-Altman plots. To gain more insight, the EDP_{1200} data (blue) and $EDP_{600\text{-}1100}$ data (red) were plotted separately. Panel A shows that the slope of the $EDP_{600\text{-}1100}$ patterns differed from EDP_{1200} ones, which argued for allowing the slope to change towards lower current levels. Panel C confirms the importance of a width parameter, as it shows that the width of both the $EDP_{600\text{-}1100}$ and EDP_{1200} patterns varies

highly across the different cochleae and neural conditions. Panel E shows that the center of excitation of the sEDPs varied between –0.47 and 0.23 electrode contacts, indicating that the parameterization of the shift was useful as well. The mountain plots at the right side of Figure 5.3 show that for most EDPs the difference from the sEDPs was small; the peak of the mountain plot is steep around 0. Note that we rotated the mountain plot 90° clockwise to align the y-axes of the Bland-Altman and mountain plots.

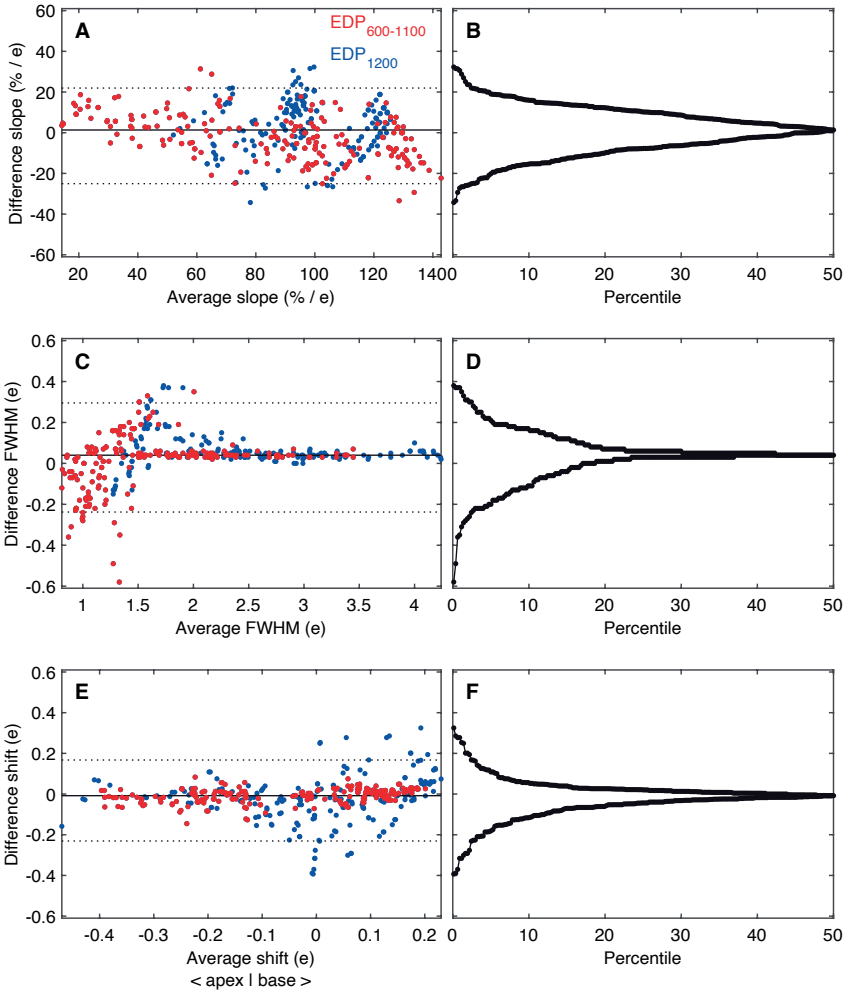

Figure 5.3. Quantitative analysis showing how well the updated EDP parameterization could fit sEDPs simulated at different current levels in five different cochleae and three different neural states. The panels at the left side represents Bland-Altman plots, in which the difference between an sEDPs and EDP parameter (y-axis) was plotted as a function of its average (x-axis). Each dot represents the result of fitting an EDP to a sEDP, whereby the EDP1200 data (blue) and the $EDP_{600\text{-}1100}$ data (red) were plotted separately. The slope (panel A) is calculated using the density decay between 40 and 60% of the maximum EDP amplitude. The black solid line shows the median and the dashed lines show the 2.5 and 97.5 percentiles. At the right side, mountain plots are plotted, wherein each ranked difference (y-axis) is plotted as function of percentile, or as 100-percentile if percentile > 50 (x-axis). EDP indicates excitation density profile; sEDP, simulated excitation density profile; e, electrode contact.

Based on the aforementioned outcomes, we assessed that the new EDP parameterization was suitable for the purpose of answering the aim of the study.

5.3. Analyzing human SFM curves

5.3.1. Materials and methods

5.3.1.1. Patients and data collection

The patient data consist of intraoperative SOE recordings from 24 CI recipients, collected in the period from April 2015 to March 2017. The demographics of these subjects are shown in Table 5.2. All subjects were implanted with a HiRes90K device with a HiFocus Mid-Scala electrode array from Advanced Bionics (Valencia, CA, USA). The electrode array contained 16 electrode contacts, numbered from apex (1) to base (16). The SFM curves were collected using the Bionic Ear Data Collection System (BEDCS) research software from Advanced Bionics, controlled by a custom-made MATLAB (Mathworks, Inc., Natick, MA) interface. The neural responses were measured using monopolar biphasic pulses (anodic first) with a duration of 32 μs per phase. The sampling rate of the eCAP recording system was 56 kHz and its gain 100. The SFM curves were recorded using the forward-masking paradigm with a fixed probe contact and roving masker (Cohen et al. 2003; Hughes 2013; Biesheuvel et al. 2016). The masker-probe stimulus interval was 500 μs and the recording contact was two electrodes away from the probe contact in the apical direction. To save time, the probe and signature frames were recorded once for each SFM curve, and they were reused in all eCAP measurements of that SFM curve. This was possible because the probe and signature frames are independent from the masker location. To reduce the amount of noise in the recordings, the reused frames were measured with 64 averages and the masker and masker-probe frames with 16 averages (Klop et al. 2009). The eCAPs were processed as described by Biesheuvel et al. (2016), followed by a visual check to avoid erroneous processing of abnormal eCAPs (double peaks, shallow P_2, etc.). In case of wrong peak detections, the peaks were corrected manually.

For each patient, two sets of SFM curves were collected. The first set consisted of SFM curves measured at probe contacts 3 through 16 with both masker and probe stimulus levels at 1200 μA. Note that no SFM_{1200} curves were measured for probe contacts 1 and 2 due to the requirement for an apically located recording contact. The second set consisted of SFM curves measured with a masker level of 1200 μA and different probe current levels. For most subjects, the probe current levels ranged from 600 to 1100 μA with a step size of 100 μA. For subjects S0125, S0126, and S0129, the probe current levels ranged from 600 to 1000 μA with a step size of 200 μA because of time limitation during surgery. The $SFM_{600\text{-}1100}$ curves were recorded at three probe contacts along the array: 3 (apex), 9 (middle), and

15 (base). In more than half of the patients, we could not measure the $SFM_{600-1100}$ curves on all three probe contacts (see Table 5.2). The reasons were that sometimes there were time limitations during surgery, and sometimes the amplitudes of the SFM_{1200} curves were already so small (< 0.2 mV) that reliable measurement of $SFM_{600-1100}$ curves was not possible.

Table 5.2. Subject demographics. SFM indicates spatial forward masking.

				Measured electrode contacts			
	Gender	**Age (y)**	**Etiology**	**SFM_{1200} curves**	**$SFM_{600-1100}$ curves**		
S103	F	1	DFNB1	1-16	3	9	15
S106	F	12	Unknown	1-16			15
S107	M	3	Unknown	1-16	3		
S108	M	26	Rubella	2-9, 11-16		9	15
S112	M	3	Unknown	1-16	3	9	15
S114	M	55	Congenital	1-16	3	9	
S115	M	2	Unknown	1-9, 11-16	3	9	15
S116	M	2	Unknown	1-16	3	9	15
S119	F	20	Congenital	1-16	3	9	15
S121	F	12	Unknown	1-2, 4-16		9	15
S122	M	2	Unknown	1-16			15
S124	F	12	DFNB25	1-16	3		
S125	F	58	DFNA9	1-16	3		
S126	F	1	DFNB1	1-16	3	9	
S129	F	60	Congenital	1-16	3	9	
S133	M	60	Unknown	1-16	3		
S135	F	4	Congenital	1-16	3		15
S137	F	39	Unknown	1-16	3	9	15
S138	M	57	Unknown	1-16	3	9	15
S141	M	2	Unknown	1-16	3	9	15
S142	M	3	Usher	1-16	3	9	
S144	F	49	Unknown	1-16	3	9	
S147	M	1	DFNB1	1-16	3		15
S149	F	8	Congenital	1-16	3		
#24	#12 F	ȳ 21			#20	#15	#14

5.3.1.2. Deconvolution of SFM curves

The SFM curves were analyzed according to the deconvolution method of Biesheuvel et al. (2016), using a custom MATLAB application. Note that, if the maximum amplitude from the SFM curves decreased below 0.15 mV, these SFM curves were not included for further analysis, since the low eCAP amplitudes and bad signal-to-noise ratio of these curves caused unreliable EDP estimations. Due to this, 44 SFM curves (15%) were not included for further analysis. For each subject, the SFM_{1200} and $SFM_{600-1100}$ curves were all deconvolved at the same time in one minimization routine. The SFM_{1200} curves were deconvolved into

EDP_{1200} patterns, reflecting the excitation areas of a 1200 μA stimulus at each electrode contact. Next, using the EDP_{1200} estimations as masker EDPs, the $SFM_{600\text{-}1100}$ curves were deconvolved into the probe $EDP_{600\text{-}1100}$ patterns.

5.3.1.3. Analysis

Linear mixed models (LMMs) were used to test the effects of current level and electrode contact on the $SFM_{600\text{-}1100}$ curves and $EDP_{600\text{-}1100}$ estimates. The variables of interest were the maximum amplitude of the SFM curves, the width of the SFM curves (i.e., FWHM), the amplitude of the EDPs, the width of the EDPs (FWHM) and the shift in the center of the EDPs. Note that, if a side of the SFM curve did not drop to the FWHM-level, the width of the curve was set to the limit of the array in the apical direction (contact 3), or in the basal direction (contact 15) (Abbas et al. 2004). The effect of current level and electrode contact on each of these variables was tested using separate models, including both current level and electrode contact as fixed effects, while subject was included as random effect. In addition, we repeated the EDP analyses on sEDPs as well in order to compare the human-based results with the output of the computational model. The output from the linear mixed models is displayed in Table 5.3.

5.3.2. Results

An example of the deconvolution of $SFM_{600\text{-}1100}$ curves is shown in Figure 5.4. The data were recorded at electrodes 3, 9, and 15 in subject S0119. The SFM curves in the upper half of the figure illustrate that an increase in stimulus level led to an increase in amplitude as well. No major change in the width of the SFM curves is visible as a result of changing the stimulus level. Deconvolution of the SFM curves resulted in the EDPs plotted directly underneath them, in the lower row of the figure. The area under all EDP curves became greater when the stimulus level grew, which implies that lower stimulus levels excited fewer neurons. However, the EDPs at electrode 3 mainly increased in amplitude, while the EDPs at electrode 9 and 15 became wider.

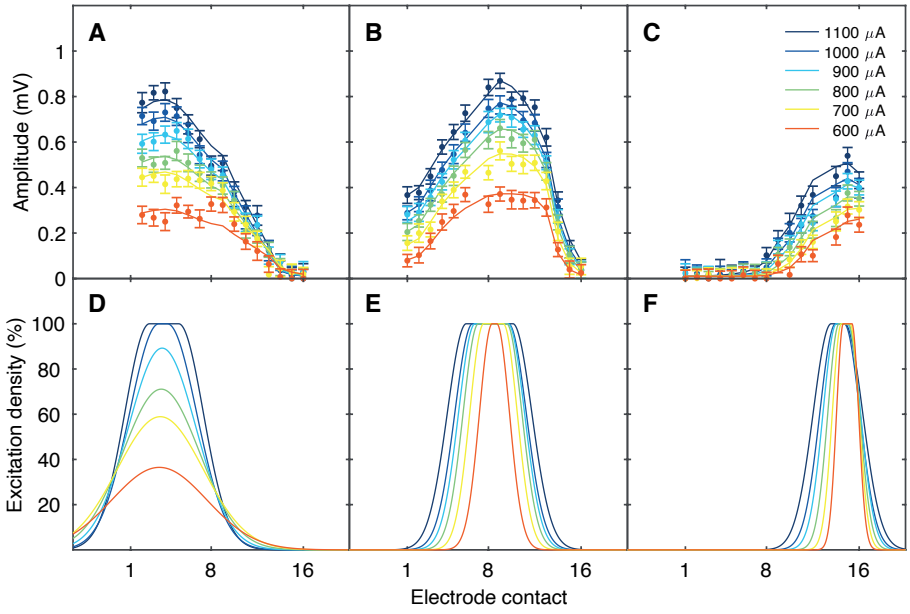

Figure 5.4. Example of SFM curves recorded at different probe stimulus levels on electrode contacts 3, 9 and 15 (respectively panel A, B and C) in subject S0119. The error bar represents the eCAP amplitude with measurement error and the color shade represents the descending probe current level. The deconvolution of these SFM curves resulted in the EDPs directly shown below the curves (panel D-F). SFM indicates spatial forward masking; eCAP, electrically evoked compound action potential; EDP, excitation density profile.

Figure 5.5 shows the effect of current level on all $EDP_{600\text{-}1100}$ series in more detail for all subjects. We plotted the area under the EDP, the amplitude, the FWHM, and the shift in center of excitation of each EDP as a function of stimulus level. In all cases, the area under the EDP became bigger with increasing current level (Figure 5.5A-C), which is consistent with more neurons being excited at higher current levels. The smaller EDPs at lower current levels are mainly caused by narrower EDPs (Figure 5.5G-I, increasing line towards higher current level) in combination with a still high EDP amplitude (Figure 5.5D-F, flat top line). In a few cases, an increasing current level led to greater EDP amplitudes in combination with a quite stable EDP width (Figure 5.5G-I, horizontal lines). Some lines in Figure 5.5G-I are v-shaped; the FHWM became smaller from 600 μA upwards, while from a certain point it became wider again. Such a result belongs to a case like in Figure 5.4D. At electrode contact 15, the current level mainly affected the EDP width and not the EDP amplitude (Figure 5.5F, most lines fall on top of each other). Furthermore, the effect of current level on the shift in center of excitation was variable across subjects and electrode contacts (Figure 5.5J-L). The LMM analyses revealed that, in general, the current level had a significant effect on the EDP amplitude ($p < 0.001$), on the EDP width ($p < 0.001$), and on the shift in EDP center ($p < 0.05$). More details from the LMMs can be found in Table 5.3.

We also compared the $EDP_{600\text{-}1100}$ outcomes with the effect of current level on the SFM curves and the sEDPs from the computational model. Figure 5.6 shows how the amplitude, FWHM and shift (if applicable) of the $EDP_{600\text{-}1100}$, $sEDP_{600\text{-}1100}$ and $SFM_{600\text{-}1100}$ curves changed as function of stimulus level. Observe that the sEDP amplitudes in Figure 5.6 panel A and C show an irregular pattern; they increased from 600 to 700 µA, decreased until 800 µA and then increased again. This effect is caused by some missing data at 600 and 700 µA, as some sEDPs did not show any excitation at the lowest stimulus levels. So, the remaining data at 600 and 700 µA came from model simulations with a relatively high excitation density at these levels. The LMM analyses showed that current level had a significant effect on the amplitude of the SFM curve ($p < 0.001$), while the FWHM of the SFM curve did not change significantly ($p = 0.62$). Concerning the sEDPs, the analysis shows that current level had a significant effect on the amplitude ($p < 0.001$) and the width ($p < 0.001$), but not on the shift ($p = 0.11$). See Table 5.3 for more details from the linear mixed-model analyses, including the effect of the electrode contact on the SOE.

Table 5.3. Output from the linear mixed model, analyzing the effect of stimulus level on the amplitude, width and shift of the excitation patterns. SFM indicates spatial forward masking; EDP, excitation density profile; sEDP, simulated excitation density profile.

		Electrode	**Current**
Amplitude	SFM_{IO} curve	$p = 6.47 \times 10^{-13}$ **	$p = 3.97 \times 10^{-50}$ **
Amplitude	EDP_{IO}	p = 0.20	$p = 2.54 \times 10^{-11}$ **
Amplitude	$sEDP_{IO}$	$p = 1.98 \times 10^{-7}$ **	$p = 9.37 \times 10^{-26}$ **
Width	SFM_{IO} curve	$p = 4.17 \times 10^{-20}$ **	p = 0.62
Width	EDP_{IO}	$p = 5.33 \times 10^{-13}$ **	$p = 2.58 \times 10^{-24}$ **
Width	$sEDP_{IO}$	$p = 5.91 \times 10^{-5}$ **	$p = 2.74 \times 10^{-70}$ **
Shift	EDP_{IO}	p = 0.14	$p = 3.80 \times 10^{-2}$ *
Shift	$sEDP_{IO}$	p = 0.66	p = 0.11

* $p < 0.05$; ** $p < 0.001$

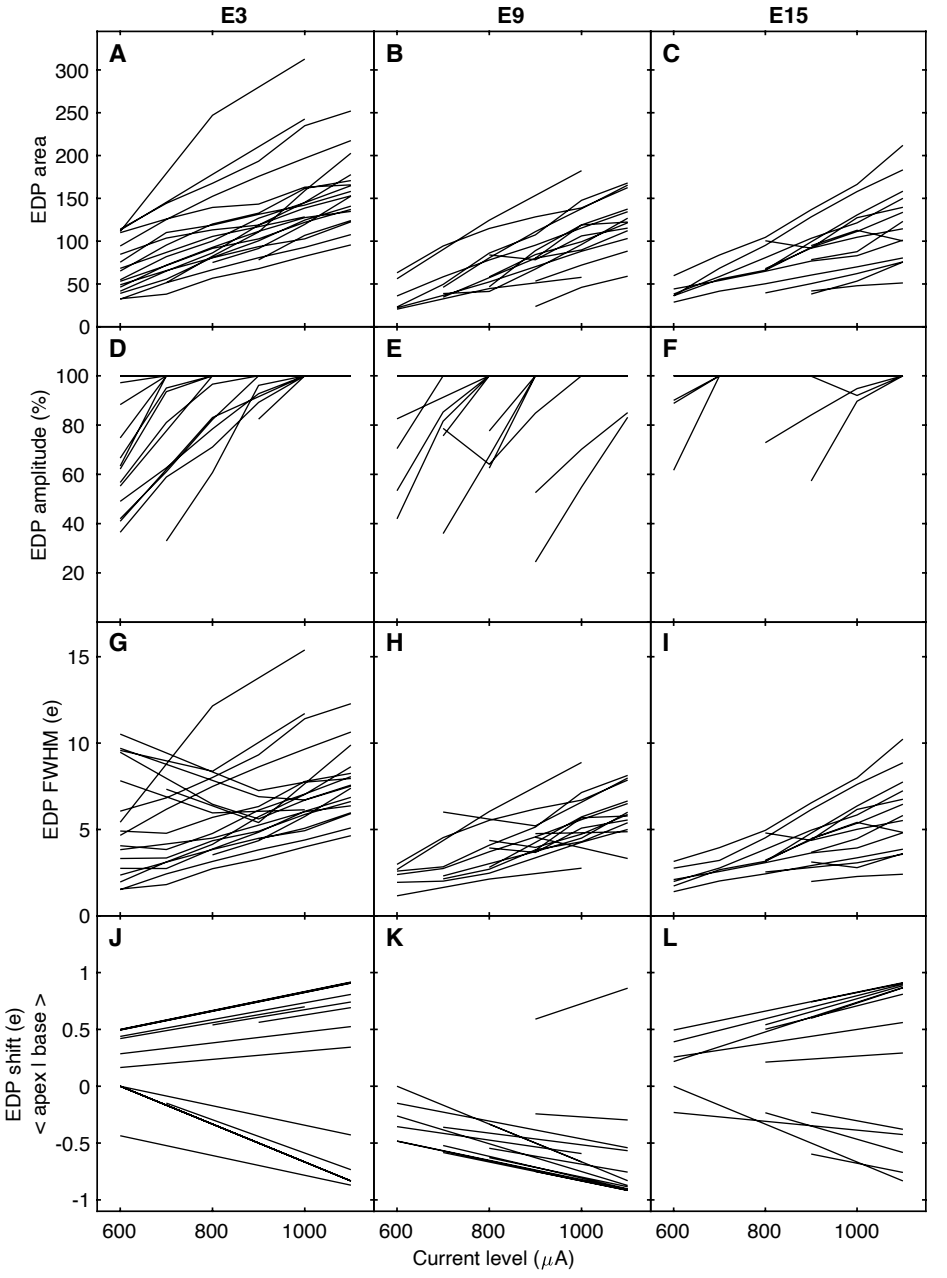

Figure 5.5. Effect of probe stimulus level on the EDPs. Each line represents a series of EDPs measured with varying probe current level in one subject. The columns show the results for electrode contacts 3, 9, and 15 separately. The rows show, respectively from top to bottom, the effect of stimulus level on the EDP area, EDP amplitude, EDP width, and EDP shift. EDP indicates excitation density profile; e, electrode contact.

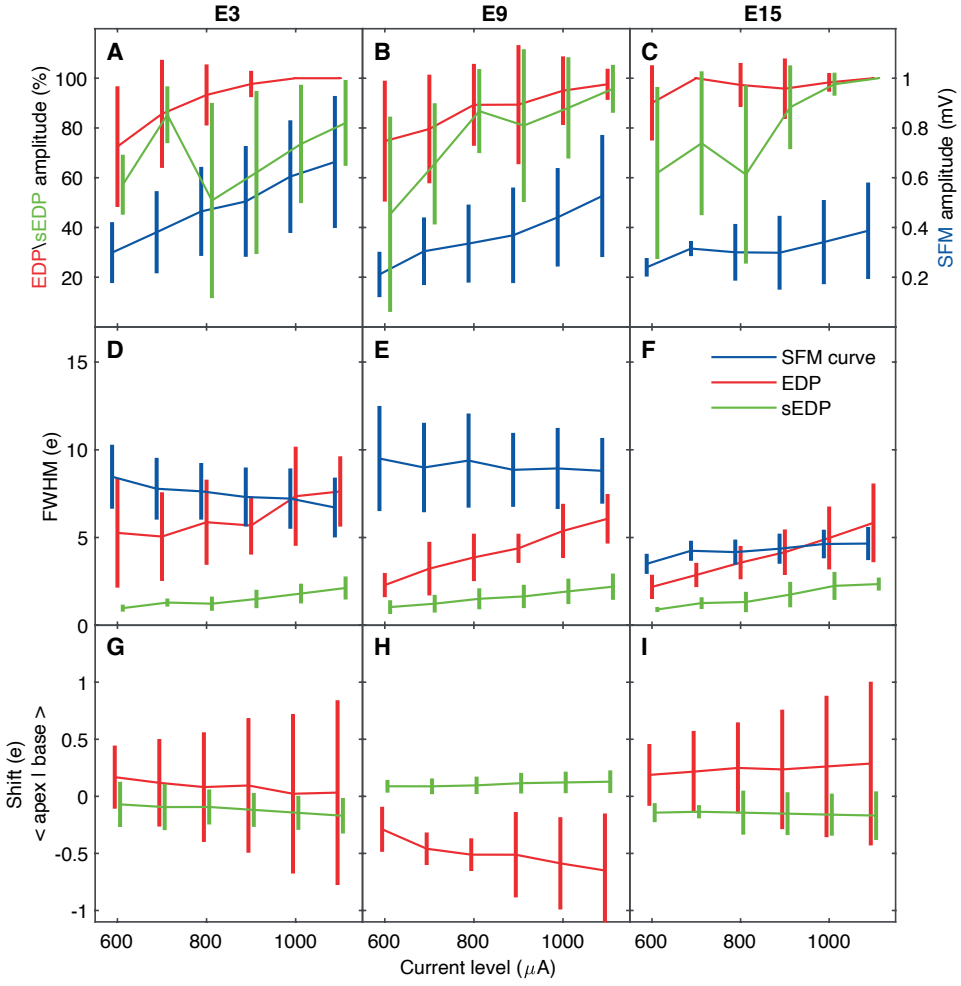

Figure 5.6. Effect of probe stimulus level on the SFM curves (blue), the EDPs (red) and the sEDPs (green). The parameters of interest (y-axis) were plotted as function of probe current level (x-axis). The line shows the average and the vertical bars indicate the standard deviation. The columns show the results for electrode contact 3, 9 and 15 separately. SFM indicates spatial forward masking; EDP, excitation density profile; sEDP, simulated excitation density profile; e, electrode contact.

5.4. Discussion

In this study, we investigated how excitation density profiles of cochlear implants change as a result of varying the stimulus level. Our hypothesis was that lower stimulus levels cause narrower excitation areas or at least excite fewer neurons. We studied this effect using our newly extended method for deconvolving SFM curves into so-called EDPs, which reflect the neural excitation by individual electrode contacts. The results of the present study support our hypothesis: lower stimulus levels excite fewer neurons, mainly represented by narrower EDPs.

In our previous study (Biesheuvel et al. 2016), the parameterization of the EDPs was kept simple to clearly demonstrate the principle of (de)convolution. As we have explained in the introduction, the EDP parameterization had to be extended to account for stimulus level effects. Initially we implemented an EDP parameter for 'slope' and 'shift' per stimulus level. However, it turned out that this parameterization caused the EDPs to become physiologically unrealistic. For example, it was possible that the EDP at 1200 µA was centered around the stimulating electrode contact, while the EDPs at lower stimulus levels (600–1100 µA) were all shifted by a full electrode contact; such a large and sudden shift cannot be explained physiologically. Therefore, we implemented a shift parameter that was linearly interpolated and must be zero somewhere at a lower stimulus level (<600 µA). In that way, we were able to study relative shifts caused by the stimulus level. Consequently, we could not account for another physiological phenomena that there might be an absolute shift at the lower stimulus levels depending on the position of the electrode contact in the cochlea. However, we think that an absolute shift depending on the position of the electrode array in the cochlea might be negligible, as all subjects had a HiFocus Mid-Scala electrode array which can be seen as a fixed factor.

Regarding the slope, it could happen that the EDP was shaped like a Gaussian curve at 1200 µA, while the EDPs at all other lower stimulus levels were almost rectangular. From a mathematical point of view, these rectangular EDPs are a valid solution in the deconvolution method. However, rectangular EDPs are physically and physiologically implausible (Biesheuvel et al. 2016). Defining the EDP parameterization turned out to be a challenging task and, in order to verify whether the EDP parameterization was realistic, we compared the EDP parameterization with sEDPs from our computational model of the human cochlea (Kalkman et al. 2014; Kalkman et al. 2015; Kalkman et al. 2022). Using the Bland-Altman analysis (Figure 5.3) and Jaccard index, we have improved the EDP parameterization stepwise and, finally, we came to the parameterization as described in section 5.2.1.1. Based on the results shown in Figure 5.3 and the similarity median of more than 92%, we think that the final EDP parameterization presented in this study is good for the purpose of answering the central question of this study. Note that the EDPs are robust enough to predict excitation areas simulated in five anatomically different cochleae, including three states of neural health (i.e., intact nerve fibers, neurons with a shortened peripheral terminal node, and neurons that suffered a complete loss of their peripheral processes). Therefore, we conclude that the extended deconvolution method can now be used to study the effect of stimulus level on excitation areas.

Before we go into detail about the effect of stimulus level on SOE, we want to discuss another aspect regarding the validity of the deconvolution method. Thus far, the deconvolution method was based on eCAP data collected with anodic-leading stimuli, while both the literature and current CI systems often use cathodic-leading stimuli. The deconvolution method, however, was developed using anodic-first stimuli and we continued on this in the current study (Biesheuvel et al. 2016). We think that the used anodic-leading stimuli did not have major consequences for the outcomes in the current study; we performed within-subject-analyses with anodic-leading data only. Further, research from Hughes et al., (2016) showed no difference in eCAP amplitude measured with either anodic-first or cathodic-first forward masking in AB recipients and our method is based on these eCAP amplitudes. Nevertheless, the excitation patterns underlying the anodic-first and cathodic-first stimuli may differ. A preliminary analysis comparing the sEDPs with sEDPs simulated under equal conditions but with cathodic-first stimuli, showed a similarity of 81.6% (according to equation 5.1). Visual inspection revealed that the differences between cathodic-first and anodic-first sEDPs were mainly in the form of changes in the widths and amplitudes of the excitation patterns. Both the width and amplitude are parameterized in our EDPs and the deconvolution method. So, we think that our method can deal with the different stimulus polarities correctly. In a follow-up study, the stimulus polarity can be an area of interest, especially if we want to compare the EDPs with behavioral data collected with cathodic-leading stimuli.

Regarding the stimulus level effects on SOE, our hypothesis was that a lower stimulus level will excite fewer neurons, due especially to a narrowing of the excitation areas. The results presented in this study confirm this hypothesis (Figure 5.5). Both the EDPs and sEDPs became significantly wider when the stimulus level increased ($p < 0.001$). A few cases showed that the EDPs did not necessarily become wider with increasing stimulus level. Higher stimulus level could initially also lead to higher EDP amplitudes, as shown in Figure 5.4D, reflecting deeper excitation in the spiral ganglion. In general, the stimulus level was always related to the area under the EDP, which reflects the number of excited neurons. This is consistent with previous findings that the area under the EDP is highly correlated to the eCAP amplitude, given that eCAP amplitudes depend on current level (Biesheuvel et al. 2016).

Figure 5.6D-F shows that the sEDPs are narrower, or more selective, than the EDPs found in patients. Unfortunately, we do not yet have a definitive explanation for this outcome. It is possible that neural excitation patterns in the computational model are too selective compared with SOE data collected in humans. In that case, the results of the present study

invite us to critically review the computational model, especially the parameters that are involved in simulating SOE. Meanwhile, it is important to realize that, although EDPs and sEDPs are conceptually very similar, strictly speaking they are different. The sEDPs are derived from simulated excitation patterns; the modeled nerve fibers are characterized by their positions along the BM and each excited neuron contributes to the sEDPs equally. Additionally, the widths of the sEDPs are affected by the length of the segment along the BM over which the excitation density is averaged. This length was set to 1 mm for this study, but this is essentially an arbitrary value. In contrast, EDPs are obtained from mathematical deconvolution of SFM curves recorded in humans and they are a function of electrode contact spacing, rather than distance along the BM. In short, although the EDP and the sEDPs are both intended to represent neural excitation densities, their differences should be kept in mind when comparing the two to each other directly. Regardless, for the purpose of this study, which is validation of the EDP parameterization, the fact that the sEDPs appears to be more selective does not matter, since the width of the EDP is a variable in the deconvolution method as well.

The updated EDP parameterization allows the center of excitation to shift as a function of stimulus level. The bottom row of Figure 5.5 shows how the center of the EDPs shifted with the current level in our patient data. Note that for all three electrode contacts a number of EDPs shifted to the maximum of the fitting range, plus or minus a full contact at 1200 µA. Although it is undesirable for the minimization routine to reach the minimum or maximum of the fitting range, extending the fitting range would be unrealistic. It turned out that when the shift parameter was not constrained, some EDPs tended to shift 4 or 5 electrode contacts. It is not likely that an EDP would shift so far (even more than one electrode contact) when the current level is increased from 600 µA to 1200 µA. We think we encountered a limitation of the deconvolution method that is likely caused by the incomplete SFM curves at distal electrode contacts. At electrode contacts 3 and 15, the SFM curves are asymmetric and most of the masker contacts involved in the deconvolution are unilateral from the probe contact. When the probe stimulus level was lowered the eCAP amplitudes became smaller and we would expect smaller probe EDPs. However, in the deconvolution method, smaller eCAP amplitudes are coded by decreased overlap between the masker and probe EDPs. We have seen that this can be achieved by narrowing the EDPs, but it can also be represented in a mathematically correct way by shifting the probe EDPs away from the masker EDPs, especially for distal electrode contacts (see also Figure 5.5J-L). However, the shift parameter did not reach the boundaries of its fitting range in all subjects. So, we can also speculate that this problem of reaching the fitting range is caused by a within-subject factor, rather than by the edges of the SFM curves. For

example, in the case of a dead neural region we would expect a smaller EDP, but a dead neural region can also be represented mathematically by shifting the adjacent EDPs away. Unfortunately, in the context of this study, we cannot rule out such dead-region effects. To estimate dead regions, we would need a different EDP parametrization followed by a validation step using an independent measure for neural status.

Dead neural regions, however, are interesting as they are directly related to the clinical applicability of the deconvolution method. If the deconvolution method can detect poor neural survival, such information can be used to optimize the cochlear implant fitting, e.g., by de-activating less effective electrode contacts. Thus far, our studies regarding the deconvolution method are quite fundamental. Nevertheless, the present results about stimulus level effects on excitation patterns can help audiologist with CI fitting, especially making them aware that higher stimulus levels may limit the spatial resolution in most subjects. In a next step, it would be valuable to work on the detection of poor neural regions. Garcia et al., (2021) recently published a study in which they investigated the assessment of neural health using the panoramic eCAP method. They concluded that the panoramic eCAP method can detect neural survival patterns with high accuracy (at least 90%). However, a disadvantage of their method is that they used computer simulations with a backward approach, so that both the generated and solved dead regions are based on the same model assumptions. Instead, it would be better to validate the detection of dead regions by an independent model, in order to increase the clinical feasibility. For instance, it would be possible to model poor neural regions with our computational model. Subsequently, based on these poor neural regions, eCAP-based SFM curves can be simulated, and these curves can be translated back to EDPs using the deconvolution method. Next, the obtained EDPs can be compared with the simulated dead regions to validate them.

The observed shift in the center of the EDPs might indicate a change in pitch percept, assuming that the center of excitation is involved in pitch perception by cochlear implant users (McKay et al. 1999; Laneau et al. 2004; McDermott & McKay 2005). Such a pitch shift with intensity is a well-known phenomenon in normal hearing (Stevens 1935; Terhardt 1979), but also in line with several studies reporting an effect of stimulation level on perceived pitch in electrical hearing (Shannon 1983; Townshend et al. 1987; Arnoldner et al. 2006; Carlyon et al. 2010). Shannon (1983) asked a CI user to judge pitch as function of loudness level and this subject perceived an increase in pitch with increased loudness. Townshend et al. (1987) studied pitch perception in three implant subjects and they found that pitch percepts were primarily affected by the place and rate of stimulation,

while the stimulus level appeared to be a secondary effector. Among these three patients, one perceived an increased pitch at higher stimulus levels, while the other two perceived a decreased pitch at higher levels. About 20 years later, other studies still show varying results. Arnoldner et al. (2006) showed an increase in pitch at higher current levels in 10 patients, whereas only one patient showed the opposite effect. Carlyon et al. (2010) studied the effect of stimulus level and place of stimulation on temporal pitch perception by cochlear implant users. They found that in 16 of 21 cases the pitch increased with signal level, while the opposite effect was observed in the other five cases. If we assume that pitch perception is linked to the excitation area, the results of the present study show similar outcomes, especially at electrode contacts 3 and 15 where the shift in the excitation center varied between –1 and +1 (Figure 5.5G-I). Carlyon et al. (2010) concluded that the stimulus-level effects observed in their study cannot entirely be assigned to changes in current spread with increasing level and they also speculated that temporal coding might play a role in pitch perception. So, to further elucidate the relationship between stimulus level and pitch perception, we suggest combining the eCAP-based EDPs with psychophysical measures of pitch perception.

5.5. Conclusions

The deconvolution method enables us to study the effect of stimulus level on excitation areas in an objective and physiological way. The validation step showed that the updated parameterization of the EDPs describes the excitation areas simulated in our computational model well. Using this updated EDP parameterization, eCAP-based SFM curves measured with different probe current levels can be deconvolved in EDPs, thereby unraveling the effect of stimulus level on the excitation areas. It turned out that excitation areas are smaller, mainly narrower, at lower stimulus levels, which could not be derived from the SFM curves included in this study. Lastly, the comparison of the EDP parameterization with simulations from our computational model provided new insights about the validity of the deconvolution method.

CHAPTER

6

Channel discrimination along all contacts of the cochlear implant electrode array and its relation to speech perception

Jan Dirk Biesheuvel, Jeroen J. Briaire, Monique A.M. de Jong, Stefan Boehringer, Johan H.M. Frijns

International Journal of Audiology, 2019, 58(5):262-268

Objective: To test the channel discrimination of cochlear implant (CI) users along all contacts of the electrode array and assess whether this is related to speech perception.

Design: CI recipients were tested with a custom-made channel discrimination test. They were asked to distinguish a target stimulus from two reference stimuli in a three-alternative forced choice task. The target stimulus was evoked using current steering, with current steering coefficients (α) of 1, 0.5, and 0.25. The test provided a discrimination score (Dα) for each electrode contact along the array.

Study sample: Thirty adults implanted with a CI from Advanced Bionics.

Results: Large variations in Dα scores were observed, both across the electrode array and between subjects. Statistical analysis revealed a significant channel-to-channel variability in Dα score ($p < 0.01$). Further, there was a significant relationship between subjects' Dα scores and their speech perception in quiet ($p < 0.001$).

Conclusion: The large variations in Dα score emphasize the importance of testing pitch discrimination across the complete electrode array. The relationship between Dα score and speech perception indicates that pitch discrimination might be a contributing factor to the performance of individual implant users.

Abstract

6.1. Introduction

The electrode array of cochlear implants (CIs) is located along the basilar membrane and takes advantage of the tonotopic organization of the cochlea to evoke different pitches. Contemporary electrode arrays contain 12-22 contacts, which ideally activate restricted and distinct areas of the auditory nerve. In practice, however, the excitation area of adjacent electrode contacts do overlap, leading to a reduced number of discriminable pitches and limited efficacy of the CI (Shannon, Fu, and Galvin 2004; Zeng 2004; Snel-Bongers et al. 2012; Jones et al. 2013). Previous research showed that there was no improvement in speech recognition as the number of active electrodes increased beyond eight (Friesen et al. 2001; Frijns et al. 2003; Shannon et al. 2004). This suggests that CI listeners are not able to take full advantage of the spectral information provided.

Several studies investigated whether the speech perception of CI users depends on their ability to distinguish pitches evoked by the different channels. Note that pitch perception is influenced by place of excitation as well as by stimulus rate. This article focusses on place-pitch only, and the term pitch will refer to place-pitch throughout this article. Subject's ability to perceive pitch is commonly assessed by using pitch ranking. In a pitch ranking task, the subject is typically asked to judge which of the stimulating electrode contacts has a higher pitch. Several studies based on pitch ranking tasks showed a positive relationship between the ability to distinguish pitches and speech perception (Nelson et al. 1995; Collins et al. 1997). Furthermore, Kenway et al. (2015) found that pitch ranking ability is an independent predictor of overall CI outcome. However, pitch ranking is difficult to accomplish for some CI users. Judging pitch as higher or lower is a challenge for individuals who have a hard time recalling what higher or lower pitch means.

Alternatively, channel discrimination can be tested using three-alternative forced choice (3AFC) tasks. In a 3AFC task, subjects indicate which of three stimuli sound different from the rest, which is easier to perform than pitch ranking. Recent 3AFC discrimination tasks use virtual channels next to the physical channels to estimate the discrimination ability more precisely. These virtual channels are created by simultaneously stimulating two adjacent physical contacts with different relative weighting of current, creating an intermediate pitch (Firszt et al. 2007; Frijns et al. 2009). While conducting the 3AFC discrimination task with virtual channels, Snel-Bongers et al. (2012) found that the mean pitch discrimination correlates negatively with speech perception scores; smaller just noticeable differences (JND) in pitch correspond with higher monosyllabic phoneme scores.

A disadvantage of the pitch discrimination tests encountered in the current literature, however, is that they are time-consuming. Consequently, the discrimination tasks were performed on only a limited number of electrode contacts; for example, those in three cochlear regions. The estimated JNDs on these few electrode contacts were then used to estimate the total amount of discriminable pitches along the whole electrode array. Doing this, some studies reported that CI users on average could hear 93 (Koch et al. 2007), 64 (Firszt et al. 2007) or 20 (Snel-Bongers et al. 2012) spectral channels. The interpretation of these results, however, is complicated by the fact that channel interaction varies across the electrode array (Jones et al. 2013). It is known that across-electrode differences in other psychophysical measures, e.g., detection thresholds, have a negative effect on speech understanding (Pfingst et al. 2004; Pfingst & Xu 2004; Bierer 2007; Long et al. 2014). Therefore, we propose that it is valuable to examine pitch discrimination across the entire electrode array rather than at only a few electrode contacts.

From a clinical perspective, there might also be interest in testing channel discrimination at individual electrode contacts. Potentially, it can help clinicians to optimize the CI fitting, e.g., to deactivate ineffective electrode contacts. Furthermore, it has been shown that subjects' speech perception is related to their pitch discrimination ability (Snel-Bongers et al. 2012; Goehring et al. 2014). In these studies, however, the discrimination scores were obtained at a few electrode contacts only. To further evaluate pitch discrimination of CI users, we developed a tool to test channel discrimination along the whole electrode array, rather than at a few contacts. Doing this with an adaptive procedure is time-consuming. Therefore, we tested pitch discrimination at predefined inter-channel distances (ICDs) of 1.0, 0.5, and 0.25 electrode contacts in order to save time. To distinguish our metric of channel discrimination from the JND of α (JNDα), as is commonly used in literature (Snel-Bongers et al. 2012; Shannon 1983), we called our metric Dα. This article shows the first results of conducting our channel discrimination test in 30 CI users. Additionally, we examined whether the found discrimination scores are related to subjects' speech perception.

6.2. Materials and methods

6.2.1. Subjects

Channel discrimination was tested in 30 adults implanted with a CI from Advanced Bionics (Sylmar, CA). All electrode arrays contained 16 electrode contacts, which are numbered from 1 to 16 (apex to base). Table 6.1 shows the subject demographics. The reported strategy is each subject's everyday life speech processing program, and the next column shows which contacts are not active in their program. The center frequencies allocated to the active electrode contacts were approximately evenly spaced on a logarithmic frequency scale

from 333 to 6665 Hz. All subjects were unilateral CI users, except S0408 who was implanted bilaterally. Subjects were randomly recruited from adult CI users who had at least 6 months of experience with their implant and an annual appointment at the audiology department of the Leiden University Medical Center, the Netherlands, in the period from October 2015 to June 2016. One subject (S0419) was excluded from further analysis due to high impedance variations across the electrode contacts. Consequently, the loudness could not be optimally balanced across the electrode array, as explained in the next section. Two additional subjects (S0426 and S0429) were excluded because they were previously diagnosed with cognitive impairment and did not understand the test procedure.

Table 6.1. Subject demographics.

Subject	Gender	Age	Etiology	Implant	Strategy	Non-active contacts	Side
S0401	M	65	Congenital/Hereditary, pre-lingual	HiRes90K 1J	Fidelity 120	-	AD
S0402	F	64	Congenital/Hereditary, pre-lingual	HiRes90K 1J	HiRes-S	-	AS
S0403	F	63	Other/Unknown, post-lingual	CII + positioner	HiRes Optima-S	-	AS
S0404	M	86	Meniere, post-lingual	HiRes90K 1J	HiRes Optima-S	15,16	AS
S0405	F	63	Rubella, pre-lingual	HiRes90K 1J	HiRes-S	2,5,9,14	AD
S0406	F	49	Congenital/Hereditary, post-lingual	HiRes90K 1J	HiRes Optima-S	-	AS
S0407	M	72	Other/Unknown, post-lingual	HiRes90K MS	HiRes Optima-S	-	AS
S0408	F	71	Other/Unknown, post-lingual	HiRes90K 1J	HiRes-S	-	AD
S0409	M	79	Other/Unknown, post-lingual	HiRes90K MS	HiRes Optima-S	-	AD
S0410	M	82	ECI, post-lingual	CII + positioner	HiRes-S	-	AD
S0411	F	66	Congenital/Hereditary, post-lingual	HiRes90K 1J	HiRes-S	-	AD
S0412	M	53	Congenital/Hereditary, post-lingual	HiRes90K MS	HiRes Optima-S	-	AS
S0413	F	50	Other/Unknown, post-lingual	HiRes90K 1J	Fidelity 120	-	AS
S0414	M	59	Other/Unknown, post-lingual	HiRes90K MS	HiRes Optima-S	-	AD
S0415	M	34	Trauma, post-lingual	HiRes90K MS	HiRes Optima-S	-	AS
S0416	M	69	Other/Unknown, post-lingual	CII + positioner	HiRes-S	3,4,11,14	AS
S0417	M	83	Other/Unknown, post-lingual	HiRes90K MS	HiRes Optima-S	-	AS
S0418	M	70	Menigitis, post-lingual	HiRes90K 1J	HiRes-S	2,5,9,14	AD
S0419	M	61	Congenital/Hereditary, post-lingual	CII + positioner	HiRes-S	3,4,6,9	AS
S0420	F	54	Other/Unknown, post-lingual	CII + positioner	HiRes-S	1,3,5,9,13,15	AS
S0421	M	59	Congenital/Hereditary, post-lingual	CII + positioner	HiRes Optima-S	-	AD
S0422	F	72	Other/Unknown, post-lingual	CII + positioner	HiRes-S	2,4,8,13,15	AS
S0423	F	66	Congenital/Hereditary, post-lingual	HiRes90K 1J	HiRes-S	-	AD
S0424	M	49	Congenital/Hereditary, post-lingual	HiRes90K 1J	HiRes-S	-	AS
S0425	M	86	Congenital/Hereditary, post-lingual	HiRes90K 1J	HiRes-S	-	AS
S0426	M	47	Other/Unknown, post-lingual	HiRes90K MS	HiRes Optima-S	-	AD
S0427	F	52	Other/Unknown, post-lingual	HiRes90K MS	HiRes Optima-S	-	AS
S0428	F	77	Other/Unknown, post-lingual	HiRes90K MS	HiRes Optima-S	-	AS
S0429	M	84	Congenital/Hereditary, post-lingual	HiRes90K MS	HiRes Optima-S	-	AD
S0430	F	66	Congenital/Hereditary, post-lingual	HiRes90K MS	HiRes Optima-S	16	AS

6.2.2. Channel-discrimination test

The channel-discrimination experiment was custom-made using MATLAB (Mathworks, Inc., Natick, MA) and the Advanced Bionics' research tool, Bionic Ear Data Collection System (BEDCS). The test was based on current steering, which involves simultaneous delivery of current to adjacent electrode contacts (Townshend et al. 1987; Donaldson et al. 2005; Firszt et al. 2007). The locus of stimulation can be steered to sites between two physical contacts by varying the proportion of current delivered to each contact. The proportion of the total current directed to the basal contact of the contact pair was denoted as α, and the proportion to the apical contact as (1 – α). Consequently, α represents the distance between the spectral channels expressed in electrode contacts. Two stimuli were used; a probe stimulus based on current steering and a reference stimulus using a physical contact. These stimuli consisted of pulse trains of monopolar, symmetric biphasic pulses with phase durations of 32 μs. We used a pulse-rate of 1400 pulses per second, which is sufficiently high to avoid place-pitch and rate-pitch confusions (Shannon 1983; Townshend et al. 1987; McKay, McDermott, and Carlyon 2000; Zeng 2002). The total duration of both stimuli was 300 ms and the pause between stimuli was 500 ms.

First, electrode impedances were obtained to assess the devices' compliance limits. Next, for all electrode contacts, the most comfortable level (MCL) was determined in linear clinical units (CU) with the use of an eight-point loudness scale (Potts et al. 2007). In this ascending loudness experiment, level 1 corresponds to the hearing threshold, level 5 with MCL and level 8 with the highest acceptable loudness. To determine MCL, we started at a low level and increased the stimulus level with a step size of 5 CU until MCL was reached. If the stimulus level tended to exceed the compliance level, the phase duration was automatically increased by 10.8 μs to increase the charge according to the following formula: CU = pulse width (μs) x amplitude (μA) / 78.7. The number 78.7 is a correction factor without units, which is provided by the manufacturer. Afterwards, the MCL of each contact was subjectively balanced with the apically adjacent electrode contact.

The discrimination test itself was performed using the 3AFC paradigm, whereby the stimuli were presented in random order. The stimuli were accompanied by three different buttons displayed on a computer screen, which flashed simultaneously with the presented stimulus. The subjects were asked to indicate which stimulus was different in pitch, without receiving feedback about the correct answer. To avoid confounding effects from potential loudness cues, a level roving of ±10% relative to MCL level was applied to each stimulus. When applying level roving, one should be aware that even small level differences in the

stimulus level could have a substantial effect on pitch judgments (Shannon 1983). The level roving of 10% applied in this study was considered to be moderate.

Prior to the actual discrimination test, a familiarization task was conducted with an ICD of two physical electrode contacts. The example was performed on five different electrode pairs across the electrode array. After verifying that the experiment was clear to the subject, the real experiment was started with $\alpha = 1$. The test started at electrode 1 (apex) and all electrode pairs along the electrode array were tested consecutively. In this way, all electrode contacts were tested five times. Because 3AFC tests have a chance probability of 33.3%, 66.6% of the answers must be correct to statistically prove a true detection rate of more than 50% (Lawless 2010). Thus, based on five repetitions, we assumed that the electrode pair could be discriminated when four or five correct answers were given. In that case, we continued to a more difficult level by halving the tested α. If the number of correct answers was three or less, the electrode pair was not examined further. Following this approach, ICDs of 1, 0.5 and 0.25 were tested. The smallest α at which the probe and reference stimuli were discriminated correctly was set as the Dα score for the reference contact. If the subject could not discriminate $\alpha = 1$, the Dα score was set to '>1'.

6.2.3. Speech perception

The speech perception scores used in this study originated from the standard Dutch monosyllabic word test routinely measured at our center. The test consisted of consonant-vowel-consonant (CVC) words (Bosman & Smoorenburg 1995) and was conducted in the free field using 48 items. For the bilaterally implanted subject (S0408), only speech scores obtained with both CIs were available. Consequently, subject S0408 was excluded from the analyses that involved CVC scores. All other subjects had no contralateral hearing that could have contributed to the speech score. Percent-correct phoneme score was used as a measure of speech perception. We used CVC scores obtained at the 1-year follow-up, because after that period the CVC scores are stabilized (Snel-Bongers et al. 2018). If these scores were not available, the scores at 2-year follow-up (S0423 and S0425) or at 6-months follow-up (S0426) were included. The scores were obtained with speech in quiet at 65 and 75 dB SPL and with speech (65 dB SPL) in speech-shaped noises at signal-to-noise ratios (SNR) of +10, +5 dB. The speech in noise tests were performed by only those patients that had a score above 50% for the speech in quiet test at 65 dB SPL. The condition speech-in-noise +5 dB SNR was not tested when the phoneme score in the +10 dB SNR condition decreased below 50%.

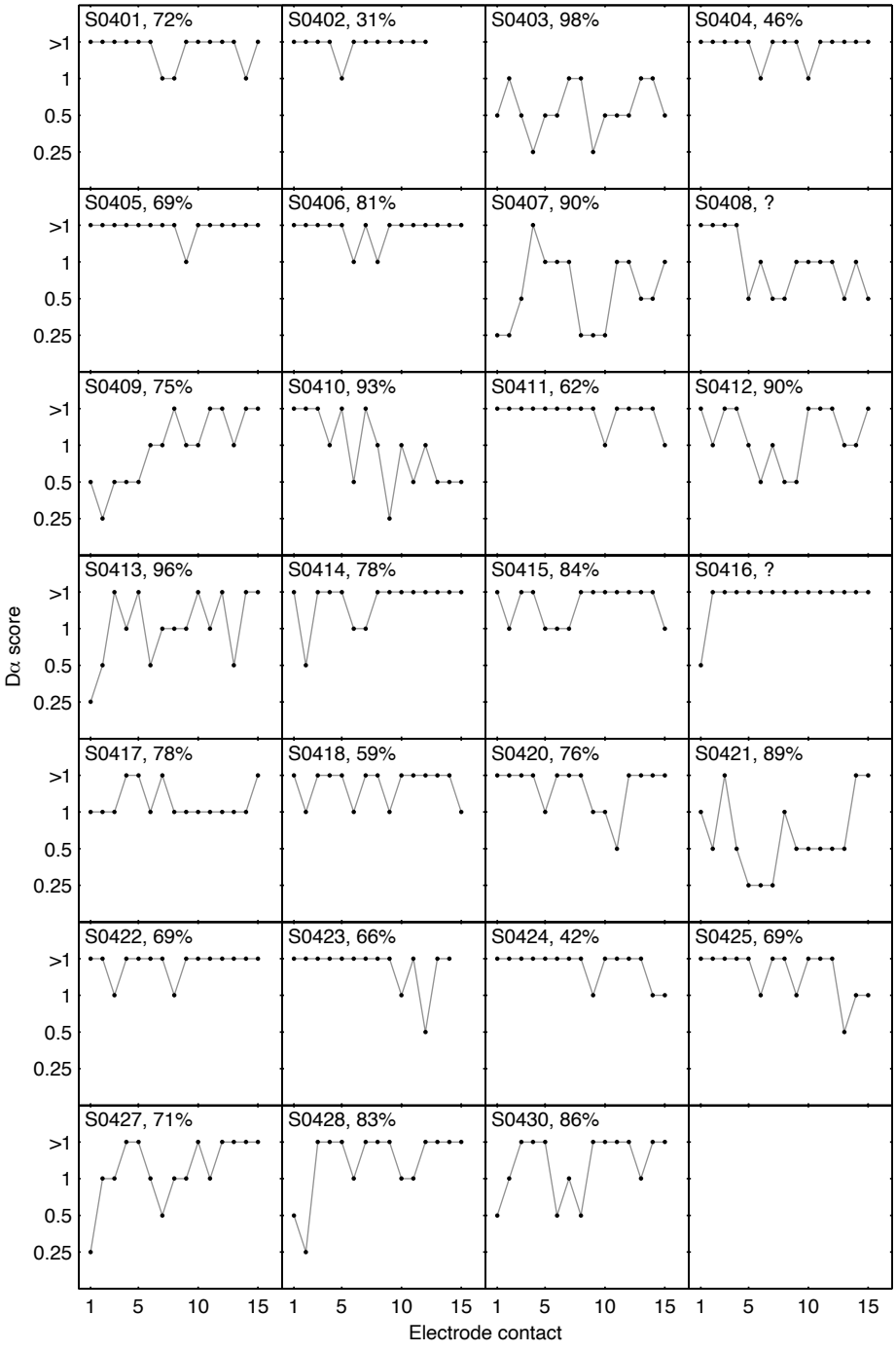

Figure 6.1. Overview showing the Dα scores (y-axis) across the electrode contacts (x-axis) for all subjects. On top of each plot subject's name and CVC score at 65 dB speech in quiet are shown. The CVC scores for subject S0408 and S0416 were unknown. CVC indicates consonant-vowel-consonant.

6.2.4. Data analysis

Heterogeneity of the Dα score across the electrode array was analyzed using a mixed-effects ordinal regression model (Agresti 2002). The model contains a random intercept per subject and the position within the electrode array, either as 'electrode contact number' or 'electrode region', both being treated as categorical variables. Electrode region was defined as apex, contact 1-5; middle, contact 6-10 and base, contact 11-16. *p* values were computed using a likelihood ratio test comparing the full model (including position within the array) to a model without position (containing both a fixed and random intercept). The variations in Dα across the electrode array were illustrated using a segmented bar graph (Figure 6.2).

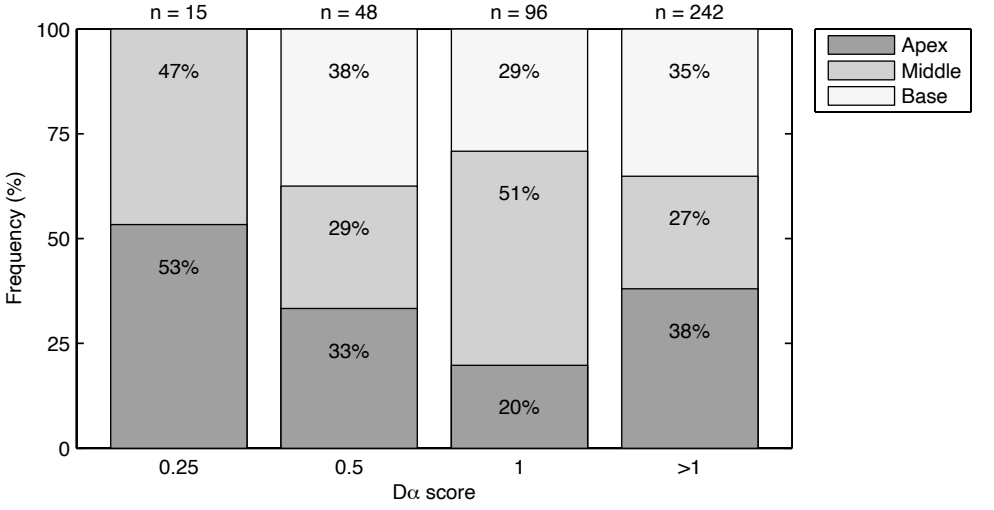

Figure 6.2. Figure showing the distribution of Dα scores across three regions of the electrode array. The apical region (dark gray) corresponds with electrode contact 1-5, the middle region (gray) with contact 6-10 and the basal region (light gray) with contact 11-15. On top of each column, the total number of Dα scores is shown.

The effect of speech perception on channel discrimination in CI users was also tested using an ordinal mixed model. The model included the variables electrode region and speech perception. To account for clustering due to multiple measurements per individual, the model had a random intercept per subject. *p* values were calculated using a likelihood ratio test for comparing a model with and without the speech perception score. All statistical analyses were conducted using R version 3.5.0 with the *ordinal* package for regression analyses. The relationship between Dα score and speech perception is visualized in Figure 6.3. In this figure, subjects' Dα scores are plotted as function of their CVC scores using boxplots. Additionally, the strength and direction of the relationship was assessed using Spearman's rank correlation coefficient (r_s), which is applicable for ordinal data.

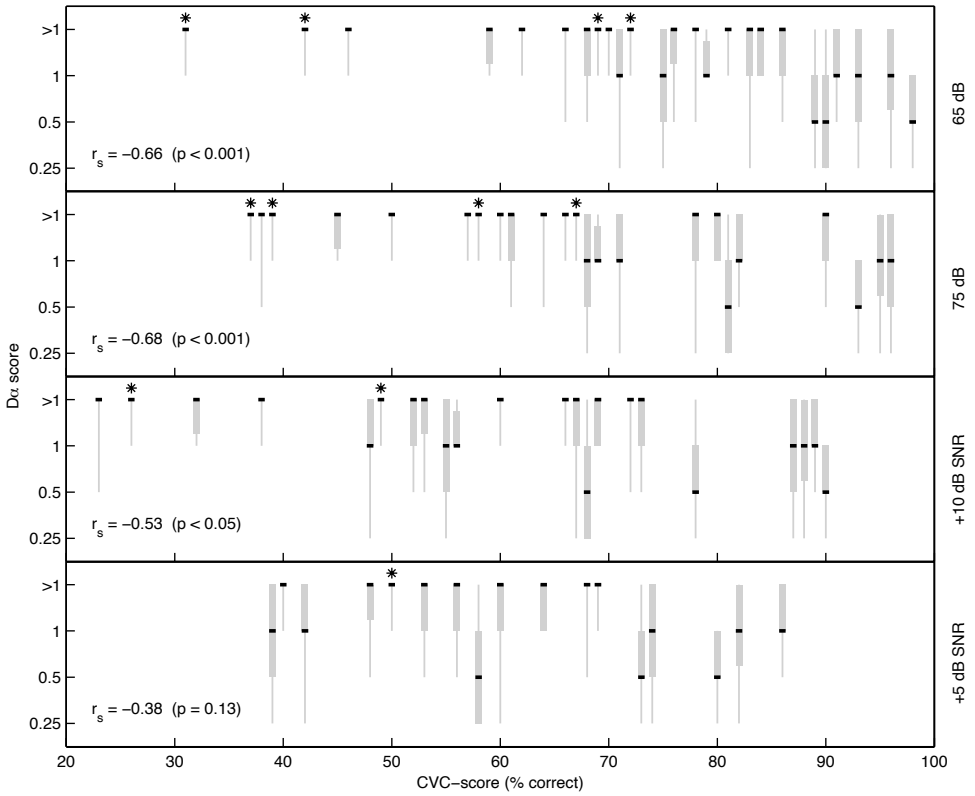

Figure 6.3. Boxplots showing the Dα scores across the electrode array (y-axis) as function of subject's CVC score (x-axis). The gray vertical line shows the range from the Dα scores and the box represents the interquartile range (25-75%). The black line indicates the median. Spearman's rank correlation (rs) was based on the median values. CVC scores were obtained in four different test conditions, resulting in one plot per condition (65 dB, 75 dB, +10 dB SNR, +5 dB SNR). Results from prelingually deafened CI users were marked with an asterisk to distinguish them from the postlinguals. CI indicates cochlear implant; CVC, consonant-vowel-consonant; SNR, signal-to-noise ratio.

6.3. Results

Figure 6.1 shows an overview of the Dα scores determined in the 27 subjects that completed the channel discrimination task. Large differences in Dα score were found between subjects (e.g. S0402 versus S0403) as well as within subjects (e.g. S0413 and S0427). Noteworthy is that, except for subject S0403, none of the patients could distinguish all the physical electrode pairs. The channel-to-channel variations in Dα score were further analyzed using a heterogeneity test. The variations in Dα score were significant, both across electrode contacts ($p < 0.01$) and across electrode region ($p < 0.01$). In addition, Figure 6.2 illustrates how often each Dα score occurs in the apical, middle and basal region of the electrode array. The Dα scores were distributed non-uniformly over the three regions, and the Dα score 0.25 even does not occur in the basal region of the electrode array.

We also examined whether the Dα score is related to the speech perception of the CI user. The ordinal regression model revealed a significant effect of CVC score on Dα score for speech perception in quiet at 65 dB ($p < 0.001$) and 75 dB ($p < 0.001$). Concerning speech perception in noise, the effect was also significant for the +10 dB SNR condition ($p < 0.01$), but not for the +5 dB SNR condition ($p = 0.10$). In Figure 6.3, subjects' Dα scores are plotted as function of their CVC scores using boxplots. Note that, if multiple subjects have equal CVC scores, these CVC scores have been varied by ±1% to increase visibility. The boxplots display the range of Dα scores (gray vertical line), the median (black horizontal line) as well as the spread around the median based on the 25% and 75% quartiles (gray box). The different panels represent the four listening conditions, as depicted on the right side of each plot. Spearman's correlation coefficients (r_s), as calculated using the median values, indicate that the relationship between Dα scores and CVC scores is negative; higher CVC scores are correlated with lower Dα scores. The correlation is significant for the conditions 65 dB ($p < 0.001$), 75 dB ($p < 0.001$) and +10 dB SNR ($p < 0.05$), which is in line with the results of the ordinal regression model. The results of the four prelingually deafened CI users are marked with the asterisk. These subjects generally have lower CVC scores and worse Dα scores than postlingually deafened subjects.

6.4. Discussion

This paper shows the first results of testing channel discrimination along all contacts of the electrode array. We developed a tool that assessed subject's ability to discriminate spectral channels using predefined ICDs of 1.0, 0.5, and 0.25 electrode contacts. In the literature, channel discrimination has been tested only at a limited number of sites along the electrode array using an adaptive procedure (Koch et al. 2007; Firszt et al. 2007; Goehring et al. 2014). In these studies, different measures for discrimination ability were used. Converted to JND of α, JNDα's of 0.14 (Koch et al. 2007), 0.21 (Firszt et al. 2007), 0.71 (Goehring et al. 2014) were found on average across the electrode array. Compared to these JNDα's, our median Dα scores were higher (see Figure 6.3). Considering the experimental designs, it is difficult to quantify differences in pitch discrimination scores across studies. For example, Koch et al. (2007) and Firszt et al. (2007) did not use loudness roving in their pitch ranking experiments. This could have led to a loudness cue and, therefore, an overestimation of the real ability to distinguish pitches. Furthermore, Goehring et al. (2014) found a mean JNDα of 0.69, 0.68, and 0.75 for the basal, middle, and apical regions, respectively. However, subjects who were unable to distinguish two adjacent physical electrodes (i.e., ICD was > 1.0) were excluded from this analysis, leading to an overestimation of overall performance. In contrast, we included the 'Dα > 1' scores in the results as well, consequently leading to higher Dα scores.

A benefit of our test procedure is that it provides insight in channel discrimination ability along the whole electrode array. The results show that the Dα scores vary largely from channel-to-channel as well as between subjects (Figure 6.1). The variations in Dα score were significant, both across electrode contact and electrode region. These results indicate the importance of testing all electrode contacts when studying electrode discrimination in CI users. Regarding clinical applicability, a detailed picture of subject's discrimination ability could potentially help clinicians to optimize the fitting procedures, e.g., to deactivate ineffective electrode contacts.

The frequently observed 'Dα > 1' indicates that testing ICDs above 1 should be included in future discrimination experiments. Testing ICDs above 1 will result in better estimates of the actual channel discrimination, especially for CI users who are poor performers (e.g., S0402, S0405 and S0416). Further, it will gain more insight in the channel-to-channel variability in Dα scores. Latter aspect would also be worthwhile for studying the effect of intra-cochlear position of the electrode array on the Dα scores. DeBruyne et al. (2017) found that basally located contacts have worse discrimination than more apically located contacts, and de Miguel et al. (2018) found that the Nucleus CI532 has a more perimodiolar placement, and that this placement is related to a better electrode discrimination. Unfortunately, due to the large number of 'Dα > 1' scores, we think that current data do not allow further analyses on factors causing the across-site variations in Dα. However, in a follow-up study, the effect of intracochlear position of the electrode array on the Dα scores will be considered.

We also assessed whether the Dα scores were related to subjects' speech perception. We found a significant relationship between subjects' median Dα scores and their CVC scores. The reported correlation coefficients can be interpreted as being strong for the 65 dB and 75 dB speech in quiet conditions, and as being moderate and weak for the +10 dB and +5 dB speech in noise conditions, respectively. Goehring et al. (2014) also investigated the relationship between mean electrode discrimination and speech scores (sentences in quiet) and found comparable results as we found. Note that, to achieve this result, they had to include 'α > 1' (meaning that no exact score was obtained) in the analysis as well. Due to the random subject selection, we also included four patients who were prelingually deaf. As expected, these subjects generally had worse CVC and Dα scores than postlingually deafened patients. These findings suggest that channel discrimination ability is a relevant factor in the performance of a CI user. Therefore, in the early phases of the rehabilitation program, the Dα score might be a useful predictor for subject's speech perception later on.

The discrimination test generally required less than 30 minutes; determining the MCLs lasted approximately 15 minutes and conducting the 3AFC task lasted another 10 minutes. This means that our test can be conducted within the time available for a regular appointment in our outpatient center. To save time, we decided to test predefined values of α only, rather than using an adaptive procedure. From a statistical point of view, the reduced number of tested α values can be seen as a measurement error with respect to the true JND of α. As the α values are pre-specified, the error is non-differential with respect to an outcome such as speech recognition. Any association found between Dα scores and speech recognition would, therefore, be weakened. On the other hand, current method does not provide precise Dα scores. In a next version, we will make the discrimination test semi-adaptive in order to estimate the Dα more precisely. In this test, the ICD was halved if the subject could discriminate the stimuli, while the test was aborted if an α was not discriminable. Alternatively, the ICD can be doubled if the subject cannot discriminate the stimuli, or one can test an α value in between a discriminable and non-discriminable α. To illustrate, while still limiting the number of test values to 3, the following sequences would be possible: ICD = 1 (fail), ICD = 2 (pass), ICD = 1.5 (pass); or ICD = 1 (pass), ICD = 0.5 (fail), ICD = 0.75 (pass). Lastly, the number of repetitions has to be weighed against the testing time. In this study, five repetitions were used. More repetitions will increase the precision and reliability of the Dα score and it will decrease the effect of chance guesses. It is our intention to evaluate these and other improvements in future versions of the discrimination test, whereby a test time below 30 min remains important for the clinical applicability of the test.

6.5. Conclusions

To conclude, this paper describes a novel custom-made pitch discrimination experiment that enables testing along the whole electrode array within 30 min. The large variations in Dα emphasize the importance of testing the complete electrode array, rather than at only a few contacts. The correlation between channel discrimination and speech perception indicates that testing channel discrimination along the whole electrode array might be a useful tool for getting insight into the performance of CI recipients. Moreover, testing this could potentially help clinicians optimize the fitting procedures, e.g., to deactivate ineffective electrode contacts.

CHAPTER

7

General discussion

The research presented in this thesis focused on the clinical applicability and relevance of electrically evoked compound action potential (eCAP) measurements. The studies covered both eCAP-based stimulation thresholds and spread of excitation (SOE). Several new insights were presented, which help researchers and clinicians to better rate eCAPs for clinical use and to understand cochlear implant (CI) stimulation. The main findings of this thesis are:

1. There is low evidence that eCAP thresholds can be used to predict fitting levels of individual CI recipients (Chapter 2: de Vos et al. 2017). Our follow-up study showed that eCAP thresholds are likely not precise enough to predict fitting levels of an individual CI user. We recommend that future research on eCAP thresholds should be accompanied by a measure of precision to correctly apply eCAP thresholds in clinical practice (Chapter 3: Biesheuvel et al. 2017).
2. eCAP-based spatial forward masking (SFM) curves show the interaction between probe and masker stimuli, but the curves need a post-processing step (i.e., mathematical deconvolution) to derive SOE from the individual stimuli, either the probe or masker (Chapter 4: Biesheuvel et al. 2016). Our newly developed deconvolution method is a valid and useful tool to study SOE, and it revealed that excitation areas become narrower when the stimulus level was lowered, which could not be derived from the SFM curves themselves (Chapter 5: Biesheuvel et al. 2021).
3. Our custom-made channel discrimination test turned out to be a useful tool for getting insight into the CI users' ability to discriminate different (virtual) channels across the electrode array. The channel discrimination score correlated with the CI users' speech performance, suggesting that the test can be used to find less effective electrode contacts, with the purpose to turn them off in the speech processing strategy in order to potentially increase the speech performance (Chapter 6: Biesheuvel et al. 2019a).

These findings contributed positively to our knowledge about CIs, and they also lead to new research ideas. However, we still encountered some difficulties with linking the eCAP outcomes to clinically relevant parameters. For example, we could not yet link the excitation profiles to speech intelligibility, while it is expected that more selective stimulation would increase speech performance. We also do not have a working solution for estimating the eCAP thresholds more precisely to further study the potential of eCAP thresholds in fitting cochlear implants. To guide future research on the topic presented in this thesis, we will discuss which complexities we encountered in recording the eCAPs and how to deal with them. Next, we will elaborate on the future perspectives of the (eCAP) measurements presented in this thesis and how to continue on these items.

7.1. Complexities encountered in recording eCAPs

When recording eCAPs for research or clinical use, it is important to realize that the eCAP is affected by physiological properties from the environment in which the eCAP is generated and by properties from the recording interface with which the eCAP is measured. This makes it challenging to record a good and usable eCAP, that really reflects the activity of the nerve fiber. In this section, we will discuss factors that affect the eCAP signals encountered in our studies. A comprehensive overview of all the aspects involved in recording eCAPs is outside the scope of this work, and we refer readers who are interested in a more general review of eCAPs to other literature (Mens 2007; Miller et al. 2008; Hughes 2013; He et al. 2017).

7.1.1. Stimulus level

In three of our studies, intra-operative eCAP measurements were used (Chapter 3-5). The main advantage of these measurements is that under anesthesia relatively high stimulus levels can be applied, often above the tolerability limit in awake subjects. In the intra-operative setting, stimulus levels with a maximum of around 1200 μA are typically used, while stimulus levels in the regular speech processing strategy are often a factor of two lower (depending on the pulse width as well). High stimulus levels are advantageous for measuring clear eCAP signals with a good signal-to-noise ratio, which make it is easier to recognize eCAP morphology, thereby simplifying eCAP analyses. However, it is hard to compare the intra-operative data with behavioral data. Behavioral data can, at the earliest, be collected a few months later, when the CI recipient is rehabilitated. It is known that, during the first months after implantation, physiological changes in the cochlea can occur that lead to certain electrophysiological changes, for example different impedances or eCAP thresholds (Hughes et al. 2001; Spivak et al. 2011). In this thesis, intra-operative data was compared with behavioral data, collected up to years later, whereby the effect of timing potentially affected the outcomes. Although it is difficult to avoid this in retrospective studies and using intra-operative eCAP data, it is recommended to collect all data within a limited time frame.

Later on, we collected a complete data set with both objective and subjective data measured in one session on the same day. We collected eCAP-based spatial forward masking (SFM) curves, electrical field imaging data, steered quadrupole thresholds (Bierer et al. 2015; O'Brien et al. 2016) and pitch discrimination data (Biesheuvel et al. 2019a). One of the ideas was to study electrode interaction, whereby the objective excitation density profiles (EDPs) obtained with the deconvolution method (Biesheuvel et al. 2016) would be compared with the subjective channel discrimination (data from Chapter 6).

Unfortunately, we could not measure reliable eCAPs (amplitude > 0.2 mV) in 13 of the 30 awake patients. These patients did not tolerate the high current levels required to elicit a clear eCAP response. In 17 of the 30 patients, we could measure reliable eCAPs, but not always on the required number of electrode contacts, as we defined that the deconvolution method needs reliable eCAPs on at least ten different electrode contacts in order to reliably estimate the EDPs (Biesheuvel et al. 2016). This made our post-operative eCAP data collected in awake subjects less usable for SOE analyses.

7.1.2. Voltage compliance limit

In Chapter 3, amplitude growth functions (AGFs) were analyzed, whereby we frequently observed a rollover at the top of the AGF (Figure 3.2C). However, the eCAP amplitude typically tends to increase with stimulus level, in line with most physiologically evoked responses (Hughes 2013). The roll over may be caused by the voltage compliance limit, which hindered the higher stimulus levels to be more effective. The voltage compliance limit determines the maximum amount of current that physically can be delivered through an electrode contact (Wolfe & Schafer 2014). All electrical stimulation follows Ohm's law: voltage (V) = current (A) × impedance (Ω), whereby the maximum current that can be delivered to the electrodes is determined by the voltage compliance and impedance seen between the electrode contacts. In CIs, the compliance voltage, that is, the maximum voltage that the current source in the CI can deliver, is determined by the device electronics and is approximately 7.2 V in the Advanced Bionics system. The impedance seen between the electrode contacts is determined by both the tissue (to the first order acting as a resistance) and the two electrode-tissue interfaces (to the first order acting as a capacitance). The total impedance of an electrode contact is typically 3–10 kΩ. The AGFs in Chapter 3 were measured using stimuli ranging from 0 to 500 CU, which corresponds with 0 to 1200 μA according to the equation[1]: clinical unit (CU) = pulse width (μs) × amplitude (μA) × 0.013. Suppose the impedance is 7.2 kΩ, the AGF starts to flatten at a stimulus level of 1000 μA, which is 411 CU.

The voltage compliance limit played a role in Chapter 5 as well. The SFM curves were collected at 1200 μA, but at some electrode contacts the impedance was so high that 1200 μA effectively could not be reached. We disabled these ineffective electrode contacts to be sure that our measurements were not limited by the compliance limit (e.g., in S008, S015, S021, see Table 5.2). Alternatively, the effectiveness of the stimulus can be guaranteed by widening the pulse width, because the total stimulus charge (in coulomb) is equal to the amplitude (in ampere) times the width (in seconds) of the pulse. Note that the

1 Personal communication with P. Boyle, senior director of external cooperation at Advanced Bionics.

stimulus pulse should not be too wide either, as the eCAP than further disappears into the stimulus artifact, making it more difficult to analyze the eCAP. In our custom-made eCAP measurement software, introduced in 2015 and used in Chapter 5, the option to increase the pulse width was not available. In a next version, this option should be incorporated in order to increase the number of successful eCAP recordings and usable SFM curves.

7.1.3. Noise level

One of the key messages of this thesis is that eCAP recordings have a measurement error. The measurement affects both the precision and accuracy of the eCAP metrics and should be considered when studying the clinical value of eCAPs. Note that 'accuracy' is defined as the approximation of a measurement to the actual value, 'precision' is defined as the closeness of a measurement to the same value as obtained with repeated measures (Stronks et al. 2019). In Chapter 3, we have seen that noise has a high impact on the precision of the eCAP thresholds, especially if the eCAP threshold is determined based on the last visible eCAP. Three different types of noise can be distinguished: (1) noise from electrophysiological processes inside the human body, (2) system noise from the electronic measurement circuit, and (3) interference from outside the body. In eCAP recordings, it is generally assumed that the eCAP signal is not disrupted by neural or muscle activity in the body (Miller et al. 2008; Undurraga et al. 2012). System noise is a stationary noise that originates from the electronic components inside the implant, for example, resistors and switched capacitors (Bes et al. 2010). It turned out that the Advanced Bionics (AB) measurement system has a higher system noise (20-50 μV) than the Cochlear system (2-5 μV) (Glassman & Hughes 2013). The lower the noise level, the more accurate the eCAP waveform is and the more precise the eCAP threshold can be determined (Glassman & Hughes 2013; Biesheuvel et al. 2017). A straightforward method to reduce random noise is ensemble averaging, i.e., averaging multiple eCAP waveforms obtained under identical stimulus conditions. The noise level decreases by a factor of $1/\sqrt{n}$, where n is the number of signal averages (Undurraga et al. 2012; Stronks et al. 2019). The third potential noise source in eCAP recordings is related to disturbances coming from outside the body. Because the intra-cochlear recording contact is close to the source and the recording circuit is fully implanted, disturbances from outside the body have little effect on the eCAP. However, one situation should be addressed in more detail in light of this thesis.

In the data from Chapter 3, which was recorded intra-operatively by a colleague from January 2010 to December 2015 and analyzed retrospectively, we observed that many of the eCAP recordings were contaminated with large stimulus artifacts, rendering them useless. Later on, when I did the measurements by myself, I found that these disrupted

eCAPs were likely recorded while the surgeon was closing the wound behind the ear. During that process, the skin or muscle flap that covers the ground electrode (implant casing) may be moving, causing brief disruptions in the recording circuit. During such disruptions, the stimulus builds up charge in the tissue, which cannot be returned to the reference electrode until the circuit is closed again. Consequently, stimulus artifacts are no longer synchronous, resulting in a failing of the artifact rejection paradigm and hence large stimulus artifacts. These artifacts are the reason that we had to exclude many eCAP recordings from our analysis (chapter 3). We, therefore, recommend recording eCAPs only when the surgeon is not performing surgery on the patient. For the data collection in Chapter 5, we interrupted the eCAP recordings when the surgeon was performing surgery. As a result, however, we were not able to complete the measurement on all contacts of interest (3, 9, 15) due to time constraints in the operating theatre.

7.1.4. Neural status

We noticed that, when measuring eCAPs postoperatively in awake CI users, stimuli may be audible while the eCAP is still not recordable, indicating an offset difference between eCAP threshold and behavioral thresholds. This offset is in line with what we found in Chapters 2 and 3, namely, that a shift is required to fit the eCAP threshold to the behavioral fitting levels. The offset can likely be explained by the neural health and the position of the recording contact relative to the active nerve fibers. The results of Snel-Bongers et al. (2013) indicated that the absence of unmyelinated terminals at the end of the dendrite (this represents a slight degeneration of the auditory nerve) causes a faster excitation of the dendrite and a lower subjective threshold compared to an intact auditory nerve. Further, research by Briaire & Frijns (2005) showed that degeneration of the nerve fibers causes deviant single fiber action potentials (SFAP) compared to a healthy, intact nerve. Their model simulations showed that, in degenerated dendrites and cell bodies, the antidromic SFAPs are delayed or even absent. Since the eCAP is the sum of SFAPs, deviating SFAPs will certainly affect the shape and recordability of the eCAP, and thus the precision and accuracy of the eCAP threshold level.

7.1.5. Recording contact

The observed offset difference between eCAP thresholds and behavioral thresholds can also be explained by the position of the recording contact relative to the active nerve fibers. A smaller distance between the recording contact and the excited nerve fibers would lead to a lower eCAP threshold, thereby minimizing the offset difference. However, as explained in the introduction of this thesis, due to the stimulus artifact, the recording

contact is generally situated one or two contacts away from the locus of excitation. Furthermore, it is known that the SFAPs closest to the recording contact contribute more to the eCAP than the SFAPS further away. This is demonstrated by the so-called scanning curve, which shows the eCAP amplitude evoked with a fixed probe position plotted as a function of a roved recording contact. Close to the probe, the eCAP amplitude is larger than when it is recorded at a larger distance. So, the proximity of the recording contact definitely affects the accuracy of the eCAP threshold.

The role of the recording contact is also relevant when studying spatial eCAP properties like SOE (Chapters 4 and 5). In Chapter 4, we found that in the apex of the cochlea the EDPs are generally broader than in the base. We discussed in Chapter 4 that this could be caused by the geometry of the cochlea and cross-turn stimulation. However, the scanning curves indicate that we also should consider the position of the recording contact. Scanning curves often show larger eCAP amplitudes apical from the stimulus than basal from the stimulus (van der Beek et al. 2012). Briaire & Frijns (2005) suggest that the asymmetry in the scanning curves can be explained by the different contributions of the orthodromic SFAPs and antidromic SFAPs to the eCAP. The orthodromic SFAPs propagate via the axons to the central nervous system, while the antidromic SFAPs move via the peripheral processes to the hair cells. The apical contacts of the intra-cochlear electrode array mainly record the antidromic SFAPs in the peripheral processes and the basal contacts mainly record the orthodromic SFAPs in the axons. Because the peripheral processes are closer to the recording contacts, due to the anatomy of the cochlea and the position of the electrode array, apical contacts likely record larger eCAPs than basal contacts. Thus far, the position of the recording contact is not included as a correction factor in our method, because we first worked on the validity of the deconvolution method with a limited number of parameters. Consequently, we only included spatial forward masking (SFM) curves from electrode contacts 3–16 and we excluded the two most apical SFM curves in our analyses. These curves were measured with a recording electrode located two contacts basal from the stimulus, which potentially deviates from the apically recorded curves. In future research, we would like to address the effect of the position of the recording contact on the eCAP data, in order to include all available data in our analyses.

7.2. Future perspectives

Thus far, we have discussed some complexities and complications that we encountered in eCAP recordings. In the next section, we will discuss our future perspectives on the (eCAP) measurements presented in this thesis.

7.2.1. eCAP thresholds

Our literature review showed that there is no evidence that eCAP thresholds are good predictors for the minimum (T) or maximum (C/M) stimulation levels (Chapter 2). Our follow-up study about the precision of eCAP thresholds showed that the precision is too low to expect a strong correlation between eCAP threshold and behavioral fitting levels (Chapter 3). However, in clinical practice, there is still demand for a method for the objectively fitting of cochlear implants to people who provide little feedback about the adjustments made by the audiologist, for example, young children or people with intellectual disabilities.

In our opinion, the search for a clinical application of eCAP thresholds as an objective fitting method for CI users will be unsuccessful as long as the research does not meet some basic conditions as described in the systematic review. We stated that the subjects must be selected randomly, the exclusion of poor eCAP responders should be reported, the behavioral threshold levels must be measured blinded from the eCAP recordings, the recordings should be described in detail, and the correlation between eCAP and behavioral levels must be investigated within individual subjects instead of across the study population, in order to draw valid conclusions for eCAP-based fitting of individuals (de Vos et al. 2017). In addition, it would be helpful if there is a consensus between clinics, and even between audiologists within a clinic, about the way that subjective and objective data are collected. As long as each clinic collects its own data, using its own methods and in a relatively small population, there will not arise a clear picture of the usefulness of eCAP thresholds for general clinical practice. Otherwise, at best, eCAP thresholds can function as a helpful guide within the fitting practice of a single audiologist (Potts et al. 2007).

Next to a clear study design, we also need some improvements in the recording system to be able to better study the relationship between eCAP thresholds and behavioral thresholds. In the context of the ReaSONS project, we want to highlight a potential role of the newly developed neural response amplifier (NRA) for studying eCAPs and eCAP thresholds. From the technical side, there might be potential for better estimating eCAP thresholds with the NRA. The NRA has a very low systemic noise of 1.1 pV and a wide dynamic range (Bes et al. 2010). These properties are advantageous for accurate and precise eCAP measurements, especially around the threshold level. The low systemic noise is also beneficial for measuring clear amplitude growth functions (AGF), leading to small measurement errors when estimating eCAP thresholds (Biesheuvel et al. 2017; Stronks et al. 2019).

7.2.2. Spatial forward masking curves

In Chapter 4, we postulated that the width of the SFM curve measured with forward masking is not an adequate measure of SOE. We proposed a new approach to determine SOE using the mathematical principle of (de)convolution. With the deconvolution method, we translated SFM curves into excitation areas attributable to either the masker or probe stimuli, the so-called EDPs (Chapter 4). The method explained inter-subject variations, e.g., differences in eCAP amplitudes, as well as across-the-array variations, e.g., asymmetry in the SFM curve. In addition, the excitation profiles from the deconvolution method matched well with the excitation profiles simulated in our computational model of the human cochlea (Chapter 5). We also showed that the deconvolution method, which was developed with HiRes90K implants from Advanced Bionics, is suitable for analyzing SFM curves recorded with Nucleus 422/532 implants from Cochlear (Biesheuvel et al. 2019b). Unfortunately, we could not yet link the EDPs to clinical measures like speech performance or channel discrimination. So, in future research, we will further elucidate the EDP as an outcome measure of SOE, to answer the many unknowns and to bring this technique to the clinic. Among the questions we have are: What does the EDP actually reflect; is it a relative or an absolute measure of nerve excitation? How well reflect two-dimensional EDPs the three-dimensional nerve fiber distributions in the cochlea? Which EDP property is relevant for pitch coding: the locus of the center of excitation, or the position of the EDP edges? Is the width of the EDP related to speech performance, or is the EDP not precise enough?

Parallel to our work, which was at first presented at the Objective Measures congress in Toronto (Briaire et al. 2014), a similar method for analyzing SFM curves was developed by Cosentino et al. (2015): the so-called 'panoramic eCAP' method. The underlying principles of the deconvolution method and the 'panoramic eCAP' method were quite similar; both methods were based on an optimization routine to estimate the excitation patterns underlying the SFM curves. However, there were also some fundamental methodological differences. The following section discusses the main differences between the two methods to find out which (methodological) aspects should be considered in future research.

Firstly, our deconvolution method is developed using intra-operative SFM curves recorded with high stimulation levels. The stimulus levels were set equally across all electrode contacts of the array. In awake subjects, the SFM curves were collected using maximum acceptable loudness (MAL), whereby the lowest MAL level across the electrode array was set to all other contacts as well. A limitation of this procedure is that, in case of substantial

MAL level variation across the array, the lowest MAL level is not so effective for the other contacts. Due to the equal stimulus level across the array, smaller eCAP amplitudes must lead to less excitation or smaller EDPs and vice versa. Cosentino et al. (2015) used the most comfortable loudness (MCL) level per electrode contract along the array. The use of MCL levels implicates that each active contact must lead to an excitation profile, because the stimulus is clearly heard at the MCL level. Further, these excitation profiles must have approximately equal areas, as they encode for equal loudness. The MCL levels are more practical in awake subjects, as they are less exhaustive for the subject and allow recording both the eCAPs and behavioral data in one session. However, the use of either MCL or MAL stimulus levels has consequences for the EDP parameterization. To illustrate, Cosentino et al. (2016) assumed that poor neural regions were reflected by shifted excitation patterns, because the stimulus is heard at MCL level and thus the excitation pattern must exist. In our deconvolution method, all stimulus levels were equal and poor neural regions were reflected by smaller eCAPs, consequently leading to locally smaller or absent EDPs. Whether a poor neural region is best reflected by a shifted or an absent excitation pattern must be further validated. Ideally, this validation is performed with an independent method or model. Garcia et al. (2021) recently published a follow-up regarding 'panoramic eCAP', whereby they used computer simulations to create SFM curves with poor neural regions and, subsequently, tried to detect them with the 'panoramic eCAP' method. However, such a backward approach has the limitation that both the generated and solved dead regions are based on the same model assumptions. We suggest to validate the dead-region-detection of both methods using simulations in an independent model, for instance, our computational model of the human cochlea (Frijns et al. 1995; Frijns et al. 2000; Briaire & Frijns 2000b; Briaire & Frijns 2000a; Kalkman et al. 2014; Kalkman et al. 2015; Kalkman et al. 2022). With our computational model, it would be possible to model poor neural regions. Subsequently, based on these poor neural regions, eCAP-based SFM curves can be simulated, and these curves can be translated back to EDPs using the deconvolution method. Next, the obtained EDPs can be compared with the simulated dead regions to validate them. Garcia et al. (2021) proposed another nice idea to validate the detection of poor neural regions. They introduced 'tired regions' in the SFM curves by presenting pre-pulses on a specific electrode contact before every eCAP recording. Next, the underlying excitation patterns were estimated, whereby the contribution of the excitation patterns to the SFM curves with tired regions was weighted using a neural health factor. However, excitation patterns that are reduced by a neural health factor do no longer match the initial stimulation at MCL level, coded by unity area under the Gaussian curve. So, it is more likely that, when using stimuli at MCL level, a poor neural region is reflected by a shifted excitation pattern (neighboring nerve fibers contribute to the loudness) than by

a smaller excitation pattern. We think that our deconvolution method, based on equal MAL levels across the electrode array, deals better with tired regions simulated with pre-pulses. Our EDPs have more free parameters and are not bound to loudness. Further, the EDP sizes are directly related to the eCAP amplitudes (see Figure 4.8). So, tired regions reflected by smaller eCAPs can be translated into smaller EDPs. It would be nice to study the tired regions concept in more detail with our deconvolution in future research.

Secondly, both our deconvolution method and the 'panoramic eCAP' method do not consider the effect of the recording contact. However, as described earlier, the recording contact might play a role in the shape of the SFM curve and thus in the EDPs derived from the SFM curve. Yet, we do not know how the recording effect best can be implemented in the deconvolution method. We might develop a correction factor like the offset parameter (representing the noise floor) and the scaling parameter (required for an arithmetic correction). Alternatively, the NRA in combination with a new and efficient electrode design (Lawand 2015) can play a role here. Due to the companding technique, the NRA can record eCAPs while they were not distorted by the stimulus artifact (Bes et al. 2010). In that case, it is no longer necessary to place the recording contact several electrode contacts away from the stimulating contact. In combination with a new horse-shoe-shaped electrode design, with a recording contact surrounding the stimulus contact the effect of the recording position can be minimized and be studied in more detail (Lawand 2015, Page 129).

7.2.3. Channel discrimination

Finally, we will discuss the future perspectives of our custom-made channel discrimination test. We developed a test that assessed the channel discrimination ability of CI users along the whole electrode array within 30 minutes. The test provided insight into the variation of discrimination scores (Dα) across the electrode array. Further, we found that channel discrimination is positively correlated with speech perception (Chapter 6). We also explored whether the Dα scores correlate with the eCAP-based EDPs. However, at first glance, no relationship was found between the Dα scores and the EDP sizes, or between the Dα scores and the overlap ration of adjacent EDPs. It is likely that the precision of the channel discrimination test played a role here. The current test provided a rough estimate of channel discrimination which was accepted as a consequence of limiting the test time. The EDPs were also a rough estimate, as we tried to estimate the excitation density of many nerve fibers by parameterized Gaussian functions. We think that both the Dα scores and EDPs need some refinement before we can study CI performance using eCAP-based EDPs.

Further, the accuracy of the Dα scores, which has not yet been studied in detail, may play a role as well. To study the accuracy, the ICDs could be compared with the more accurate and even more time-consuming just noticeable difference (Snel-Bongers et al. 2012), which can be seen as the golden standard. Alternatively, the Dα scores could be validated using psychometric functions. A psychometric function depicts the discrimination ability (y-axis) as function of a range of ICDs (x-axis), assuming a high Dα score for large ICDs (>2) and a low Dα score for ICDs close to zero. The point where 50% of the ICDs were properly distinguished is typically chosen as the 'threshold' or the discrimination score. Collecting psychometric curves may also be time-consuming, but the curves could provide accurate ICDs, including estimates of the threshold reliability (Wichmann & Hill 2001a; Wichmann & Hill 2001b). Further, the ICDs at which the discrimination test was performed should be reconsidered, because our current test led to too many '> 1' outcomes. In the current test, we started at ICD = 1 and the ICD was halved if the subject could discriminate the stimuli, while the test was aborted if an α was not discriminable. Alternatively, the ICD can be doubled if the subject cannot discriminate the stimuli, or one can test an α value in between a discriminable and non-discriminable α. Next, the number of repetitions has to be weighed against the testing time. In the current test, five repetitions were used to save time. However, with six of seven repetitions, we could better approach the turning point of the 3AFC test (66%). Further, more repetitions will also decrease the effect of chance guesses.

We think that, after further improving the accuracy and precision, the channel discrimination test has potential for both research and clinical practice. We will work on linking the Dα scores to the eCAP-based EDPs in order to further investigate SOE and its relation to CI performance. Moreover, accurate and precise Dα scores could potentially help clinicians optimize the fitting procedures, e.g., to deactivate ineffective electrode contacts.

7.3. Concluding remark

This thesis showed that eCAP research in cochlear implants is challenging and remains challenging. The studies provided a closer look at stimulation thresholds and spread of excitation in cochlear implants, which for sure helps CI researchers in their work. We are curious how the items addressed in this thesis evolve, and where the CI research stands within 10 years. Will new recording techniques, more precise eCAP measurements and intelligent analyses lead to totally objective CI fittings, attuned to the characteristics of the auditory nerve and the needs of the CI user?

CHAPTER

Nederlandse samenvatting

8.1. Algemene introductie

Hoofdstuk 1: Goed kunnen horen is heel belangrijk voor het welzijn van de mens. Het is daarom essentieel dat een gehoorverlies goed wordt gerevalideerd. Bij een ernstig, perceptief gehoorverlies kan de geluidsverwerking in de cochlea (ook wel het slakkenhuis genoemd) zodanig verstoord zijn dat een hoortoestel onvoldoende ondersteuning biedt. Een cochleair implantaat (CI) kan dan een oplossing zijn. Een CI is een apparaat dat geluid direct doorgeeft aan de gehoorzenuw, door de zenuw elektrisch te prikkelen via een elektrode array in het slakkenhuis. Deze elektrische prikkels worden waargenomen als geluid.

Het CI heeft ook een telemetrie functie waarmee de 'electrically evoked compound action potential' (eCAP) kan worden gemeten. De eCAP is de optelsom van alle actiepotentialen die na elektrische stimulatie ontstaan in de zenuwvezels in het slakkenhuis. In het verleden is er veel onderzoek gedaan naar de eCAP. Men was vooral benieuwd of de eCAP informatie kon geven over de werking van het CI en de gehoorzenuw. In de praktijk bleek het lastig om de eCAP-signalen goed te kunnen analyseren en om een relatie te vinden tussen de eCAP en klinische uitkomstmaten zoals spraakverstaan. Het lijkt erop dat de technische beperkingen van de telemetrie functie grote invloed hebben op de nauwkeurigheid van de eCAP en daarmee ook op de klinische toepasbaarheid van de eCAP. Met het project Real-time Sensing Of Neural Signals (ReaSONS) is geprobeerd een stap verder te komen met het eCAP onderzoek. Het ReaSONS-project is een samenwerking tussen het Leids Universitair Medisch Centrum en de Technische Universiteit Delft en het is gefinancierd door Stichting Technologische Wetenschappen (projectnummer 11693). Het project had twee doelen: (1) het ontwikkelen van een neurale responsieversterker om betrouwbaar en nauwkeurig eCAPs te kunnen meten; (2) het onderzoeken van de klinische toepasbaarheid en relevantie van eCAP metingen. Het eerste doel is uitgewerkt door een promovendus bij de Technische Universiteit van Delft. Het tweede doel is uitgewerkt in dit proefschrift.

8.2. Systematisch literatuuronderzoek naar het objectief instellen van CI's

Hoofdstuk 2: Als eerste hebben we gekeken naar de toepasbaarheid van eCAPs als objectieve maat voor het instellen van het CI. Bij een bepaalde groep CI-gebruikers, bijvoorbeeld jonge kinderen, is het lastig om het CI goed in te stellen. Dit komt onder andere doordat zij geen goede feedback kunnen geven over het functioneren van het CI. In het verleden is er onderzoek gedaan naar de vraag of eCAP metingen bruikbaar zijn als hulpmiddel voor het instellen van het CI. Sommige onderzoeken concluderen dat de objectieve eCAP-drempel, dat is de minimale hoeveelheden stroom die nodig is om een eCAP op te wekken, een goede voorspeller is van de subjectieve gehoordrempel op

hetzelfde elektrode contact. Bij veel van deze onderzoeken leken de onderzoeksmethoden en conclusies echter niet valide. Door middel van een systematische review van de literatuur hebben we gekeken hoeveel bewijs er nu eigenlijk is dat eCAPs bruikbaar zijn voor het aanpassen van CI's. Uiteindelijk bleken slechts enkele studies een goede onderzoeksmethode te gebruiken en deze studies kwamen tot de conclusie dat de eCAP drempel geen goede uitkomstmaat is voor het instellen van het CI.

8.3. De nauwkeurigheid van eCAP drempels

Hoofdstuk 3: De volgende vraag over eCAP drempels die ons bezig hield was: waarom is er geen verband tussen de eCAP drempels en de subjectieve gehoordrempels van de CI-gebruiker, terwijl de meeste onderzoekers deze relatie wel verwachten? Om dit te onderzoeken hebben we gekeken hoe nauwkeurig eCAP drempels zijn en of deze in de huidige vorm bruikbaar zijn voor het voorspellen van subjectieve gehoordrempels. Het onderzoek liet zien dat de eCAP-drempels, zoals bepaald met de veelgebruikte 'linear regression' methode en 'last visible' methode, te onnauwkeurig zijn voor het voorspellen van subjectieve gehoordrempels van CI-gebruikers.

Kort samengevat: hoofdstuk 2 en 3 laten zien dat, wil men eCAPs gebruiken voor het instellen van CI's, er betere meetsystemen en nauwkeurigere onderzoeksmethoden ontwikkeld moeten worden.

8.4. Nieuwe methode voor het bepalen van excitatiegebieden

Hoofdstuk 4: Naast het analyseren van de eCAP-drempels, hebben we ook gekeken hoe de eCAP gebruikt kan worden om de grootte van het excitatiegebieden te bepalen. Er is veel belangstelling voor de vraag of de grootte van de excitatiegebieden, oftewel de 'spread of excitation' (SOE), correleert met het spraakverstaan van de CI-gebruiker. De verwachting is dat kleinere excitatiegebieden zorgen voor een betere spatiële resolutie (onderscheiding van verschillende electrode contacten) en daarmee ook voor een beter spraakverstaan. We hebben kritisch gekeken naar de huidige methoden voor het bepalen van de SOE met behulp van eCAPs. We zagen dat deze methoden te simplistisch waren en geen recht doen aan de eCAP metingen. Daarom hebben we een nieuwe methode ontwikkeld om de neurale excitatie per electrode contact te kunnen voorspellen. Onze methode maakt gebruik van het wiskundige principe van (de)convolutie om eCAP metingen te vertalen naar zogenaamde 'excitation density profiles' (EDPs). We hebben de deconvolutiemethode toegepast op eCAP metingen bij patiënten en op basis van de eerste resultaten konden we concluderen dat de methode werkt. Het was mogelijk om eCAP metingen bij patiënten te vertalen naar excitatiegebieden per electrode

contact. Vervolgonderzoek moet uitwijzen of de EDPs vertaald kunnen worden naar een toepassing in de klinische praktijk.

8.5. Het effect van stimulusniveau op excitatiegebieden

Hoofdstuk 5: In het vervolgonderzoek naar excitatieprofielen hebben we gekeken wat er met de EDP's gebeurde als we het stimulatieniveau veranderden. De verwachting was dat lagere stimulatieniveaus zouden leiden tot kleinere excitatiegebieden, maar dat was nog niet eerder aangetoond met objectieve eCAP metingen. De methode die we ontwikkeld hebben in hoofdstuk 4 bood nieuwe kansen om dit verder te onderzoeken. We bestudeerden het effect van stimulatieniveau op het excitatiegebied bij 24 proefpersonen en we ontdekten dat lagere stimulusniveaus inderdaad kleinere EDP's veroorzaakten. Een kleinere EDP betekende in de meeste gevallen een smallere EDP (dus selectievere excitatie) en in sommige gevallen een lagere EDP (dus kleinere excitatiedichtheid). Ook zagen we dat bij het wijzigen van het stimulatieniveau het excitatiegebied een beetje opschoof langs de electrode array, met als gevolg dat de toonhoogte waarneming een klein beetje verandert. Deze resultaten bieden meer inzicht in de werking van het CI en kunnen gebruikt worden bij het optimaliseren van CI's in de klinische praktijk.

Ter validatie hebben we in deze studie de EDP's ook vergeleken met excitatieprofielen die we simuleerden in het Leidse computermodel van de humane cochlea. Het bleek dat de EDP's die we vonden bij CI-gebruikers sterk lijken op voorspellingen van neurale excitatie in het computermodel. Dit bevestigde de juistheid van onze deconvolutiemethode.

8.6. Het onderscheiden van verschillende geluidskanalen

Hoofdstuk 6: Het laatste onderzoek betrof het ontwikkelen van een nieuwe test voor het subjectief meten van spatiële resolutie langs de electrode array. De resultaten van deze test zijn ook interessant als vergelijkingsmateriaal voor de EDPs, die een objectieve maat van spatiële resolutie geven. We hebben gekeken hoe goed een CI-gebruiker onderscheid kan maken tussen tonen die geproduceerd worden via de verschillende geluidskanalen van het CI. Dit wordt ook wel 'channel discrimination' genoemd, in dit proefschrift aangeduid met de 'Dα-score'. Bij andere studies was het gebruikelijk om de Dα-score heel nauwkeurig te meten. Maar omdat dit veel tijd kostte, kon de Dα-score dan slechts op een beperkt aantal elektrode contacten worden gemeten. We hebben een nieuwe methode ontwikkeld voor het testen van 'channel discrimination' langs alle elektrode contacten van de elektrode-array in een relatief korte tijd, maar dan wel met een beperktere nauwkeurigheid. In deze studie hebben we ook gekeken of er een relatie is tussen de gemeten Dα-scores en het spraakverstaan van dezelfde CI-gebruiker. Het

onderzoek liet zien dat er een relatie is tussen spraakverstaan en de Dα-score. Als een CI-gebruiker geluidskanalen die dicht bij elkaar liggen goed kon onderscheiden dan was het spraakverstaan ook beter. Daarnaast vonden we dat de Dα-score sterk varieerde tussen de verschillende geluidskanalen. Dit pleit ervoor om, bij toekomstig onderzoek naar 'channel discrimination', de Dα-score langs de hele electrode-array te meten en niet slechts op een paar elektrode contacten, zoals tot nu toe vaak werd gedaan. Tijdens het onderzoek kwamen er nog een paar verbeterpunten naar boven met betrekking tot de nauwkeurigheid van de test. Na implementatie van deze punten kunnen de Dα-scores verder toegepast worden. Te denken valt aan het vergelijken van de Dα-scores met de EDP uitkomsten, met als doel de EDP's en de deconvolutiemethode verder te valideren. Daarnaast zouden de test en de Dα-scores ook een rol kunnen gaan spelen in de klinische praktijk. Bijvoorbeeld, om tijdens de CI controles de effectiviteit van de verschillende contacten te beoordelen en zo de CI aanpassing te optimaliseren.

8.7. Algemene discussie

Hoofdstuk 7: Het proefschrift sluit af met een uitgebreide discussie over het meten van eCAPs en het toekomstperspectief voor het eCAP onderzoek. Het proefschrift laat zien dat het eCAP onderzoek uitdagend is en blijft. We zijn benieuwd hoe de onderwerpen die in dit proefschrift aan bod kwamen zich ontwikkelen en waar het eCAP onderzoek over 10 jaar staat. Zullen nieuwe meettechnieken, nauwkeurigere eCAP metingen en 'artificial intelligence' leiden tot objectieve CI aanpassingen, volledig afgestemd op de individuele gehoorzenuw en situatie?

CHAPTER

9

Bibliography

Abbas, P.J., Brown, C.J., Shallop, J.K., et al. (1999). Summary of results using the nucleus CI24M implant to record the electrically evoked compound action potential. *Ear Hear.*, 20, 45–59.

Abbas, P.J., Hughes, M.L., Brown, C.J., et al. (2004). Channel interaction in cochlear implant users evaluated using the electrically evoked compound action potential. *Audiol. Neurootol.*, 9, 203–213.

Agresti, A. (2002). *Categorical Data Analysis*, Hoboken, NJ, USA: John Wiley & Sons, Inc.

Akhoun, I., Bestel, J., Pracht, P., et al. (2015). Automated classification of electrically-evoked compound action potentials. In *2015 7th International IEEE/EMBS Conference on Neural Engineering (NER)*. (*pp. 687–690*). IEEE.

Akin, I., Kuran, G., Saka, C., et al. (2006). Preliminary results on correlation between neural response imaging and "most comfortable levels" in cochlear implantation. *J. Laryngol. Otol.*, 120, 261–5.

Akin, I., Mutlu, M., Kuran, G., et al. (2008). One-year results of the banded neural response imaging study. *Otol. Neurotol.*, 29, 635–8.

Alvarez, I., de la Torre, A., Sainz, M., et al. (2010). Using evoked compound action potentials to assess activation of electrodes and predict C-levels in the Tempo+ cochlear implant speech processor. *Ear Hear.*, 31, 134–45.

Arnoldner, C., Kaider, A., Hamzavi, J. (2006). The role of intensity upon pitch perception in cochlear implant recipients. *Laryngoscope*, 116, 1760–5.

Arora, K., Dowell, R., Dawson, P. (2012). Cochlear Implant Stimulation Rates and Speech Perception. *Mod. speech Recognit. approaches with case Stud.*, 215–254.

Baudhuin, J.L., Hughes, M.L., Goehring, J.L. (2016). A Comparison of Alternating Polarity and Forward Masking Artifact-Reduction Methods to Resolve the Electrically Evoked Compound Action Potential. *Ear Hear.*, 1–9.

Beek, F.B. van der., Briaire, J.J., Frijns, J.H.M. (2015). Population-Based Prediction of Fitting Levels for Individual Cochlear Implant Recipients. *Audiol. Neurotol.*, 20, 1–16.

van der Beek, F.B., Briaire, J.J., Frijns, J.H.M. (2012). Effects of parameter manipulations on spread of excitation measured with electrically-evoked compound action potentials. *Int. J. Audiol.*, 51, 465–74.

Bes, C.J., Chutham, S., Serdijn, W.A. (2010). An Additive Instantaneously Companding Readout System for Cochlear Implants. *2010 Biomed. Circuits Syst. Conf.*, 126–29.

Bierer, J. a., Litvak, L. (2016). Reducing Channel Interaction Through Cochlear Implant Programming May Improve Speech Perception: Current Focusing and Channel Deactivation. *Trends Hear.*, 20, 1–12.

Bierer, J.A. (2007). Threshold and channel interaction in cochlear implant users: evaluation of the tripolar electrode configuration. *J. Acoust. Soc. Am.*, 121, 1642–1653.

Bierer, J.A., Bierer, S.M., Kreft, H. a., et al. (2015). A Fast Method for Measuring Psychophysical Thresholds Across the Cochlear Implant Array. *Trends Hear.*, 19, 1–12.

Biesheuvel, J.D., Briaire, J.J., Frijns, J.H.M. (2016). A Novel Algorithm to Derive Spread of Excitation Based on Deconvolution. *Ear Hear.*, 37, 572–81.

Biesheuvel, J.D., Briaire, J.J., Frijns, J.H.M. (2017). The Precision of eCAP Thresholds Derived From Amplitude Growth Functions. *Ear Hear.*, 39, 701–711.

Biesheuvel, J.D., Briaire, J.J., de Jong, M.A.M., et al. (2019a). Channel discrimination along all contacts of the cochlear implant electrode array and its relation to speech perception. *Int. J. Audiol.*, 58, 262–268.

Biesheuvel, J.D., Briaire, J.J., Kalkman, R.K., et al. (2021). The effect of stimulus level on the spread of excitation in cochlear implants. *Hear. Res.*, Submitted.

Biesheuvel, J.D., Goffi-Gomez, M.V.S., James, C.J., et al. (2019b). Applying the deconvolution method in Nucleus CIs to better characterize spread of excitation. *Congr. Eur. Fed. Audiol. Soc.*, Lisbon, Portugal.

Bonham, B.H., Litvak, L.M. (2008). Current focusing and steering: Modeling, physiology, and psychophysics. *Hear. Res.*, 242, 141–53.

Borenstein, M. (2009). Effect Sizes for Continuous Data. In H. . Cooper, L. V. Hedges, & J. C. Valentine, eds. *The Handbook of Research Synthesis and Meta-analysis*. (*pp. 221–235*). New York: Russell Sage Foundation.

Bosman, A.J., Smoorenburg, G.F. (1995). Intelligibility of Dutch CVC syllables and sentences for listeners with normal hearing and with three types of hearing impairment. *Audiology*, 34, 260–84.

Botros, A., van Dijk, B., Killian, M. (2007). AutoNR: an automated system that measures ECAP thresholds with the Nucleus Freedom cochlear implant via machine intelligence. *Artif. Intell. Med.*, 40, 15–28.

Botros, A., Psarros, C. (2010). Neural response telemetry reconsidered: I. The relevance of ECAP threshold profiles and scaled profiles to cochlear implant fitting. *Ear Hear.*, 31, 367–79.

Bournique, J.L., Hughes, M.L., Baudhuin, J.L., et al. (2014). Effect of ECAP-based choice of stimulation rate on speech-perception performance. *Ear Hear.*, 34, 437–46.

Briaire, J., Biesheuvel, D., Frijns, J. (2014). Deconvolution of the spread of excitation curves measured in cochlear implants. *Int. Conf. Object. Meas. Audit. Implant.*, Toronto, Canada.

Briaire, J.J., Frijns, J.H. (2000a). Field patterns in a 3D tapered spiral model of the electrically stimulated cochlea. *Hear. Res.*, 148, 18–30.

Briaire, J.J., Frijns, J.H.M. (2000b). 3D mesh generation to solve the electrical volume conduction problem in the implanted inner ear. *Simul. Pract. Theory*, 8, 57–73.

Briaire, J.J., Frijns, J.H.M. (2005). Unraveling the electrically evoked compound action potential. *Hear. Res.*, 205, 143–56.

Brown, C.J., Abbas, P.J., Borland, J., et al. (1996). Electrically evoked whole nerve action potentials in Ineraid cochlear implant users: responses to different stimulating electrode configurations and comparison to psychophysical responses. *J. Speech Hear. Res.*, 39, 453–67.

Brown, C.J., Abbas, P.J., Gantz, B.J. (1998). Preliminary experience with neural response telemetry in the nucleus CI24M cochlear implant. *Am. J. Otol.*, 19, 320–7.

Brown, C.J., Hughes, M.L., Luk, B., et al. (2000). The relationship between EAP and EABR thresholds and levels used to program the nucleus 24 speech processor: data from adults. *Ear Hear.*, 21, 151–63.

Busby, P. a, Battmer, R.D., Pesch, J. (2008). Electrophysiological spread of excitation and pitch perception for dual and single electrodes using the Nucleus Freedom cochlear implant. *Ear Hear.*, 29, 853–864.

Cafarelli Dees, D., Dillier, N., Lai, W.K., et al. (2005). Normative findings of electrically evoked compound action potential measurements uing the neural response telemetry of the nucleus CI24M cochlear implant system. *Audiol. Neurotol.*, 10, 105–116.

Caner, G., Olgun, L., Gültekin, G., et al. (2007). Optimizing fitting in children using objective measures such as neural response imaging and electrically evoked stapedius reflex threshold. *Otol. Neurotol.*, 28, 637–40.

Carlyon, R.P., Lynch, C., Deeks, J.M. (2010). Effect of stimulus level and place of stimulation on temporal pitch perception by cochlear implant users. *J. Acoust. Soc. Am.*, 127, 2997–3008.

Charasse, B., Chanal, J.M., Berger-Vachon, C., et al. (2004). Influence of stimulus frequency on NRT recordings. *Int. J. Audiol.*, 43, 236–44.

Cohen, L.T. (2009). Practical model description of peripheral neural excitation in cochlear implant recipients: 2. Spread of the effective stimulation field (ESF), from ECAP and FEA. *Hear. Res.*, 247, 100–111.

Cohen, L.T., Richardson, L.M., Saunders, E., et al. (2003). Spatial spread of neural excitation in cochlear implant recipients: Comparison of improved ECAP method and psychophysical forward masking. *Hear. Res.*, 179, 72–87.

Cohen, L.T., Saunders, E., Richardson, L.M. (2004). Spatial spread of neural excitation: comparison of compound action potential and forward-masking data in cochlear implant recipients. *Int. J. Audiol.*, 43, 346–55.

Collins, L.M., Zwolan, T. a, Wakefield, G.H. (1997). Comparison of electrode discrimination, pitch ranking, and pitch scaling data in postlingually deafened adult cochlear implant subjects. *J. Acoust. Soc. Am.*, 101, 440–55.

Cosentino, S., Gaudrain, E., Deeks, J., et al. (2015). Multistage nonlinear optimization to recover neural activation patterns from evoked compound action potentials of cochlear implant users. *IEEE Trans. Biomed. Eng.*, 7, 1–1.

Cosentino, S., Vries, L. De, Scheperle, R., et al. (2016). Dual-stage algorithm to identify channels with poor electrode-to-neuron interface in cochlear implant users. In *2016 IEEE International Conference on Acoustics, Speech and Signal Processing (ICASSP)*. (*pp. 834–838*). IEEE.

Cosetti, M.K., Shapiro, W.H., Green, J.E., et al. (2010). Intraoperative neural response telemetry as a predictor of performance. *Otol. Neurotol.*, 31, 1095–9.

Cullington, H. (2000). Preliminary neural response telemetry results. *Br. J. Audiol.*, 34, 131–40.

D'Elia, A., Bartoli, R., Giagnotti, F., et al. (2012). The Role of Hearing Preservation on Electrical Thresholds and Speech Performances in Cochlear Implantation. *Otol. Neurotol.*, 33, 343–347.

Debruyne, J.A., Francart, T., Janssen, A.M.L., et al. (2017). Fitting prelingually deafened adult cochlear implant users based on electrode discrimination performance. *Int. J. Audiol.*, 56, 174–185.

DerSimonian, R., Laird, N. (1986). Meta-analysis in clinical trials. *Control. Clin. Trials*, 7, 177–88.

Donaldson, G.S., Kreft, H. a, Litvak, L. (2005). Place-pitch discrimination of single- versus dual-electrode stimuli by cochlear implant users (L). *J. Acoust. Soc. Am.*, 118, 623–6.

Dumville, J.C., Torgerson, D.J., Hewitt, C.E. (2006). Research methods - Reporting attrition in randomised controlled trials. *BMJ Br. Med. J.*, 332, 969.

Firszt, J.B., Koch, D.B., Downing, M., et al. (2007). Current steering creates additional pitch percepts in adult cochlear implant recipients. *Otol. Neurotol.*, 28, 629–36.

Franck, K.H. (2002). A model of a nucleus 24 cochlear implant fitting protocol based on the electrically evoked whole nerve action potential. *Ear Hear.*, 23, 67S-71S.

Franck, K.H., Norton, S.J. (2001). Estimation of psychophysical levels using the electrically evoked compound action potential measured with the neural response telemetry capabilities of Cochlear Corporation's CI24M device. *Ear Hear.*, 22, 289–99.

Friesen, L.M., Shannon, R. V, Baskent, D., et al. (2001). Speech recognition in noise as a function of the number of spectral channels: comparison of acoustic hearing and cochlear implants. *J. Acoust. Soc. Am.*, 110, 1150–63.

Frijns, J.H., Briaire, J.J., Grote, J.J. (2001). The importance of human cochlear anatomy for the results of modiolus-hugging multichannel cochlear implants. *Otol. Neurotol.*, 22, 340–349.

Frijns, J.H.M., Briaire, J.J., de Laat, J.A.P.M., et al. (2002). Initial evaluation of the Clarion CII cochlear implant: speech perception and neural response imaging. *Ear Hear.*, 23, 184–197.

Frijns, J.H.M., Briaire, J.J., Schoonhoven, R. (2000). Integrated use of volume conduction and neural models to simulate the response to cochlear implants. *Simul. Pract. Theory*, 8, 75–97.

Frijns, J.H.M., Kalkman, R.K., Vanpoucke, F.J., et al. (2009). Simultaneous and non-simultaneous dual electrode stimulation in cochlear implants: evidence for two neural response modalities. *Acta Otolaryngol.*, 129, 433–9.

Frijns, J.H.M., Klop, W.M.C., Bonnet, R.M., et al. (2003). Optimizing the number of electrodes with high-rate stimulation of the clarion CII cochlear implant. *Acta Otolaryngol.*, 123, 138–42.

Frijns, J.H.M., De Snoo, S.L., Schoonhoven, R. (1995). Potential distributions and neural excitation patterns in a rotationally symmetric model of the electrically stimulated cochlea. *Hear. Res.*, 87, 170–186.

Garcia, C., Goehring, T., Cosentino, S., et al. (2021). The Panoramic ECAP Method: Estimating Patient-Specific Patterns of Current Spread and Neural Health in Cochlear Implant Users. *J. Assoc. Res. Otolaryngol.*, 22, 567–589.

Giavarina, D. (2015). Understanding Bland Altman analysis. *Biochem. Medica*, 25, 141–151.

Glassman, E.K., Hughes, M.L. (2013). Determining electrically evoked compound action potential thresholds: a comparison of computer versus human analysis methods. *Ear Hear.*, 34, 96–109.

Goehring, J.L., Neff, D.L., Baudhuin, J.L., et al. (2014). Pitch ranking, electrode discrimination, and physiological spread of excitation using current steering in cochlear implants. *J. Acoust. Soc. Am.*, 136, 3159.

Gordon, K. a, Papsin, B.C., Harrison, R. V (2004a). Toward a battery of behavioral and objective measures to achieve optimal cochlear implant stimulation levels in children. *Ear Hear.*, 25, 447–63.

Gordon, K., Papsin, B.C., Harrison, R. V (2004b). Programming cochlear implant stimulation levels in infants and children with a combination of objective measures. *Int. J. Audiol.*, 43 Suppl 1, S28-32.

Guedes, M.C., Weber, R., Gomez, M.V.S.G., et al. (2007). Influence of evoked compound action potential on speech perception in cochlear implant users. *Braz. J. Otorhinolaryngol.*, 73, 439–45.

Han, D.-M., Chen, X.-Q., Zhao, X.-T., et al. (2005). Comparisons between neural response imaging thresholds, electrically evoked auditory reflex thresholds and most

comfortable loudness levels in CII bionic ear users with HiResolution sound processing strategies. *Acta Otolaryngol.*, 125, 732–5.

He, S., Teagle, H.F.B., Buchman, C.A. (2017). The Electrically Evoked Compound Action Potential: From Laboratory to Clinic. *Front. Neurosci.*, 11, 339.

Hedges, L., Olkin, I. (1985). Meta-analysis from a small sample. In *Statistical methods for meta-analysis*. (*p. 32*). Orlando: Academic Press.

Holstad, B. a, Sonneveldt, V.G., Fears, B.T., et al. (2009). Relation of electrically evoked compound action potential thresholds to behavioral T- and C-levels in children with cochlear implants. *Ear Hear.*, 30, 115–27.

Hughes, M.L. (2013). *Objective Measures in Cochlear Implants*, San Diego: Plural Publishing.

Hughes, M.L., Abbas, P.J. (2006a). Electrophysiologic channel interaction, electrode pitch ranking, and behavioral threshold in straight versus perimodiolar cochlear implant electrode arrays. *J. Acoust. Soc. Am.*, 119, 1538–1547.

Hughes, M.L., Abbas, P.J. (2006b). The relation between electrophysiologic channel interaction and electrode pitch ranking in cochlear implant recipients. *J Acoust Soc Am*, 119, 1527–1537.

Hughes, M.L., Baudhuin, J.L., Goehring, J.L. (2014). The relation between auditory-nerve temporal responses and perceptual rate integration in cochlear implants. *Hear. Res.*, 316, 44–56.

Hughes, M.L., Brown, C.J., Abbas, P.J., et al. (2000). Comparison of EAP thresholds with MAP levels in the nucleus 24 cochlear implant: data from children. *Ear Hear.*, 21, 164–74.

Hughes, M.L., Goehring, J.L., Baudhuin, J.L. (2016). Effects of Stimulus Polarity and Artifact Reduction Method on the Electrically Evoked Compound Action Potential. *Ear Hear.*, 1.

Hughes, M.L., Stille, L.J. (2010). Effect of stimulus and recording parameters on spatial spread of excitation and masking patterns obtained with the electrically evoked compound action potential in cochlear implants. *Ear Hear.*, 31, 679–692.

Hughes, M.L., Stille, L.J., Baudhuin, J.L., et al. (2013). ECAP spread of excitation with virtual channels and physical electrodes. *Hear. Res.*, 306C, 93–103.

Hughes, M.L., Vander Werff, K.R., Brown, C.J., et al. (2001). A longitudinal study of electrode impedance, the electrically evoked compound action potential, and behavioral measures in nucleus 24 cochlear implant users. *Ear Hear.*, 22, 471–486.

Jeon, E.K., Brown, C.J., Etler, C.P., et al. (2010). Comparison of electrically evoked compound action potential thresholds and loudness estimates for the stimuli used to program the Advanced Bionics cochlear implant. *J. Am. Acad. Audiol.*, 21, 16–27.

Jones, G.L., Won, J.H., Drennan, W.R., et al. (2013). Relationship between channel interaction and spectral-ripple discrimination in cochlear implant users. *J. Acoust. Soc. Am.*, 133, 425–33.

Julious, S.A., Mullee, M.A. (1994). Confounding and Simpson's paradox. *BMJ*, 309, 1480–1.

Kalkman, R.K., Briaire, J.J., Dekker, D.M.T., et al. (2014). Place pitch versus electrode location in a realistic computational model of the implanted human cochlea. *Hear. Res.*, 315, 10–24.

Kalkman, R.K., Briaire, J.J., Dekker, D.M.T., et al. (2022). The relation between polarity sensitivity and neural degeneration in a computational model of cochlear implant stimulation. *Hear. Res.*, 415, 108413.

Kalkman, R.K., Briaire, J.J., Frijns, J.H.M. (2015). Current focussing in cochlear implants: an analysis of neural recruitment in a computational model. *Hear. Res.*, 322, 89–98.

Kalkman, R.K., Briaire, J.J., Frijns, J.H.M., et al. (2016). Stimulation strategies and electrode design in computational models of the electrically stimulated cochlea: An overview of existing literature. *Netw. Comput. Neural Syst.*, 6536, 0–28.

Kaplan-Neeman, R., Henkin, Y., Yakir, Z., et al. (2004). NRT-based versus behavioral-based MAP: a comparison of parameters and speech perception in young children. *J. Basic Clin. Physiol. Pharmacol.*, 15, 57–69.

Kenway, B., Tam, Y.C., Vanat, Z., et al. (2015). Pitch Discrimination: An Independent Factor in Cochlear Implant Performance Outcomes. *Otol. Neurotol.*, 36, 1472–9.

King, J.E., Polak, M., Hodges, A. V, et al. (2006). Use of neural response telemetry measures to objectively set the comfort levels in the Nucleus 24 cochlear implant. *J. Am. Acad. Audiol.*, 17, 413–31;

Kiss, J.G., Tóth, F., Nagy, A.L., et al. (2003). Neural response telemetry in cochlear implant users. *Int. Tinnitus J.*, 9, 59–60.

Klop, W.M.C., Frijns, J.H.M., Soede, W., et al. (2009). An objective method to measure electrode independence in cochlear implant patients with a dual-masker forward masking technique. *Hear. Res.*, 253, 3–14.

Klop, W.M.C., Hartlooper, A., Briaire, J.J., et al. (2004). A new method for dealing with the stimulus artefact in electrically evoked compound action potential measurements. *Acta Otolaryngol.*, 124, 137–43.

Koch, D.B., Downing, M., Osberger, M.J., et al. (2007). Using current steering to increase spectral resolution in CII and HiRes 90K users. *Ear Hear.*, 28, 38S-41S.

Lai, W.K., Dillier, N. (2007). Comparing neural response telemetry amplitude growth functions with loudness growth functions: preliminary results. *Ear Hear.*, 28, 42S-45S.

Lai, W.K., Dillier, N., Weber, B.P., et al. (2009). TNRT profiles with the nucleus research platform 8 system. *Int. J. Audiol.*, 48, 645–54.

Laneau, J., Wouters, J., Moonen, M. (2004). Relative contributions of temporal and place pitch cues to fundamental frequency discrimination in cochlear implantees. *J. Acoust. Soc. Am.*, 116, 3606–19.

Lawand, N.S. (2015). *Micromachining technologies for future cochleair implants*. Delft University.

Lawless, H.T. (2010). A simple alternative analysis for threshold data determined by ascending forced-choice methods of limits. *J. Sens. Stud.*, 25, 332–346.

Long, C.J., Holden, T. a., McClelland, G.H., et al. (2014). Examining the electro-neural interface of cochlear implant users using psychophysics, CT scans, and speech understanding. *J. Assoc. Res. Otolaryngol.*, 15, 293–304.

Lorens, A., Walkowiak, A., Piotrowska, A., et al. (2004). ESRT and MCL correlations in experienced paediatric cochlear implant users. *Cochlear Implants Int.*, 5, 28–37.

McDermott, H.J., McKay, C.M. (2005). Pitch ranking with nonsimultaneous dual-electrode electrical stimulation of the cochlea. *J. Acoust. Soc. Am.*, 96, 155–162.

McKay, C.M., Fewster, L., Dawson, P. (2005). A different approach to using neural response telemetry for automated cochlear implant processor programming. *Ear Hear.*, 26, 38S-44S.

McKay, C.M., McDermott, H.J., Carlyon, R.P. (2000). Place and temporal cues in pitch perception: are they truly independent? *Acoust. Res. Lett. Online*, 1, 25–30.

McKay, C.M., O'Brien, A., James, C.J. (1999). Effect of current level on electrode discrimination in electrical stimulation. *Hear. Res.*, 136, 159–64.

McKay, C.M.C.M., Chandan, K., Akhoun, I., et al. (2013). Can ECAP Measures Be Used for Totally Objective Programming of Cochlear Implants? *J. Assoc. Res. Otolaryngol.*, 14, 879–90.

Mens, L.H.M. (2007). Advances in cochlear implant telemetry: evoked neural responses, electrical field imaging, and technical integrity. *Trends Amplif.*, 11, 143–59.

de Miguel, Á.R., Argudo, A.A., Borkoski Barreiro, S.A., et al. (2018). Imaging evaluation of electrode placement and effect on electrode discrimination on different cochlear implant electrode arrays. *Eur. Arch. Oto-Rhino-Laryngology*, 0, 0.

Miller, C.A., Abbas, P.J., Brown, C.J. (2000). An Improved Method of Reducing Stimulus Artifact in the Electrically Evoked Whole-Nerve Potential. *Ear Hear.*, 21, 280–290.

Miller, C.A., Brown, C.J., Abbas, P.J., et al. (2008). The clinical application of potentials evoked from the peripheral auditory system. *Hear. Res.*, 242, 184–197.

Mittal, R., Panwar, S.S. (2009). Correlation between intra-operative high rate neural response telemetry measurements and behaviourally obtained threshold and comfort levels in patients using Nucleus 24 cochlear implants. *Cochlear Implants Int.*, 10, 103–11.

Morita, T., Naito, Y., Hirai, T., et al. (2003). The relationship between the intraoperative ECAP threshold and postoperative behavioral levels: the difference between postlingually deafened adults and prelingually deafened pediatric cochlear implant users. *Eur. Arch. Otorhinolaryngol.*, 260, 67–72.

Muhaimeed, H. Al, Anazy, F. Al, Hamed, O., et al. (2010). Correlation between NRT measurement level and behavioral levels in pediatrics cochlear implant patients. *Int. J. Pediatr. Otorhinolaryngol.*, 74, 356–60.

Di Nardo, W., Ippolito, S., Quaranta, N., et al. (2003). Correlation between NRT measurement and behavioural levels in patients with the Nucleus 24 cochlear implant. *Acta Otorhinolaryngol. Ital.*, 23, 352–5.

Nelson, D.A., Van Tasell, D.J., Schroder, A.C., et al. (1995). Electrode ranking of "place pitch" and speech recognition in electrical hearing. *J. Acoust. Soc. Am.*, 98, 1987–99.

O'Brien, G., DiNino, M., Biesheuvel, J.D., et al. (2016). Comparing auditory perceptual thresholds in pediatric and adult cochlear implant populations. *J. Acoust. Soc. Am.*, 140, 3157–3157.

Pedley, K., Psarros, C., Gardner-Berry, K., et al. (2007). Evaluation of NRT and behavioral measures for MAPping elderly cochlear implant users. *Int. J. Audiol.*, 46, 254–62.

Petersen, B., Gjedde, A., Wallentin, M., et al. (2013). Cortical plasticity after cochlear implantation. *Neural Plast.*, 2013, 318521.

Pfingst, B.E., Xu, L. (2004). Across-site variation in detection thresholds and maximum comfortable loudness levels for cochlear implants. *J. Assoc. Res. Otolaryngol.*, 5, 11–24.

Pfingst, B.E., Xu, L., Thompson, C.S. (2004). Across-site threshold variation in cochlear implants: relation to speech recognition. *Audiol. Neurootol.*, 9, 341–52.

Plant, K., Law, M.-A., Whitford, L., et al. (2005). Evaluation of streamlined programming procedures for the Nucleus cochlear implant with the Contour electrode array. *Ear Hear.*, 26, 651–68.

Polak, M., Hodges, A. V, King, J.E., et al. (2006). Objective methods in postlingually and prelingually deafened adults for programming cochlear implants: ESR and NRT. *Cochlear Implants Int.*, 7, 125–41.

Potts, L.G., Skinner, M.W., Gotter, B.D., et al. (2007). Relation between neural response telemetry thresholds, T- and C-levels, and loudness judgments in 12 adult nucleus 24 cochlear implant recipients. *Ear Hear.*, 28, 495–511.

Raghunandhan, S., Ravikumar, A., Kameswaran, M., et al. (2014). A clinical study of electrophysiological correlates of behavioural comfort levels in cochlear implantees. *Cochlear Implants Int.*, 15, 145–60.

Ramekers, D., Versnel, H., Strahl, S.B., et al. (2014). Auditory-nerve responses to varied inter-phase gap and phase duration of the electric pulse stimulus as predictors for neuronal degeneration. *J. Assoc. Res. Otolaryngol.*, 15, 187–202.

Rosenfeld, R.M. (2010). How to review journal manuscripts. *Otolaryngol. Head. Neck Surg.*, 142, 472–86.

Scheperle, R.A., Abbas, P.J. (2015). Relationships Among Peripheral and Central Electrophysiological Measures of Spatial and Spectral Selectivity and Speech Perception in Cochlear Implant Users. *Ear Hear.*, 36, 441–53.

Schwarz, J.R., Reid, G., Bostock, H. (1995). Action potentials and membrane currents in the human node of Ranvier. *Pflugers Arch.*, 430, 283–92.

Seyle, K., Brown, C.J. (2002). Speech perception using maps based on neural response telemetry measures. *Ear Hear.*, 23, 72S-79S.

Shannon, R. V. (1983). Multichannel electrical stimulation of the auditory nerve in man. I. Basic psychophysics. *Hear. Res.*, 11, 157–89.

Shannon, R. V, Fu, Q.-J., Galvin, J. (2004). The number of spectral channels required for speech recognition depends on the difficulty of the listening situation. *Acta Otolaryngol. Suppl.*, 124, 50–4.

Smit, J.E., Hanekom, T., Hanekom, J.J. (2009). Estimation of stimulus attenuation in cochlear implants. *J. Neurosci. Methods*, 180, 363–373.

Smoorenburg, G.F., Willeboer, C., van Dijk, J.E. (2002). Speech perception in nucleus CI24M cochlear implant users with processor settings based on electrically evoked compound action potential thresholds. *Audiol. Neurootol.*, 7, 335–47.

Snel-Bongers, J., Briaire, J.J., Vanpoucke, F.J., et al. (2012). Spread of excitation and channel interaction in single- and dual-electrode cochlear implant stimulation. *Ear Hear.*, 33, 367–76.

Snel-Bongers, J., Briaire, J.J., Veen, E.H. van der, et al. (2013). Threshold levels of dual electrode stimulation in cochlear implants. *J. Assoc. Res. Otolaryngol.*, 14, 781–90.

Snel-Bongers, J., Netten, A.P., Boermans, P.-P.B.M., et al. (2018). Evidence-Based Inclusion Criteria for Cochlear Implantation in Patients With Postlingual Deafness. *Ear Hear.*, 39, 1008–1014.

Spivak, L., Auerbach, C., Vambutas, A., et al. (2011). Electrical compound action potentials recorded with automated neural response telemetry: threshold changes as a function of time and electrode position. *Ear Hear.*, 32, 104–13.

Stevens, S.S. (1935). The Relation of Pitch to Intensity. *J. Acoust. Soc. Am.*, 6, 150–154.

Stronks, H.C., Biesheuvel, J.D., de Vos, J.J., et al. (2019). Test/Retest Variability of the eCAP Threshold in Advanced Bionics Cochlear Implant Users. *Ear Hear.*, 40, 1457–1466.

Sun, Y.-S., Wu, C.-M., Liu, T.-C. (2004). Mandarin speech perception in nucleus CI 24 implantees using MAPs based on neural response telemetry. *ORL. J. Otorhinolaryngol. Relat. Spec.*, 66, 255–61.

Tang, Q., Benítez, R., Zeng, F. (2011). Spatial channel interactions in cochlear implants. *J. Neural Eng.*, 8.

Terhardt, E. (1979). Calculating virtual pitch. *Hear. Res.*, 1, 155–82.

Thai-Van, H., Chanal, J.M., Coudert, C., et al. (2001). Relationship between NRT measurements and behavioral levels in children with the Nucleus 24 cochlear implant may change over time: preliminary report. *Int. J. Pediatr. Otorhinolaryngol.*, 58, 153–62.

Thai-Van, H., Truy, E., Charasse, B., et al. (2004). Modeling the relationship between psychophysical perception and electrically evoked compound action potential threshold in young cochlear implant recipients: clinical implications for implant fitting. *Clin. Neurophysiol.*, 115, 2811–24.

Townshend, B., Cotter, N., Van Compernolle, D., et al. (1987). Pitch perception by cochlear implant subjects. *J. Acoust. Soc. Am.*, 82, 106–15.

Undurraga, J.A., Carlyon, R.P., Wouters, J., et al. (2012). Evaluating the Noise in Electrically Evoked Compound Action Potential Measurements in Cochlear Implants. *IEEE Trans. Biomed. Eng.*, 59, 1912–1923.

Vaerenberg, B., Smits, C., DeCeulaer, G., et al. (2014). Cochlear Implant Programming: A Global Survey on the State of the Art. *Sci. World J.*, 2014.

Vanpoucke, F.J., Zarowski, A.J., Peeters, S. a. (2004). Identification of the impedance model of an implanted cochlear prosthesis from intracochlear potential measurements. *IEEE Trans. Biomed. Eng.*, 51, 2174–2183.

de Vos, J.J., Biesheuvel, J.D., Briaire, J.J., et al. (2017). Use of Electrically Evoked Compound Action Potentials for Cochlear Implant Fitting: A Systematic Review. *Ear Hear.*, 39, 401–411.

Walkowiak, A., Lorens, A., Polak, M., et al. (2011). Evoked stapedius reflex and compound action potential thresholds versus most comfortable loudness level: assessment of their relation for charge-based fitting strategies in implant users. *ORL. J. Otorhinolaryngol. Relat. Spec.*, 73, 189–95.

Wesarg, T., Battmer, R.-D., Garrido, L.C., et al. (2010). Effect of changing pulse rate on profile parameters of perceptual thresholds and loudness comfort levels and relation to ECAP thresholds in recipients of the Nucleus CI24RE device. *Int. J. Audiol.*, 49, 775–87.

Wichmann, F. a., Hill, N.J. (2001a). The psychometric function: I. Fitting, sampling, and goodness of fit. *Percept. Psychophys.*, 63, 1293–1313.

Wichmann, F.A., Hill, N.J. (2001b). The psychometric function: II. Bootstrap-based confidence intervals and sampling. *Percept. Psychophys.*, 63, 1314–1329.

Willeboer, C., Smoorenburg, G.F. (2006). Comparing cochlear implant users' speech performance with processor fittings based on conventionally determined T and C levels or on compound action potential thresholds and live-voice speech in a prospective balanced crossover study. *Ear Hear.*, 27, 789–98.

Wolfe, J., Kasulis, H. (2008). Relationships among objective measures and speech perception in adult users of the HiResolution Bionic Ear. *Cochlear Implants Int.*, 9, 70–81.

Wolfe, J., Schafer, E.C. (2014). *Programming Cochlear Implants* Second Edi., Plural Publishing.

Zeng, F.-G. (2004). Trends in cochlear implants. *Trends Amplif.*, 8, 1–34.

Zeng, F.G. (2002). Temporal pitch in electric hearing. *Hear. Res.*, 174, 101–6.

Zhang, F., Benson, C., Murphy, D., et al. (2013). Neural adaptation and behavioral measures of temporal processing and speech perception in cochlear implant recipients. *PLoS One*, 8, e84631.

Appendices

A.1. Abbreviations

3AFC	three alternative forced choice
AB	Advanced Bionics
AGF	amplitude growth function
AP	alternating polarity
ART	auditory response telemetry
BEDCS	bionic ear data collection system
BM	basilar membrane
CI	cochlear implant
CU	clinical unit
CVC	consonant vowel consonant
eCAP	electrically evoked compound action potential
EDP	excitation density profile
FM	forward masking
ICD	inter channel distance
JND	just noticeable difference
LE	linear extrapolation
LV	last visible
M	masker
MAL	maximum acceptable loudness
MCL	most comfortable loudness
MP	masker-probe
mSOE	measured spread of excitation
NRA	neural response amplifier
NRI	neural response imaging
NRT	neural response telemetry
P	probe
PRISMA	preferred reporting items for systematic reviews and meta-analyses
pSOE	predicted spread of excitation
RMSE	root mean square error
RSPOM	research studies platform objective meausures
sEDP	simulated excitation density profile
SFAP	single fiber action potential
SFM	spatial forward masking
SNR	signal to noise ratio
SOE	spread of excitation
TCI	threshold confidence interval

A.2. List of publications

1. The effect of stimulus level on the excitation patterns of individual stimuli in cochlear implants, J.D. Biesheuvel, J.J. Briaire, R.K. Kalkman, J.H.M. Frijns, Hearing Research, 2022, 420:108490
2. Full array channel discrimination in cochlear implants: validation and clinical application, C.A.A. Windmeijer, J.D. Biesheuvel, J.J. Briaire, P.P.B.M. Boermans, J.H.M. Frijns, International Journal of Audiology, 2022, Jul 23:1-10
3. Unravelling the temporal properties of human eCAPs through an iterative deconvolution model, Y. Dong, J.J. Briaire, J.D. Biesheuvel, H.C. Stronks, J.H.M. Frijns, Hearing Research, 2020, 395:108037
4. Effectiveness of phantom stimulation in shifting the pitch percept in cochlear implant users, M.A.M. de Jong, J.J. Briaire, J.D. Biesheuvel, J. Snel-Bongers, S. Böhringer, G.R.F.M. Timp, J.H.M. Frijns, Ear and Hearing, 2020, 41(5):1258-1269
5. Test/retest variability of the eCAP threshold in advanced bionics cochlear implant users, H.C. Stronks, J.D. Biesheuvel, J.J. de Vos, P.S. Boot, J.J. Briaire, J.H.M. Frijns, Ear and Hearing, 2019, 40(6):1457-1466
6. Channel discrimination along all contacts of the cochlear implant electrode array and its relation to speech perception, J.D. Biesheuvel, J.J. Briaire, M.A.M. de Jong, S. Boehringer, J.H.M. Frijns, International Journal of Audiology, 2019, 58(5):262-268
7. The precision of eCAP thresholds derived from amplitude growth functions, J.D. Biesheuvel, J.J. Briaire, J.H.M. Frijns, Ear and Hearing, 2018, 39(4):701-711
8. Use of electrically evoked compound action potentials for cochlear implant fitting: a systematic review, J.J. de Vos, J.D. Biesheuvel, J.J. Briaire, P.S. Boot, M.J. van Gendt, O.M. Dekkers, M. Fiocco, J.H. M. Frijns, Ear and Hearing, 2018, 39(3):401-411
9. A novel algorithm to derive spread of excitation based on deconvolution, J.D. Biesheuvel, J.J. Briaire, J.H.M. Frijns, Ear and Hearing, 2016, 37(5):572-581
10. Initial systolic time interval (ISTI) as a predictor of intradialytic hypotension (IDH), J.D. Biesheuvel, M.G. Vervloet, R.M. Verdaasdonk, J.H. Meijer, Journal of Physics: Conference Series, 2013, 434

A.3. Curriculum vitae

Personalia

Name: Jan Dirk Biesheuvel
Born: 13-05-1990, Lienden

Education

2017-2021	Klinisch fysicus - audioloog in opleiding	LUMC, Leiden
2013-2017	PhD student	LUMC, Leiden
2011-2013	Master Medical Natural Sciences	Vrije Universiteit, Amsterdam
2008-2011	Bachelor Medische Natuurwetenschappen	Vrije Universiteit, Amsterdam
2002-2008	Voorbereidend Wetenschappelijk Onderwijs	Van Lodenstein College, Amersfoort

Work experience

2021-now	Klinisch fysicus - audioloog	LUMC, Leiden
2017-2021	Klinisch fysicus - audioloog in opleiding	LUMC, Leiden
2013-2017	PhD student	LUMC, Leiden